DESIGN OF AN ANTI CONCUSSION HEADGEAR

A THESIS SUBMITTED TO
THE GRADUATE SCHOOL OF NATURAL AND APPLIED SCIENCES
OF
MIDDLE EAST TECHNICAL UNIVERSITY

BY

ALPEREN VAROL

IN PARTIAL FULFILLMENT OF THE REQUIREMENTS
FOR
THE DEGREE OF MASTER OF SCIENCE
IN
MECHANICAL ENGINEERING

APRIL 2023

Approval of the thesis:

DESIGN OF AN ANTI CONCUSSION HEADGEAR

submitted by **ALPEREN VAROL** in partial fulfillment of the requirements for the degree of **Master of Science** in **Mechanical Engineering, Middle East Technical University** by,

Prof. Dr. Halil Kalıpçılar
Dean, Graduate School of **Natural and Applied Sciences**

Prof. Dr. M. A. Sahir Arıkan
Head of the Department, **Mechanical Engineering**

Assist. Prof. Dr. Gökhan Osman Özgen
Supervisor, **Mechanical Engineering, METU**

Examining Committee Members:

Prof. Dr. Fevzi Suat Kadıoğlu
Mechanical Engineering, METU

Assist. Prof. Dr. Gökhan Osman Özgen
Mechanical Engineering, METU

Prof. Dr. Serkan Dağ
Mechanical Engineering, METU

Assist. Prof. Dr. Orkun Özşahin
Mechanical Engineering, METU

Assist. Prof. Dr. Selçuk Himmetoğlu
Mechanical Engineering, Hacettepe University

Date: 25.04.2023

Name Last name : Alperen Varol

Signature :

ABSTRACT

DESIGN OF AN ANTI CONCUSSION HEADGEAR

Varol, Alperen
Master of Science, Mechanical Engineering
Supervisor: Assist. Prof. Dr. Gökhan Osman Özgen

April 2023, - 111 pages

In this thesis, a FE model of improved boxing headgear is modeled through the implementation of a TVA to reduce the risk of TBI in boxing, a valid human head FE model is constructed, and a boxing hook punch is simulated. A surface-to-surface tied contact is defined between the head components. The human head model is validated by experimental data available in the literature. The neck is modeled by using axial and torsional springs, whose material properties are acquired from the literature. On the human head model, a damping ratio of 5% is added to the model using Rayleigh damping. The protective headgear, glove, and hand are modeled. A TVA is modeled at the tuning frequency of the first natural mode of the head, a torsional motion around the neck. With a known tuning frequency, sweeps of the TVA tuning mass and damping ratio are conducted. The change in the lateral response of the nasal area in FRF plots at TVA tuning frequency is examined. The least response is decided to be most beneficial. For both undamped and Rayleigh-damped models, TVA tuning is conducted. TBI happens when high stress and strain rates occur on the brain tissues, as a result of rapid head movements. The hook punch, which is the most dangerous punch type in boxing in terms of TBI, is simulated. Hook punch simulations are performed on the head model without headgear, with standard headgear, and with TVA-implemented headgear for both undamped and Rayleigh-damped head models. The linear acceleration of the head as well as the

rotational movement, velocity, and acceleration are monitored. Three different severity metrics are used in TBI risk calculations: HIC, BrIC, and CM. It is observed that the implementation of the TVA tuned at the first torsional natural frequency of the head on protective headgear does not reduce the risk of TBI effectively.

Keywords: Traumatic Brain Injury, Boxing, Headgear Design, Concussion, Tuned Vibration Absorber

ÖZ

SARSINTI ENGELLEYİCİ BAŞLIK TASARIMI

Varol, Alperen
Yüksek Lisans, Makina Mühendisliği
Tez Yöneticisi: Dr. Öğr. Üy. Gökhan Osman Özgen

Nisan 2023, - 111 sayfa

Bu tezde; beyin sarsıntısı riskini azaltmak amacıyla ayarlı kütle sönümleyicisi eklenerek geliştirilmiş boks kaskı sonlu eleman modeli tasarlandı, geçerli bir insan kafası sonlu eleman modeli oluşturuldu ve kroşe yumruk için sonlu eleman simülasyonu modellendi. Kafa kısımları arasında yüzey yüzeye bağlı kontak tanımlandı. Kafa modelinin doğrulamasında mevcut deneysel veriler kullanıldı. Boyun modellemesi doğrusal ve burulma yayları ile modellendi. Kafa modeline 5% sönümleme Rayleigh sönüm modeli ile eklendi. Koruyucu kask, eldiven ve el modellendi. Ayarlı kütle sönümleyicisi frekansı, kafanın ilk doğal frekansı olan boyun etrafında burulma yönündeki moduna ayarlandı. Ayarlı kütle sönümleyicisinin frekansı belirlendikten sonra kütle ve sönümleme oranını belirlemek için taramalar gerçekleştirildi. Frekans davranış fonksiyonunun; burun kemiği bölgesinde, yatay yöndeki büyüklüğü ayarlı kütle sönümleyicisinin değişkenlerine bağlı olarak değiştiği gözlemlendi. Bölgedeki düşük tepkinin daha faydalı olduğuna karar verildi. Sönümsüz ve Rayleigh sönümlü kafa modelleri için ayarlı kütle sönümleyicisi değişkenleri belirlendi. Beyin sarsıntısına sebep olan yüksek gerilim ve gerinim kafanın hızlı hareketleri ile meydana geldiği görüldü. Beyin sarsıntısı için kroşe yumruk simülasyonları gerçekleştirildi. Sönümsüz ve Rayleigh sönümlü modeller için; kasksız model, standart kasklı model ve ayarlı kütle sönümleyicisi eklenmiş kasklı model analizleri yapıldı. Kafanın doğrusal ivmesi, açısal dönüşü, açısal hızı ve açısal ivmesi bu simülasyonlarda takip edildi. Sonuçlar için üç farklı şiddet indeksi hesaplandı; HIC, BrIC ve CM. Simülasyonlar neticesinde, kafanın ilk burkulma doğal frekansına ayarlanmış ayarlı kütle sönümleyicisi eklenmiş boks kaskının beyin sarsıntısı riskini azaltmakta yeterli fayda sağlamadığı görüldü.

Anahtar Kelimeler: Travmatik Beyin Sarsıntısı, Boks, Kask Tasarımı, Sarsıntı, Ayarlı Kütle Sönümleyicisi

To my luck in this realm.

ACKNOWLEDGMENTS

First and foremost, I would like to express my gratitude to my thesis supervisor, Assist. Prof. Dr. Gökhan Osman Özgen for his guidance, support, and patience through this study.

I would like to thank the examining committee members: Prof. Dr. Fevzi Suat Kadıoğlu, Prof. Dr. Serkan Dağ, Assist. Prof. Dr. Orkun Şahin, and Assist. Prof. Dr. Selçuk Himmetoğlu for their valuable comments and guidance.

I also would like to thank my co-workers Mehmet Yahşi, Emre Bilen, Orhun Çiçek, and Umut Yılmaz for their constant support in this study.

I am grateful to my family members for their unending support and encouragement.

Finally, I would like to express my deepest gratitude to my wife, Aliye Bihter, for her endless support, patience, and love. Her presence gives me strength to accomplish my goals.

TABLE OF CONTENTS

LIST OF TABLES

TABLES

LIST OF FIGURES

FIGURES

LIST OF ABBREVIATIONS

ABBREVIATIONS

AIBA	:	L'Association Internationale de Boxe Amateur
AOB	:	AIBA Open Boxing
BrIC	:	Brain Injury Criteria
CAD	:	Computer Aided Design
CM	:	Combined Metric
CSF	:	Cerebrospinal Fluid
CT	:	Computerized Tomography
HIC	:	Head Injury Criterion
IBA	:	International Boxing Association
LUSN	:	Loughborough University Surrogate Neck
MR	:	Magnetic Resonance
MRI	:	Magnetic Resonance Imaging
NFL	:	National Football League
TBI	:	Traumatic Brain Injury
TVA	:	Tuned Vibration Absorber

CHAPTER 1

INTRODUCTION

1.1 GENERAL

Boxing has been one of the most popular sports around the globe for centuries. Numerous people follow boxing or participate as amateur or professional players. Even though all sports activities involve a risk of injury at some level, the injuries in boxing are rather critical, even resulting in deaths. Studies show the number of fatalities in boxing has decreased over the years due to regulations in the rules, yet the number of deaths still averages around 7 per year [1]–[3]. Many of the fatalities in boxing result from brain injuries due to high impact loads on the head [3], [4]. The impact on the head results in a sudden movement of the head, which causes high stress and strain rates in brain tissues, which cause traumatic brain injuries (TBI) [4]. The aim of this study is to reduce the risk of TBI by reducing the critical movement of the head after an impact. For this reason, the implementation of a tuned vibration absorber (TVA) on boxing headgear is selected. TVA implementation on a headgear will absorb the motion of the head at a selected (tuned) frequency, and thus the movement of the head will be reduced, as well as the risk of TBI.

TBIs can be divided into three categories: concussions, intracranial hemorrhage, and second-impact syndrome. Among these three categories, intracranial hemorrhage is the most crucial one with a higher risk of death than others. Second-impact syndrome is a condition where a person suffers a second concussion before the first one heals completely, and the results of second-impact syndrome are often fatal. Concussion is the most common type of TBI, with ordinary end-effects of loss of consciousness, drowsiness, and slowed reaction. However, there is also a possible long-term effect of micro concussions, which is punch-drunk syndrome. Punch-drunk syndrome is a condition that occurs when a person is repeatedly exposed to low-level brain injuries for a long time, resulting in symptoms such as mental confusion, slowness, tremors at the hands, and so on. Since the effect of punch-drunk syndrome emerges after a long time, preventing it from happening is not easy for boxers who experience not noticeable brain injuries frequently [3]. Even though it is not possible to quantify the long-term injury in the brain, it is assumed that lowering the risk of concussion should reduce the risk of both fatalities by knockout and punch-drunk syndrome since the main source of all types of TBI is the same: high stress and strain rates in brain tissues due to rapid movement of the head.

1.2 PROCESS OF STUDY

The aim of this study is to reduce the risk of concussion for boxers. Since the risk of concussion is highly linked with the rapid movement of the head, the idea behind this study is to lower the sudden movement of the head by a TVA implementation on the headgear.

For the study at hand, the first step was understanding the main reason for TBI. After it is determined that the linear and rotational rapid movement of the head is the main reason for TBI occurrence, the punch types in boxing are investigated, which are the impact loads in this study. Among the three main punch types in boxing, the hook punch is decidedly the most crucial one since its impact on the head results in more rotational movement of the head than other punch types. A finite element simulation method is decidedly used in the study, for which a verified human head model is needed. For the verification of a human head finite element model, Nahum's experimental data on human cadavers was determined to be used [5]. After modeling and verification of the human head, boxing protective headgear and glove are modeled. A literature survey is conducted on the average hook punch speeds and impact loads on the head to be used in the simulations. Human head damping values are investigated based on experimental articles to be used in the head model for more realistic results. The simulations are conducted under three different conditions: when there is no protective headgear, when there is a protective headgear with no

TVA implementation, and finally with a protective headgear with a TVA implementation. The quantification of TBI risk is performed by using three different methods: Head Injury Criterion (HIC), Brain Injury Criteria (BrIC), and Combined Metric (CM), which use linear and rotational velocity and acceleration values of the human head based on experimental data.

CHAPTER 2

LITERATURE REVIEW

For the development of an improved boxing headgear to reduce the risk of TBI, understanding the nature of TBI and what causes its occurrence was the first step. The known causes of TBI are investigated at both the brain tissue and head movement levels. After conducting research on TBI, the reasons for concussion during boxing matches are investigated, and the hook punch on the side of the head is decided to be the most critical one because of its effect on rapid angular movement of the head. After deciding the risk factor of the study is the rapid torsional movement of the head due to a hook punch, the severity indices for risk of TBI are investigated, and three metrics are selected to be used for TBI risk quantification in this study. For the problem at hand, a method of finite element simulations is decided to be used. For the simulations, a human head model was needed, and studies with similar problems where a finite element simulation was held with an impact on the human head were examined. In order to acquire more realistic simulation results, damping is decided to be added to the model, and for this goal, different damping methods used in FE analyses are reviewed. For the simulation of the process, boxing headgear and gloves are investigated, as well as average hook punch speeds and impact forces.

2.1 Investigation on TBI

The reason behind concussion is well known as the rapid linear and rotational movement of the head. However, the movement of the head does not quite explain the injury happening to the brain. Studies show that the cellular-level cause of concussion is high axonal stress and strain taking place on brain tissues due to rapid movement of the head [6], [7]. Nodes of Ranvier, also known as myelin-sheath gaps, are the ion channels that are responsible for the transportation of sodium ions on nerve cell extensions, known as axons. It is shown that the stretch on nodes of Ranvier disrupts the ion transport on axons, resulting in subcellular damage. It is suggested that the critical strain values in the nodes of Ranvier can be used as a metric of concussion. Moreover, a practical way of monitoring the strain on nodes of Ranvier is by observing the strain of corpus callosum. Where nodes of Ranvier are present at [4], corpus callosum is shown in Figure 2.1.

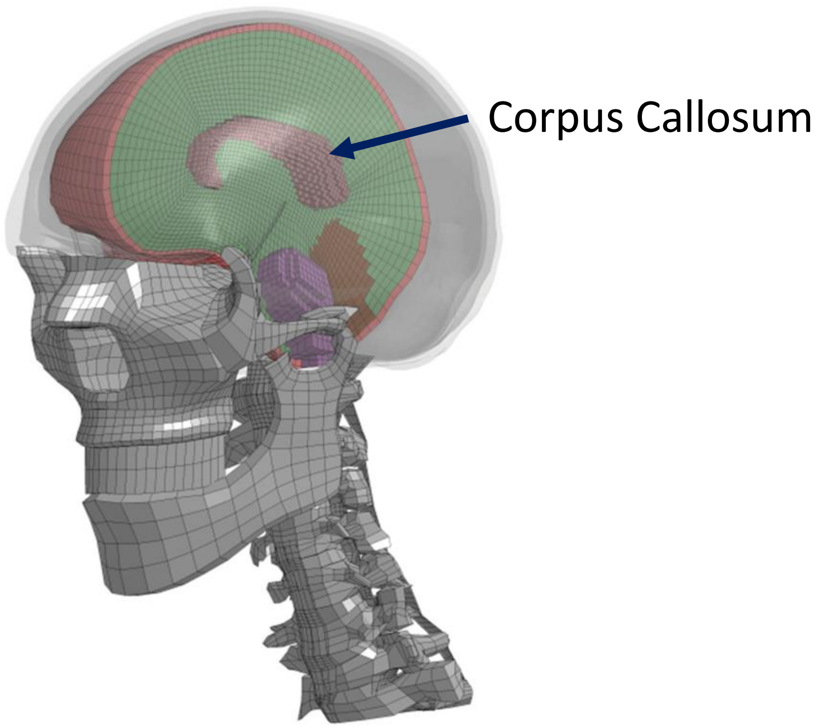

Figure 2.1. Corpus Callosum [4]

Ng et al. used a detailed human head and neck FE model and showed a correlation between concussion rates of individuals and strain rates on the corpus callosum by using datasets from National Football League (NFL) players' helmets, military combat exposure, and experiments held on non-human primates (NHP) [4].

Even though the main reason for the concussion is at the subcellular level, the gross motion of the head has been linked to TBI for decades. Studies show that there are three possible types of stress that can occur on the brain tissues due to an impact on the head: compression, tension, and shear stresses. Among these three, shear stress is the most dangerous one [4], [8]–[10] and in boxing, the hook punch carries the highest risk of concussion due to its cause of high rotational acceleration and velocity on the head, which results in high shear stresses and strains in brain tissue [3].

2.1.1 Formulation of Risk of TBI

Quantifying the brain injury risk has been studied for a long time, and the most common severity index is the Head Injury Criterion (HIC). HIC is originated from studies on the determination of acceleration and intracranial pressure due to head injuries [11] and evolved over time by real-life datasets and experiments held on dogs. HIC formulation for TBI risk calculation is as follows [11]:

$$HIC = \max\left\{(t_2 - t_1)\left[\frac{1}{t_2 - t_1}\int_{t_1}^{t_2} a(t)dt\right]^{2.5}\right\} \qquad \text{Eq. 2-1}$$

Where a is the resultant linear acceleration of the head, t_1 and t_2 are the impulse start and stop times. In literature, two variations of HIC are being used: HIC15 and HIC36. The difference between them is the maximum elapsed time during the impact. HIC15 and HIC36 are being used for maximum impact durations of 15 ms and 36 ms respectively. The higher the magnitude of HIC, the higher the risk of concussion.

Brain Injury Criteria (BrIC) is another TBI severity index developed by Takhounts et al. [12]. While HIC focuses on the resultant angular acceleration of the head, BrIC is calculated by using the angular velocities of the head. The equation for BrIC is as follows [12]:

$$BrIC = \sqrt{\left(\frac{\omega_x}{\omega_{xC}}\right)^2 + \left(\frac{\omega_y}{\omega_{yC}}\right)^2 + \left(\frac{\omega_z}{\omega_{zC}}\right)^2} \qquad \text{Eq. 2-2}$$

Where ω_x, ω_y, and ω_z are the maximum angular velocities of the head about axes X, Y, and Z, respectively, and ω_{xC}, ω_{yC}, and ω_{zC} are the critical angular velocities of their axes, the axes definition of the study is shown in Figure 2.2. The critical angular velocities of the three axes are given in Table 2.1 [12]

Table 2.1 Critical Maximum Angular Velocities for BrIC

Critical Maximum Angular Velocity	*rad/s*
ω_{xC}	66.25
ω_{yC}	56.45
ω_{zC}	42.87

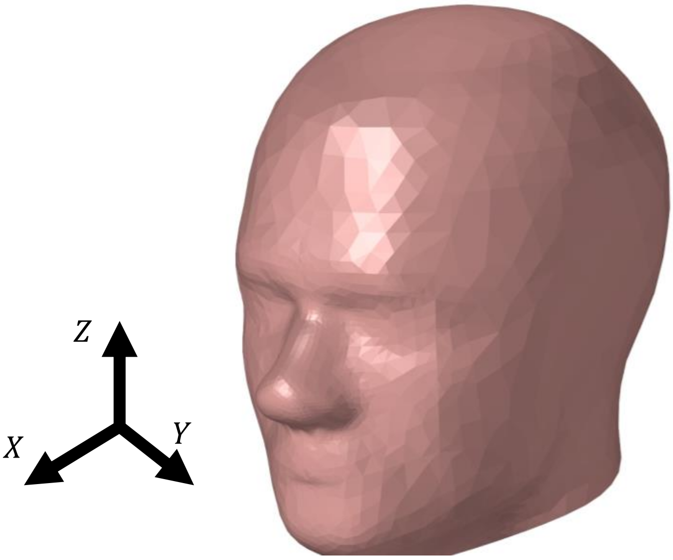

Figure 2.2. Axes Definition of the Model

There are two possible approaches to calculating BrIC. First, using the maximum values of ω_x, ω_y, and ω_z separately, even though their maxima happened at different times. The second approach is to calculate BrIC for the whole impact duration and accept the maximum value at hand [12]. This study employs the first strategy.

Other than HIC and BrIC, Combined Metric (CM) is developed by the NFL for a better evaluation of concussion risk [13]. CM takes both rotational and linear resultant head acceleration into account with HIC15 criteria, the formulation is as follows [13]:

$$CM = \frac{1}{n}\sum\left(\frac{\alpha_{peak}}{\alpha_{ave}} + \frac{\omega_{peak}}{\omega_{ave}} + \frac{HIC15}{HIC15_{ave}}\right) \qquad \text{Eq. 2-3}$$

Where n is the number of test conditions conducted, α_{peak} and ω_{peak} are the maximum rotational resultant acceleration and velocity values of the head, HIC15 is the calculated HIC value for the impact, α_{ave}, ω_{ave}, and $HIC15_{ave}$ are normalizing values developed by the NFL by using different tests with different football helmets [13]. NFL conducted 24 tests for the CM development in different years; details are given in Table 2.2 [13].

Table 2.2 Normalization Values for CM

Year	$\alpha_{ave}\ (rad/s)$	$\omega_{ave}\ (rad/s)$	$HIC15_{ave}$
2015	4102	37.8	209
2016	4127	38.0	208
2017	4088	37.7	202
Average	4105.7	37.9	206.3

A study conducted on football helmets shows linear acceleration, angular acceleration, and HIC15 values for 25, 50, and 80 percent probability of mild TBIs [13]. The mentioned values are given in Table 2.3.

Table 2.3 Probability of mild TBI

Probability of mild TBI	Linear Acceleration (g)	Angular Acceleration (rad/s^2)	$HIC15$
25%	66	4600	151
50%	82	5900	250
80%	106	7900	369

2.2 Investigation on Punch Types

In boxing, there are three main punches: straight, hook, and uppercut. A straight punch is when the opponent gets hit from directly ahead, as shown in Figure 2.3.

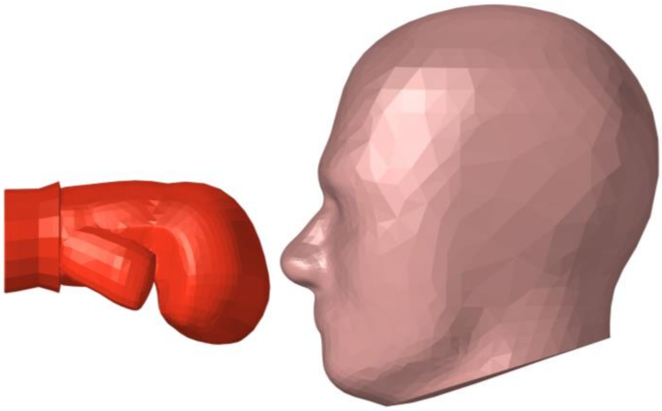

Figure 2.3. Straight Punch

Straight punches result in bending and translational movement of the head; they do not lead to rotational movement since the impact point is on the rotation axis of the head. An uppercut is a punch thrown up to the opponent's jaw from below, as shown in Figure 2.4.

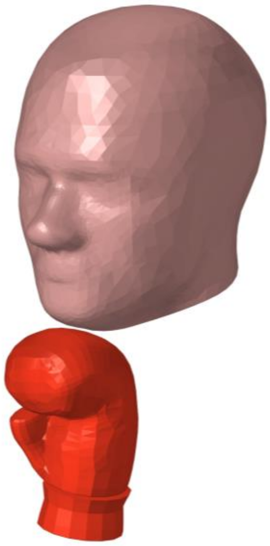

Figure 2.4. Uppercut Punch

A hook punch is thrown to the opponent from the side of the head; the punch generally hits the jaw or cheekbone, as shown in Figure 2.5.

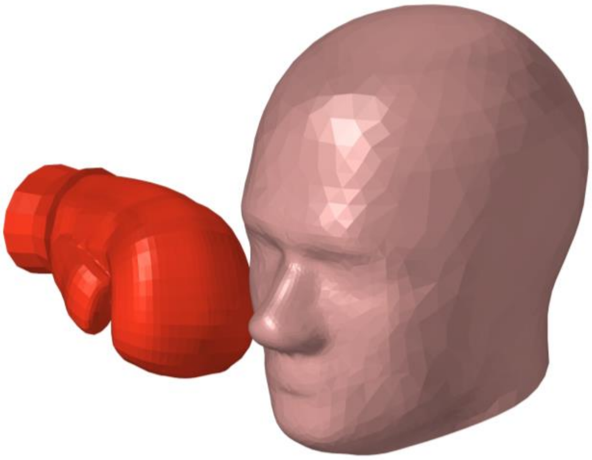

Figure 2.5. Hook Punch

A hook punch causes a higher angular movement of the head than straight or uppercut punches. It is stated that concussion occurs more due to angular movement of the head than linear motion; therefore, the hook punch is more crucial in terms of risk of concussion and was selected as the impact condition for the study at hand.

2.3 Head Modeling

The human head finite element modeling problem is discussed in two branches: modeling and validation of any modeled human head finite element model.

2.3.1 Head Modeling Validation

Nahum et al. [14] performed two sets of head impact experiments on stationary, not mummified cadavers in a seated position to examine the relationship between different impact variables and the dynamic response of the human brain to head impact. The first set of experiments is performed on different specimens, whereas the second series includes experiments repeatedly performed on the same specimen. A rigid impactor mass of 5 to 23 kg traveling at a constant velocity ranging from 4.4 to 13.0 m/s is used to hit the frontal bone in the mid-sagittal plane with an angle of 45°, as shown in Figure 2.6. A layer of padding is interposed on the free end of the impactor to alternate the impact duration and prevent skull fracture. On several specimens, dynamic measurements of force exerted by the impactor ranging from 5.20 to 14.84 kN of peak values, together with biaxial head accelerations with peak values of 1.52 x 10^3 to 3.90 x 10^3 m/s^2 are recorded during blunt impact. The cadaver heads are pressurized to maintain in vivo levels of vascular and cerebrospinal fluid pressures. Pressure transducers are inserted on the frontal bone (A), parietal bone (B, D), lambdoidal suture at the occipital bone (C), and the occipital bone at the posterior fossa (E). Cadaver cranium sizes, such as head breadth, circumference, length, and so on, are given in the study. The pressure results of experiment number 37 are given in figures with inputs on the cadaver's head. With the given input force, head acceleration, and transducer pressure reading figures, it becomes possible to create a human head model with correct brain dynamics corresponding to the movement of the cranium.

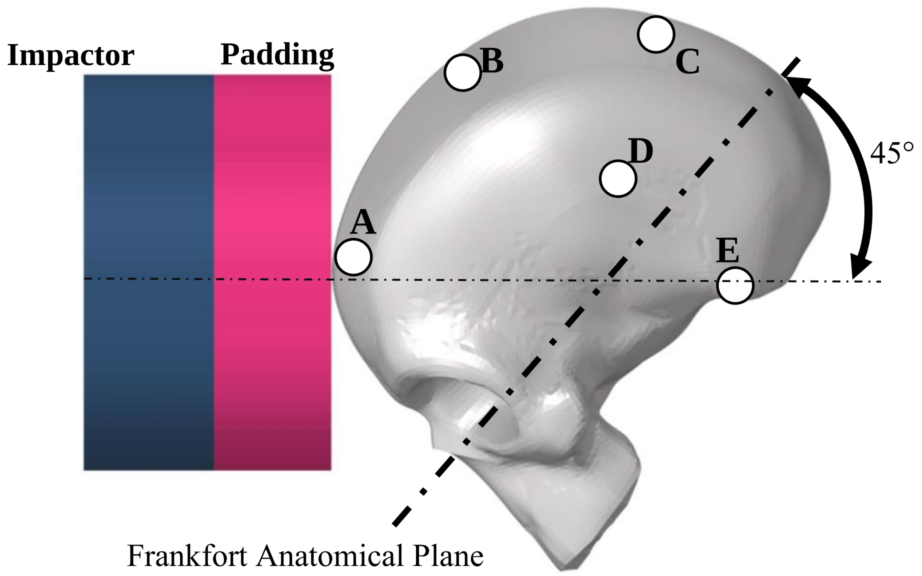

Figure 2.6. The Head, Impactor and Pressure Transducer Locations

2.3.2 Previous Human Head Modeling Studies

Numerous researchers have been using Nahum's experimental data to validate their human head finite element models. Since the experiment Nahum conducted was for understanding the dynamic behavior of the human brain under impact loadings on the skull, the models validated by this experiment can be used for many applications, such as simulations in the fields of the military, football, boxing, traffic accidents, and so on. Among these studies, the level of detail in their FE models varies; however, none use a neck model for head validation. There are two main reasons for not modeling a neck in a finite element model: the first is that, the experimental data supplied by Nahum et al. is based on cadavers, and the stiffness and damping values of relaxed human muscle are negligible; the second is that the time duration of the simulation is between 5 and 7 seconds on average, and the addition of a neck to a head model does not change the results, as the authors explain in their articles. A few examples are given in the following, with their similarities and differences.

Luo et al. modeled a human head based on a geometric model extracted from real-life medical images and applied material properties from the literature [15], [16]. The interfaces between intracranial tissues are not described in the article. The built model is validated by Nahum's experiment number 37, and the aim of the study was to understand the effectiveness of a sports helmet in preventing closed head injuries. The model contains three parts: the skull, cerebrospinal fluid (CSF), and brain. The brain is modeled as viscoelastic, and CSF is modeled as an inviscid fluid. The validation results compared to Nahum's experimental data are given in Table 2.4.

Cai et al. created a multiblock finite element head model based on geometric size adapted from medical images [17]. The model they created consists of skin, cranium, facial bone, and brain tissues and membranes with material properties gathered from the literature. Elastic material properties for bone and skin components and viscoelastic materials for brain tissue components and membranes are used. A tied contact interface condition is given between the skull and CSF and between the CSF and brain. The validation based on Nahum's experiment is given in Table 2.4.

Fernandes et al. modeled a human head based on real-life medical images, with the goal of modeling it as realistically as possible rather than using a sphere-like brain [18]. The model they created consists of three main layers: the skull, brain, and cerebrospinal fluid (CSF). As material types, the skull is modeled as a linear elastic component, the brain is modeled as a viscoelastic component, and CSF is modeled as a hyperelastic component. Sliding with friction contact is applied between the skull and CSF and between the CSF and brain. The pressure results compared with Nahum's experiment are given in Table 2.4. However, while the peak pressure values are in accordance with the experimental data, it is noticed that the trend of the pressure line is not similar to Nahum's results, especially in negative pressure conditions.

Horgan et al. modeled a human head for impact simulations [19]. The geometric data in the model is from the Visible Human Database. According to the material properties gathered from the literature, the brain is modeled as a hyperelastic material, whereas the bones and intracranial layer between the brain and skull are modeled as elastic. Tied contact interface modeling was chosen between the skull, CSF, and brain due to computational constraints. The validation of the model based on Nahum's experiment is given in Table 2.4.

Takhounts et al. created a finite element head model to investigate TBI [20]. The geometric data for the model was taken from medical images of a male patient. The outer surface of the brain is smooth, whereas the brain tissues are modeled separately with detail, such as the cerebrum, cerebellum, brainstem, blood vessels, falx, tentorium, ventricles, and the CSF layer. In the model, brain parts and the CSF layer are modeled as viscoelastic components with different properties; the falx is modeled as elastic, the skull is modeled as rigid, and the ventricles are modeled as elastic fluid. The pressure results of the simulation based on Nahum's experiment are given in Table 2.4 for comparison. Note that numerous pressure results are shared for each location, and the given values in Table 2.4 are the averages of them.

Tse et al. developed a human FE model and validated the model based on three experiments [21], including Nahum's experiment number 37. The geometric data for the head model is from CT and MR images. They modeled two distinct heads, one simpler than the other. Model 1 contains the neck, jaw, teeth, nose, skull, CSF, and brain. Whereas model 2 contains skin on top of the head, and the brain consists of gray matter, white matter, the brainstem, the cerebellum, and the centivular system. The element type of model 1 is linear hexahedral, while the element type of model 2 is linear tetrahedral. Material properties are gathered from the literature; brain components are modeled as viscoelastic, whereas CSF, skin, and other components are modeled as linear elastic with different properties. As for the interface condition, sliding with friction without separation is applied both between the skull and CSF and between CSF and brain interfaces. The validation based on experimental data is given in Table 2.4.

Table 2.4 Comparison of Different Head Models' Peak Pressure Values

	Frontal P. (kPa)	*Parietal P. (kPa)*	*Occipital P. #1 (kPa)*	*Occipital P. #2 (kPa)*	*Posterior Fossa P. (kPa)*
Experiment	141.2	73.6	-45.5	-48.4	-60.3
Luo et al.	170	85	N/A	N/A	-75
Cai et al.	150	110	-60	N/A	-70
Fernandes et al.	142	72	-60	-47	-60
Horgan et al.	142	72	-60	N/A	-75
Takhounts et al.	150	55	-75	-80	-80
Tse et al. Model 1	152	75	-45	-45	-57
Tse et al. Model 2	165	90	-55	-58	-65

In the table above, P. stands for Pressure.

2.4 Human Head Damping

Hakansson et al. investigated the free-damped natural frequencies of the human head on six patients. Patients who already had titanium implants in their cranium for hearing aids made this experiment possible. The resonant frequencies as well as damping ratios are tabulated as the result of the study [22]. The damping ratios are given as between 5 and 10%, decreasing with increased frequencies above 1 kHz.

Nahum et al. modeled a human finite element model and met their experimental results acquired from cadavers [14]. It is stated that the response of the brain was highly damped, and 20% damping was added in order to meet the experimental data.

In finite element analysis, there is more than one way to add damping to your model, besides damper elements. In Radioss (Altair Engineering Inc.), an explicit finite element solver, these methods are dynamic relaxation, kinetic relaxation, and Rayleigh mass and stiffness damping coefficients. Among these three options, Rayleigh damping is the most practical since it is possible to control the frequency dependent damping ratios given to your model.

Rayleigh damping approximates viscous damping based on mass and stiffness matrices and constant coefficient multipliers, as shown in Eq. 2-4. Where C is the model given Rayleigh damping, M and K are the mass and stiffness matrices of the model, respectively, and finally, α and β terms are the mass and stiffness damping coefficients, respectively.

$$C = \alpha M + \beta K \qquad \text{Eq. 2-4}$$

The damping ratio for any given frequency can be calculated approximately as given in Eq. 2-5. Where, ζ is the damping ratio and ω is the given frequency in rad/s.

$$\zeta = \frac{1}{2}\left(\frac{\alpha}{\omega} + \beta\omega\right) \qquad \text{Eq. 2-5}$$

For better understanding, the behavior of the damping coefficient with changing frequency is shown in Figure 2.7 for mass and stiffness matrix coefficients separately.

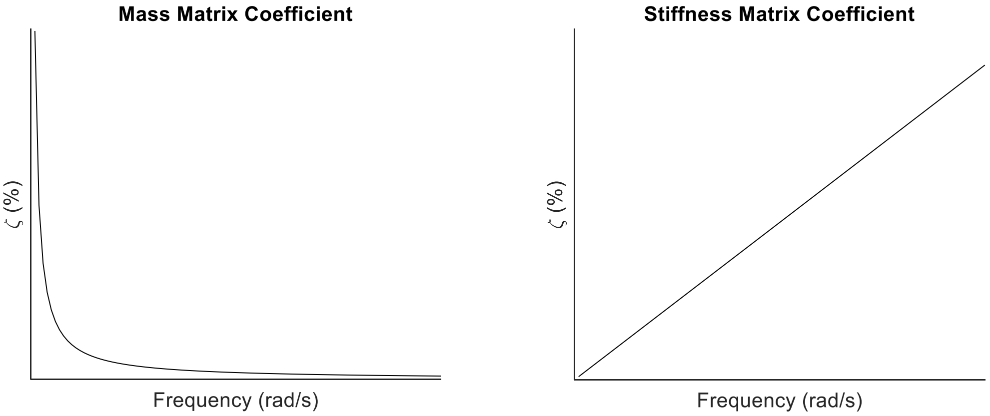

Figure 2.7. Rayleigh Damping Coefficient Proportionalities

In this study, a non-damped human head model as well as a damped human head model using Rayleigh damping coefficients are used.

2.5 Protective Headgears and Gloves in Boxing

The International Boxing Association (IBA) states that in all AOB (AIBA Open Boxing) competitions, except elite competitions, every boxer must wear a headguard. The maximum weight of the headguard is set to be 450 grams. Headguards must have Velcro strips to fit on the head safely [23].

In every event, a boxer must wear a set of gloves weighing 10 or 12 oz, depending on the competition.

CHAPTER 3

MODELING OF HOOK PUNCH IN BOXING

The study aims to use a tuned vibration absorber (TVA) on the headgear to reduce the risk of concussion caused by a delivered hook punch. To make the improvement on the existing headgear, the requirements are as follows: a verified finite element head model; a neck model added to the head model to meet realistic boundary conditions of the simulation; a model of a headgear and a glove; a simulation of the punch; and finally, an improvement on the headgear by adding a tuned vibration absorber.

3.1 Modeling

In the modeling process of the study, modeling of the head, which consists of the skull, the brain, and the cerebrospinal fluid between them, modeling of the neck, and the protective gears, which are the glove and the headgear, are taken care of.

3.1.1 Modeling of the Head

The head model of the study consists of the skull, CSF, and brain. Upon consideration of similar studies discussed before and with consideration of simulation time, it is decided that some parts of the head can be omitted from the FE model. The severity indices decided to be used in this study are all based on the rigid motions of the head; therefore, detailed or rather insignificant parts of the head are selected to not be added to the FE model. The omitted parts are the skin, jaw, nose, and different membranes between the skull and the brain. Also, the whole brain is constructed as a whole instead of the cerebellum and cerebrum, which contain white matter and gray matter, and the skull is constructed as only one bone structure instead of the facial bone and cranium. Because the validation of the human head FEM is conducted with no neck present in the model, the neck modeling is handled separately in this study.

3.1.1.1 Geometric Modeling of Skull

The skull and brain models are obtained from the GrabCAD database, a free CAD (computer-aided design) library. Geometric modeling is conducted by Hypermesh software (Altair Engineering Inc.). For the skull model, the first step was removing the mandible and considerably ineffective details from the surface model, such as details on teeth, the zygomatic arch, and the nasal area, as shown in Figure 3.1.

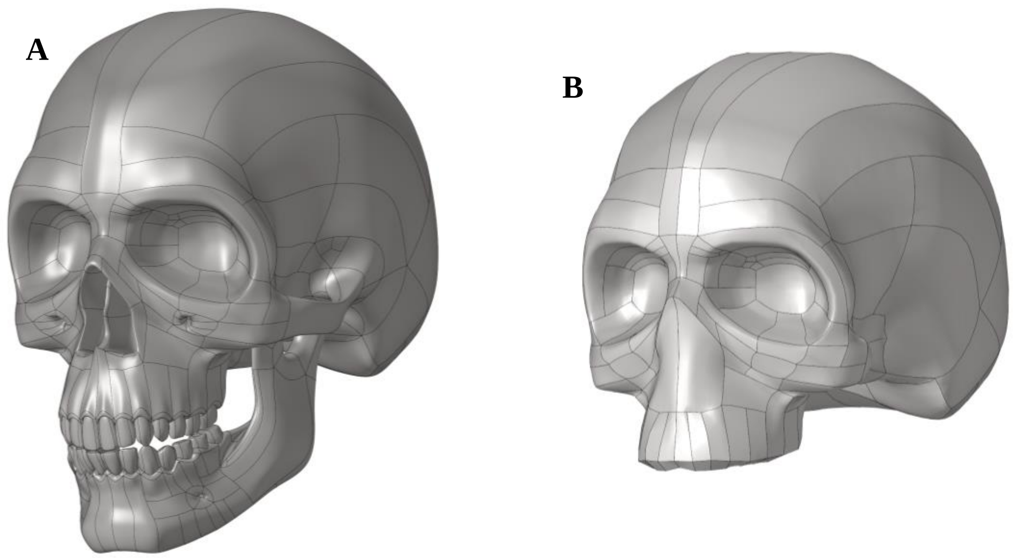

Figure 3.1. Surface Model of Skull A) Original Model B) Edited for Simplicity

After acquiring the adequate shape of the skull, the next step is altering the size of the skull based on Nahum's experiment 37 [14]. The modeled human head is validated based on Nahum's experimental data; therefore, it is important to meet the geometry of the head as much as possible to acquire more fitting results. The dimensions of both the baseline from the experiment [14] and the model of ours are given in Table 3.1, and the points of measurements are shown in Figure 3.2.

Table 3.1 Comparison of Head Dimensions Between Experiment and FEM

	A(cm)	*B(cm)*	*C(cm)*	*D(cm)*	*E(cm)*	*F(cm)*	*G(cm)*	*H(cm)*
Experiment	14.5	16.7	19.2	13.6	22.3	56.0	37.2	35.5
FEM	14.6	17.3	19.2	12.6	N/A	55.7	N/A	30.5

A: Head Breadth (maximum above ears)

B: Head Length (inion to glabella)

C: Head Length (opisthocranion to glabella)

D: Head Height (tragion to top of head)

E: Head Height (gnathion to vertex)

F: Head Circumference (across forehead, over ears, maximum)

G: Head Midsagittal Arc Length (inion to glabella)

H: Head Coronal Arc Length (tragion to tragion)

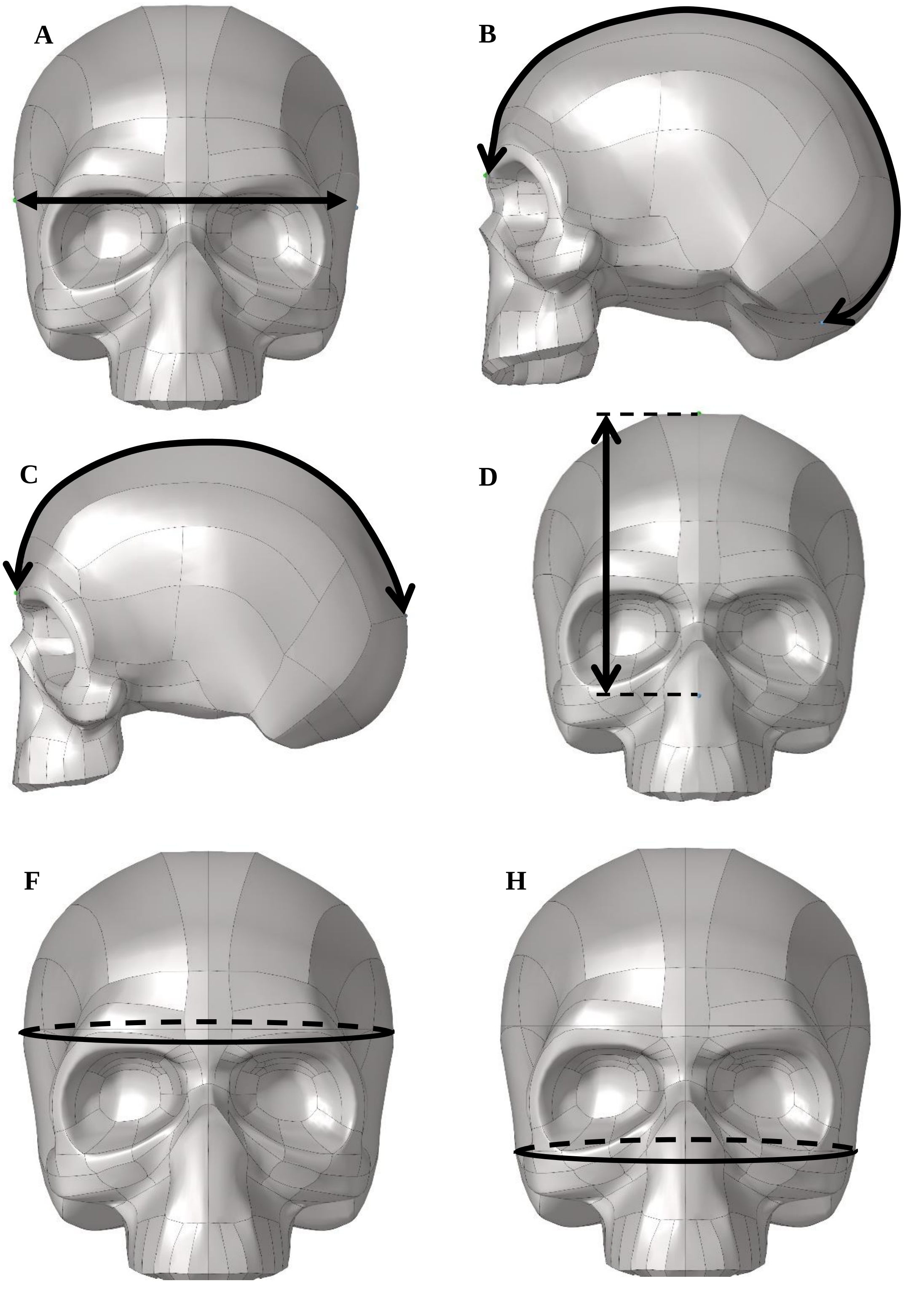

Figure 3.2. Head Size Measurement Points

Note that measurements E and G are not comparable due to the lack of jaw and skin in the model, respectively.

3.1.1.2 Geometric Modeling of the Brain

The geometric shape of the brain is set to be bulky to reduce the computational cost. In the literature, some studies worked with similar shapes [17], [19], [24], which lends credibility to this selection.

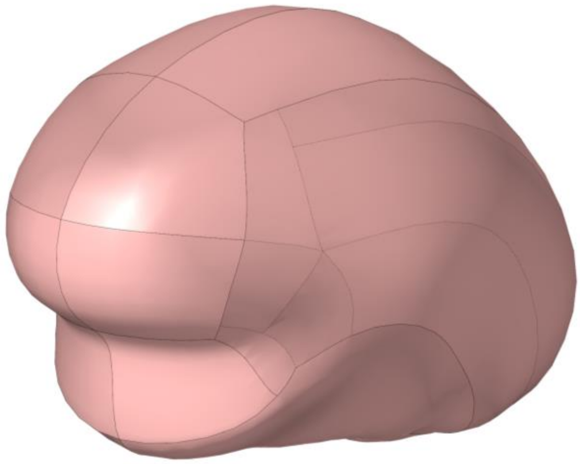

Figure 3.3. Shape of Brain Model

No data on brain size or mass is available from Nahum's experiment; therefore, the geometry of the brain is selected to be in accordance with the average female data presented in [25]. Lüders et al. submit the total volume of the brain as $1.32\ dm^3$, in the model the volume is set as $1.327\ dm^3$.

3.1.1.3 Geometric Modeling of the CSF

In the built model, only one component is used between the skull and the brain as the combination of all cerebrospinal fluid, blood vessels, brain tissues, and so on. The modeled component is named CSF (cerebrospinal fluid) because CSF is the main contributor among all layers between the skull and the brain when the dynamic behavior of the head and brain is the focus.

The surface model of the brain is duplicated and expanded to be the inner surface of the skull and the outer surface of the CSF; thus, all three parts of the head model are geometrically modeled. The thickness of the skull varies between 4.5 and 10 mm, which is in accordance with the dimensions shared by Ruan et al. [26]. Hence, the dimensions of the skull and brain are set, and the CSF thickness is settled at varying between 5 and 7 mm.

3.1.1.4 Finite Element Modeling of the Head

After the geometric modeling of the head is completed, the next step is the finite element modeling of the head. For finite element modeling, Hypermesh software (Altair Engineering Inc.) is used. For all components of the head, 2 mm first order tetrahedral elements are used, as shown in Figure 3.4 and Figure 3.5, and the details of the elements are given in Table 3.2.

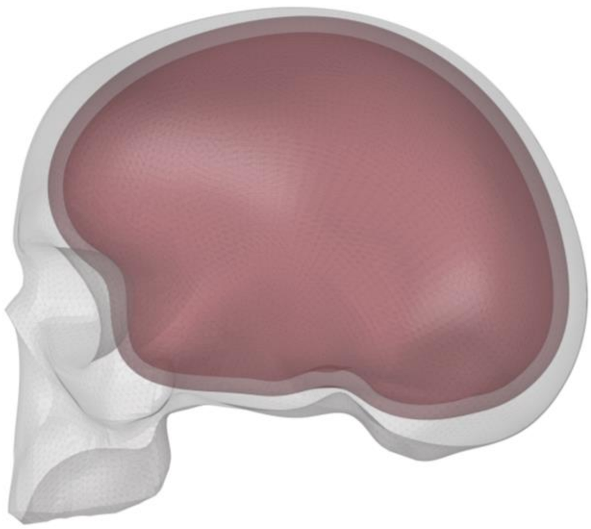

Figure 3.4. Head Finite Element Model

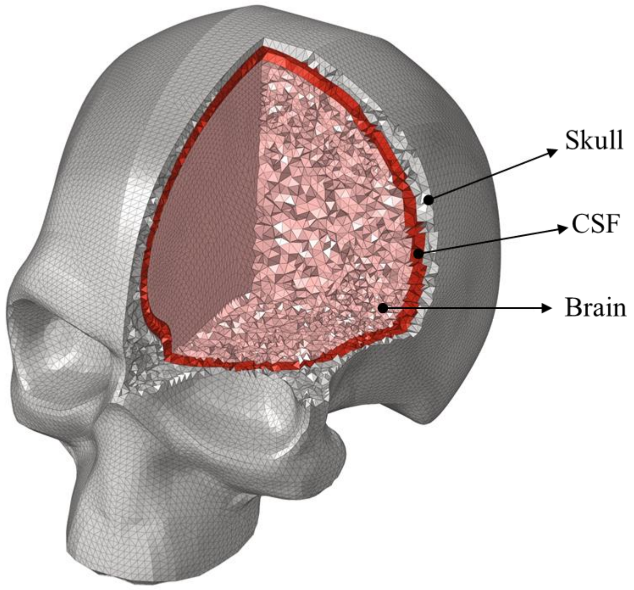

Figure 3.5. Head Finite Element Model Detail

For interface modeling between the skull and CSF and between the CSF and brain, there are three main options: first, surface-to-surface sliding with separation allowed; second, surface-to-surface sliding with no separation; and finally, surface-to-surface tied contact with neither sliding nor separation. In similar studies, all three of the aforementioned interface conditions are applied. [17]–[21]. The optimal interface modeling to use in a finite element simulation depends on the model detail, the scenario of the simulation, and the computational cost of the simulation. For the acquired model, a surface-to-surface tied contact interface is used, as in the studies of Cai et al. [17] and Horgan et al. [19]. Surface-to-surface tied contact suits the model at hand because the CSF of the human head is pressurized in reality, which results in preload between surfaces and causes a condition where two surfaces do not separate. Also, the CSF is modeled slightly thicker than usual, which gives a sliding motion effect between the brain and the skull even when the two sides of the CSF are tied to the brain and the skull.

Table 3.2 Mesh Properties of Head FEM

Component	*Element Type*	*Element Size (mm)*	*Number of Elements*	*Component Volume* (mm^3)
Skull	Linear Tetrahedral	2	509685	1.327×10^6
CSF	Linear Tetrahedral	2	121725	3.596×10^5
Brain	Linear Tetrahedral	2	297202	8.077×10^5

Material properties used for head components are in accordance with similar studies. Most of these studies have taken the brain as a viscoelastic material with nearly equal properties and the bone components as linear elastic, near rigid. Material selection of CSF varies across similar models; while some studies accepted CSF as a viscoelastic material [17], [18], others took CSF as a linear elastic material with a high Poisson's ratio and a low modulus of elasticity [21]. For the model at hand, CSF is modeled as a linear elastic material with a high Poisson's ratio and a low modulus of elasticity. The selection of such material properties gives the CSF a fluid-like, near-incompressible behavior, which is in line with the true nature of the CSF. The material properties of the skull, CSF, and brain are given in Table 3.3. and Table 3.4. The material properties for all three components are acquired from the study of Tse et al. [21]. The material properties of the brain are untouched; however, the material properties of the skull and the CSF are altered in order to meet the required pressure results for the model validation.

Table 3.3 Material Properties of Skull and CSF

Component	*Density* (kg/mm^3)	*Young's Modulus* (MPa)	*Poisson's Ratio*
Skull	2.5×10^{-6}	8000	0.21
CSF	1.04×10^{-6}	1	0.45

Brain material is selected as viscoelastic with a Maxwell-Kelvin formulation of [21]:

$$G(t) = G_\infty + \sum_i G_i e^{-\beta_i t} \qquad \text{Eq. 3-1}$$

In formula above, G_∞, G_i, β_i and t are the long-time shear modulus, the shear modulus, the time decay constant, and the time, respectively.

Table 3.4 Material Properties of Brain

Component	*Density* (kg/mm^3)	*Bulk Modulus* (MPa)	G_∞ (MPa)	G_1 (MPa)	β_1 (s^{-1})
Brain	1.04×10^{-6}	2190	0.21	0.36	35

3.1.1.5 Validation of Head Model

For the validation of the head FE model, Nahum's experiment on subject 37 [14] is used, like the studies mentioned before. The simulation is prepared for model validation of the head based on experimental data. In the experiment, an impactor with padding on the contact end is used to hit the cadaver's head at a 45-degree angle from the Frankfort anatomical plane, and the following test data are acquired: impact force, head acceleration, and intracranial pressure data from the locations shown in Figure 2.6. To use the experiment for validation, it is required to create an impactor as described in the studies. The information on the impactor is given as follows: with a 5.59 kg mass and a pad on the contact surface, and its velocity is said to be 9.94 m/s. Since Nahum does not give the geometrical information of the impactor, the information from the study of Tse et al. [21] is used. An impactor and padding with a diameter of 154 mm, and thicknesses of 45 and 40 mm, respectively, are used.

Nahum provided the force-time plot of the impactor contact; the resultant behavior of the head is due to this impact. To ensure that the simulation replicates the same impact on the head, the impactor and padding material properties are selected as given in Table 3.5, and the initial velocities of the impactor and padding are set at 6.5 m/s. The impactor and the head are shown in Figure 3.6.

Table 3.5 Material Properties of Impactor and Padding

Component	*Density* (kg/mm^3)	*Young's Modulus* (MPa)	*Poisson's Ratio*	*Mass* (kg)
Impactor	6.54×10^{-6}	85	0.1	5.96
Padding	1×10^{-6}	4	0.3	0.82

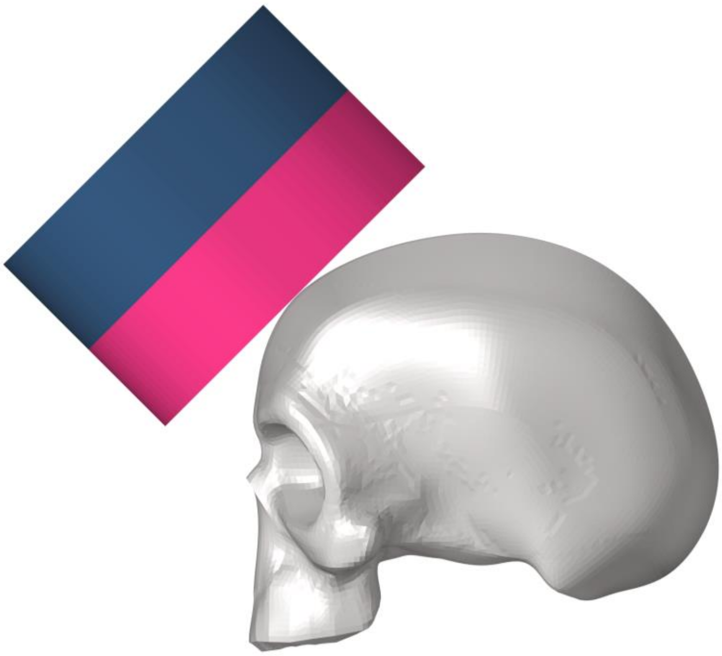

Figure 3.6. Impactor and Head Model

The simulation of impact is run by Radioss (Altair Engineering Inc.), an explicit finite element solver. The input force-time data shows that the input of the simulation is in accordance with the experiment. The head acceleration peak value states that the inertial properties of the head model are on point, as shown in Table 3.6. Pressure readings at different locations of the model show that the material properties and overall dynamic behavior of the model are valid. In Table 3.7, comparison of pressure values between the experiment, the average of literature [17]–[21], and the simulation at hand is shared. In simulation, for each pressure reading location, more than one element is selected to have more reliable data. The maximum, minimum, and average pressure readings for the selected elements are given in both Table 3.7 and figures from Figure 3.8 to Figure 3.13. The impact force on the head is shown in Figure 3.7, which shows that the impact on the head is in accordance with the experimental data. The linear resultant acceleration of the head is shown in Figure 3.8 displays the linear resultant acceleration of the head and demonstrates how the modeled head's inertial values are agree with the experiment. From Figure 3.9 to Figure 3.13, pressure readings from five different locations are shown: frontal, parietal, occipital 1, occipital 2, and posterior fossa. The figures show the dynamic accuracy of the modeled FE model.

Table 3.6 Comparison of Input Force and Head Acceleration of Simulation

	Peak Input Force (N)	*Peak Resultant Head Acceleration* (m/s^2)
Experiment	7900	2000
Simulation	7584	1937

Table 3.7 Comparison of Pressure Results of Simulation

	Frontal P. (kPa)	*Parietal P.* (kPa)	*Occipital P. #1* (kPa)	*Occipital P. #2* (kPa)	*Posterior Fossa P.* (kPa)
Experiment	141.2	73.6	−45.5	−48.4	−60.3
Literature (Average)	153	80	−59	−57	−69
Sim. Max.	154.28	84.50	−91.70	−36.39	−54.75
Sim. Min	133.06	75.12	−103.05	−44.73	−75.83
Sim. Ave.	143.67	79.81	−97.38	−40.56	−64.79

In the table above, P. stands for Pressure.

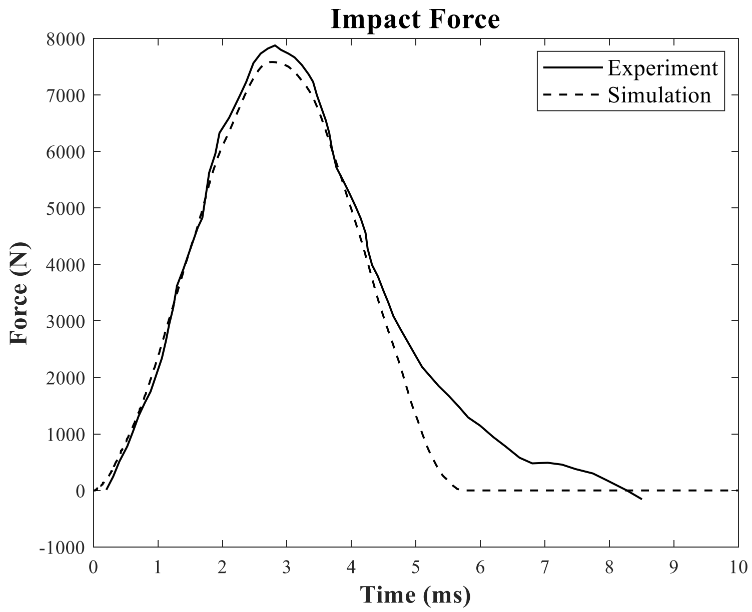

Figure 3.7. Impact Force Time History on Head

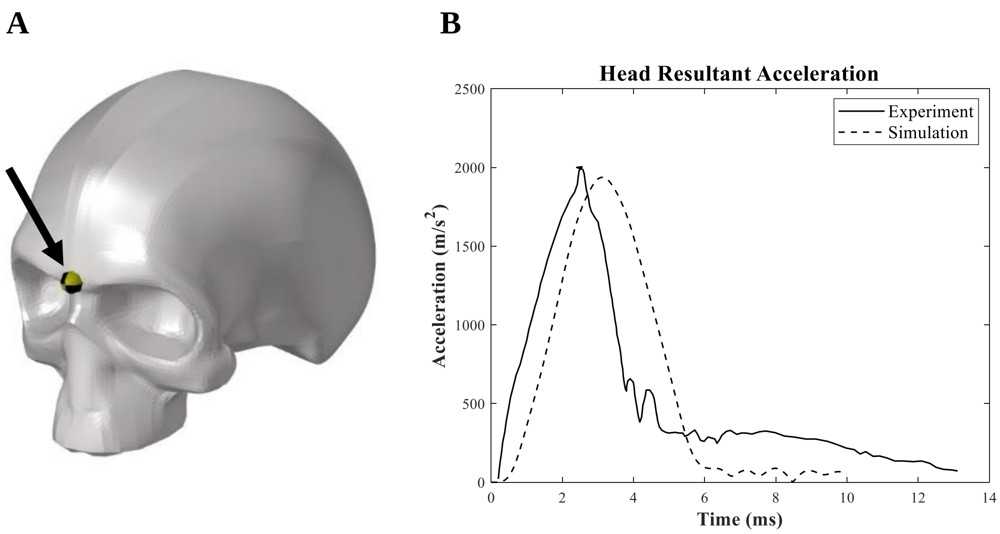

Figure 3.8. Resultant Head Acceleration Time History A) Location of Acceleration Reading B) Comparison of Acceleration Data

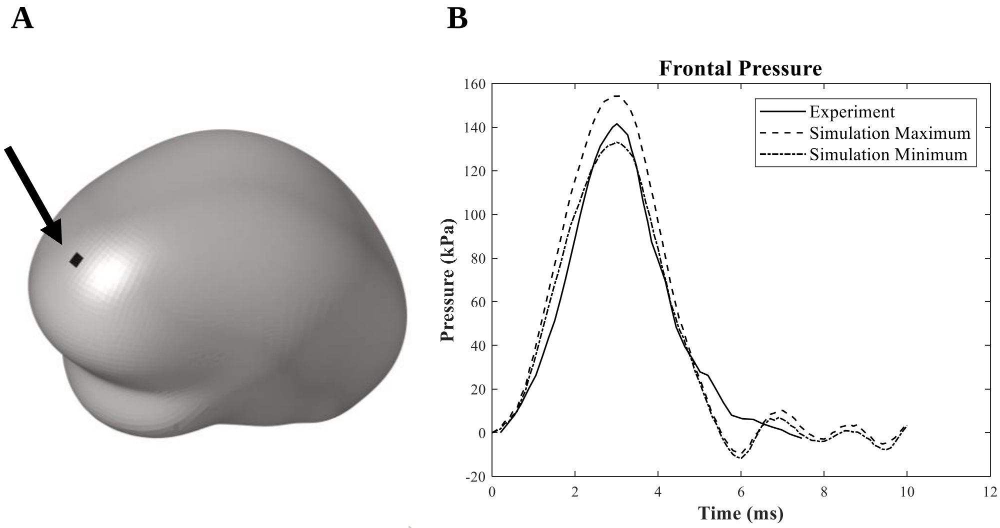

Figure 3.9. Frontal Pressure Resultant Time History A) Location of Pressure Reading on CSF B) Comparison of Pressure Data

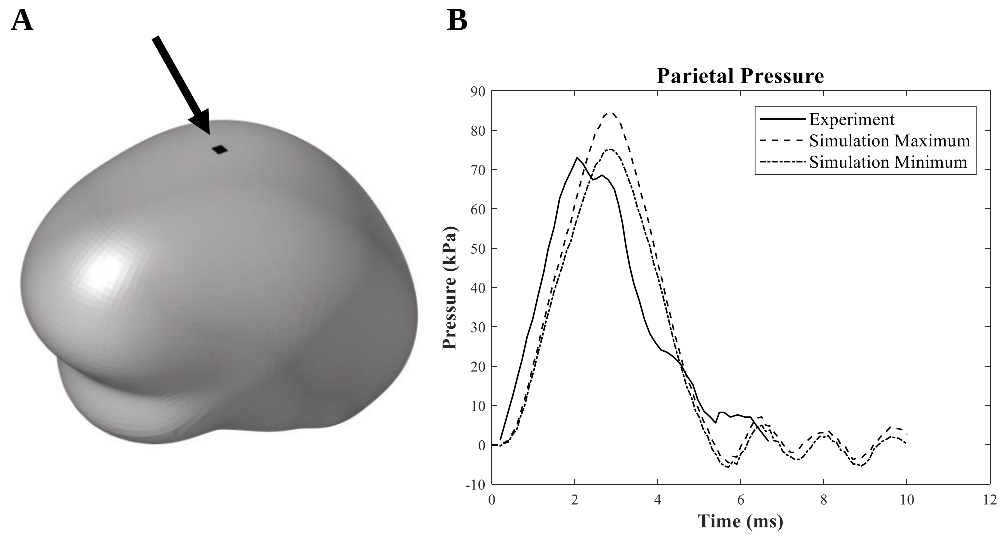

Figure 3.10. Parietal Pressure Resultant Time History A) Location of Pressure Reading on CSF B) Comparison of Pressure Data

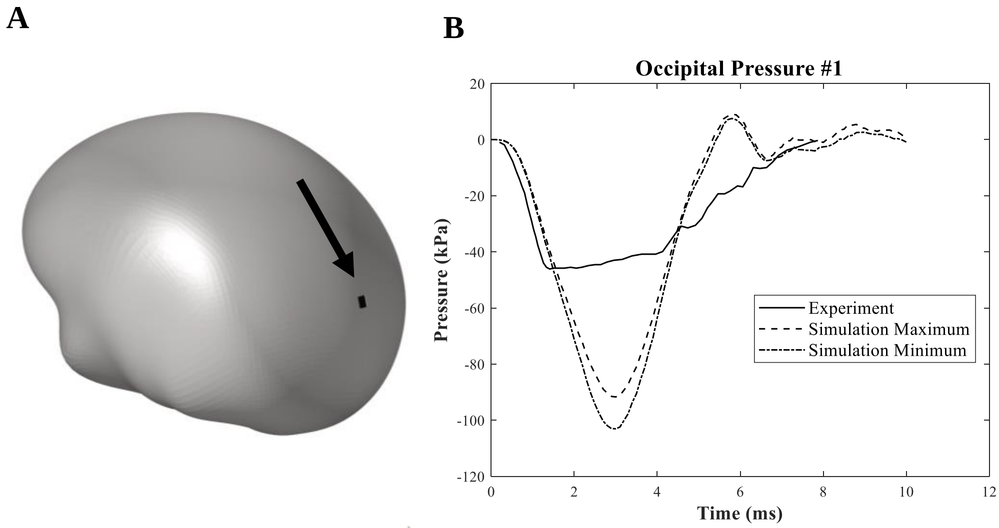

Figure 3.11. Occipital 1 Pressure Resultant Time History A) Location of Pressure Reading on CSF B) Comparison of Pressure Data

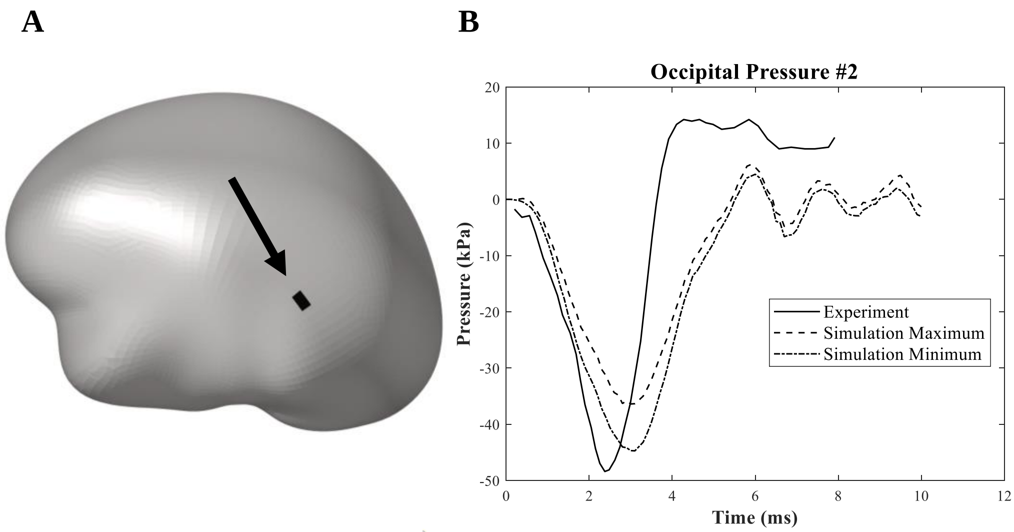

Figure 3.12. Occipital 2 Pressure Resultant Time History A) Location of Pressure Reading on CSF B) Comparison of Pressure Data

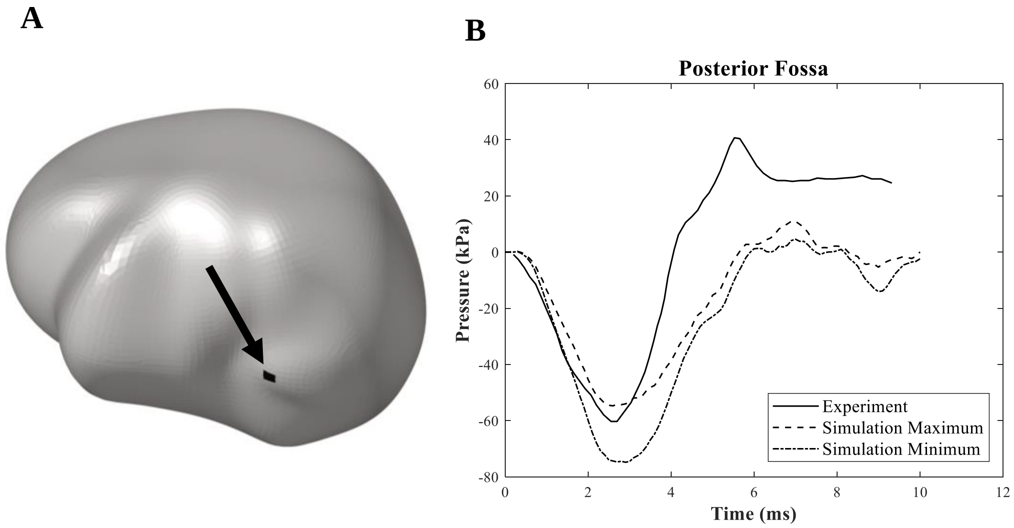

Figure 3.13. Posterior Fossa Pressure Resultant Time History A) Location of Pressure Reading on CSF B) Comparison of Pressure Data

3.1.2 Modeling of Neck

Modeling of the neck was not required in the head model validation part because it is assumed that the behavior of the head would not change in a short time of impact [18], [21], and the mechanical properties of a cadaver neck would make no significant difference to the results. However, under the impact of a hook punch, it is required to model the head with appropriate boundary conditions to acquire more reliable results.

The human neck behaves as both spring and damper in six degrees of freedom, and the stiffness value of the neck changes drastically based on the relaxation of the muscles. Dirisala et al. used 1-D linear dampers and springs in their simulation and showed that the neck model consisting of 1-D linear dampers and springs is good enough for simulations under direct loads, such as straight punches [27], as shown in Figure 3.14. Nine springs and nine dampers are placed under the skull, resembling the circumference of a neck. Approximately 80 mm of diameter is given to the neck shape, and all 1-D elements are connected to the nearest node on the skull at one end and fixed at the other end. The bottom of the neck is level with the horizontal plane, and the length of 1-D elements varies between 75 and 90 mm. However, the study at hand requires more than 1-D elements to accurately represent the reaction of the head under torsional impact, which would be caused by a hook punch, for instance.

In addition to the linear 1-D spring/damper element method, torsional stability is needed for the head. Farmer et al. shared human neck bending and torsional stiffness plots in their study [28]. The stiffness values are based on different human head dummies for crash tests and finite element models. Since the study at hand is a simulation of a boxing event, it can be assumed that the boxer who gets hit on the head flexes his or her neck before the punch lands as an immediate reflex. Therefore, taking the stiffer values for neck modeling from the literature is more realistic than assuming a soft neck muscle.

Based on the information gathered from the literature, the neck modeling is executed with linear damping and stiffness values extracted from [27] and the torsional stiffness values of DUMMY III crash dummies from [28] and [29].

The torsional spring added model is shown in Figure 3.15. In the final neck modeling, the 18 axial spring carries the same properties. Also, the axial springs are free in all directions except axial translation, whereas the torsional spring is free in all directions except torsional. All 19 spring elements are fixed at both ends; one end is a fixed boundary condition for the head, while the other end is fixed to the skull. The total mass of all 19 elements is 0.95 kg, the upper neck mass of LUSN (Loughborough University Surrogate Neck), as tabled in [28].

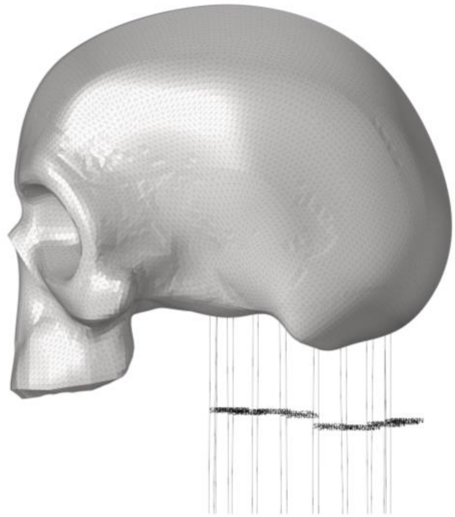

Figure 3.14. Neck Modeling – 1-D Spring Elements

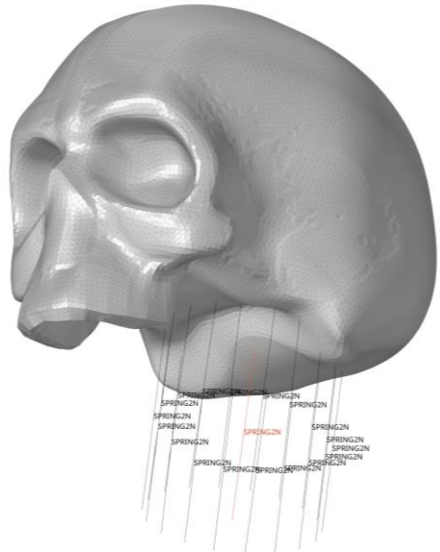

Figure 3.15. Neck Modeling with Torsional Spring

Table 3.8 Material Properties of Neck Modeling

	Axial Stiffness (N/mm)	*Torsional Stiffness* (Nmm/rad)	*Mass* (kg)
Neck	1.8×10^{6}	2.5×10^{4}	0.95

3.1.3 Modeling of Protective Gears

The goal of the study is to reduce the risk of concussion in boxing. The concussion risk is caused by the hook punch delivered on the head, and the proposed solution is to place a tuned vibration absorber on the headgear. Headgear and glove models are required.

3.1.3.1 Modeling of Headgear

There is not simply one protective headgear design in boxing; the type of headgear changes based on how open the face is. Even though the design of headgear changes, their primary objective is the same, and they all meet some regulations set by IBA, formerly known as AIBA.

An open-face headgear model is acquired from Free3D, an Internet 3D model database for design and manufacturing purposes, as shown in Figure 3.16. In boxing, headgear is needed to fit on the head with no slip; for the sake of this condition, the usage of Velcro straps with a minimum of 2-3 cm width is pinned down by the IBA [23]. To meet the fit-on-head condition, the obtained model is resized to fit as much as possible on the surface of the head. The skull and headgear are given a tied interface at six locations, three on each side, as shown in Figure 3.17, which prevents slipping between the skull and the headgear as ordered by IBA.

The material properties of the headgear were acquired from the studies by Razaghi et al. [30] and Fan [31]. In their study, Razaghi et al. studied more than one foam property for boxing headgear, and Fan shared a stress-strain curve of a headgear foam specimen. In the study at hand, for modulus of elasticity and Poisson’s ratio, average values from the aforementioned studies are used. The weight of the protective headgear is to a maximum of 450 grams in the IBA Technical and Competition Rules [23]. The headgear in our model is set to 360 grams in order to have some weight budget to be used in TVA implementation. The weight budget in our study is set to be 100 grams for TVA mass. The finite element model of headgear is built with linear tetrahedral elements; details are given in Table 3.9 and Table 3.10.

Figure 3.16. Headgear Model

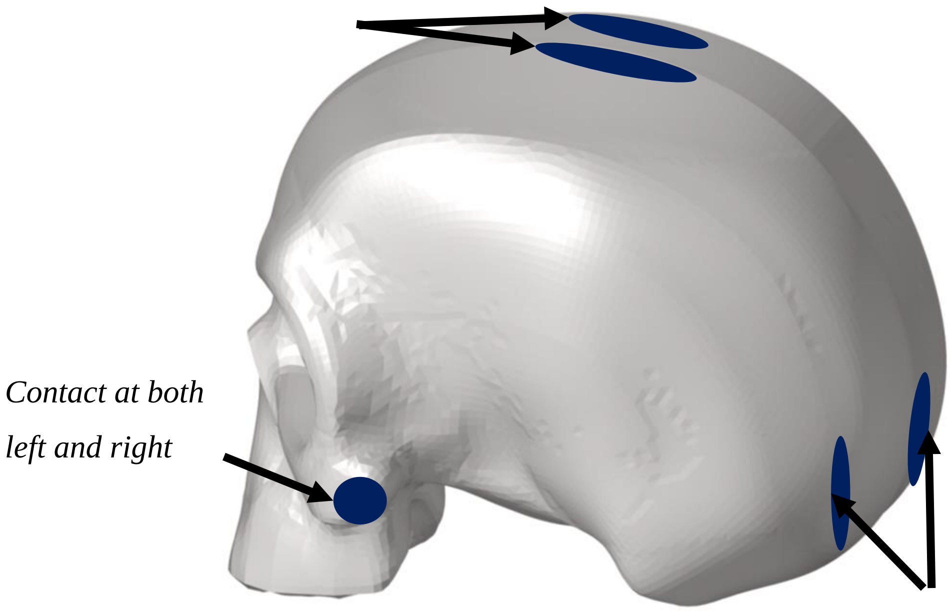

Figure 3.17. Skull and Headgear Contact Locations

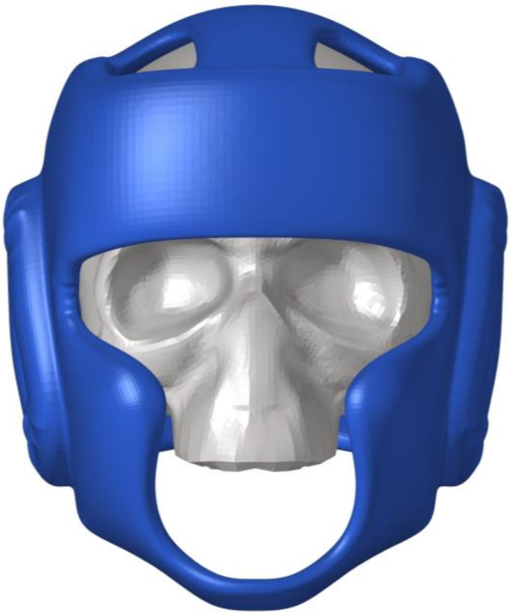

Figure 3.18. Headgear and Skull

Table 3.9 Material Properties of Protective Headgear

Component	*Density* (kg/mm^3)	*Young's Modulus* (MPa)	*Poisson's Ratio*	*Mass* (kg)
Headgear	3×10^{-7}	5	0.4	0.360

Table 3.10 Mesh Properties of Protective Headgear

Component	*Element Type*	*Element Size (mm)*	*Number of Elements*	*Component Volume* (mm^3)
Headgear	Linear Tetrahedral	2	676152	1.199×10^6

3.1.3.2 Modeling of Glove

The geometric design and weight of boxing gloves are fixed and set in IBA Technical and Competition Rules [23]. However, in our study, the aim is to simulate the punch impact on the head, so the results needed to be accurate are on the head side of the impact, not the hand side. Therefore, a simpler design of glove and hand is applicable for the study at hand, as long as the load condition on the head is realistic.

The dimensions and geometric design of the glove and hand from the study of Fan [31] are used, as shown in Figure 3.19. The material properties of the glove are selected to be the same as those of the headgear, which is in accordance with the data shared by Fan [31]. For the material properties of the hand, the initial values are selected to be the same as those of the skull, and then the density of the hand is altered to fit the total effective mass of the glove and hand data shared by Perkins et al. [32] Material and mesh properties of the hand and glove parts are given in Table 3.11 and Table 3.12. Between the glove and the hand, a surface-to-surface tied interface is defined to prevent sliding between the two components.

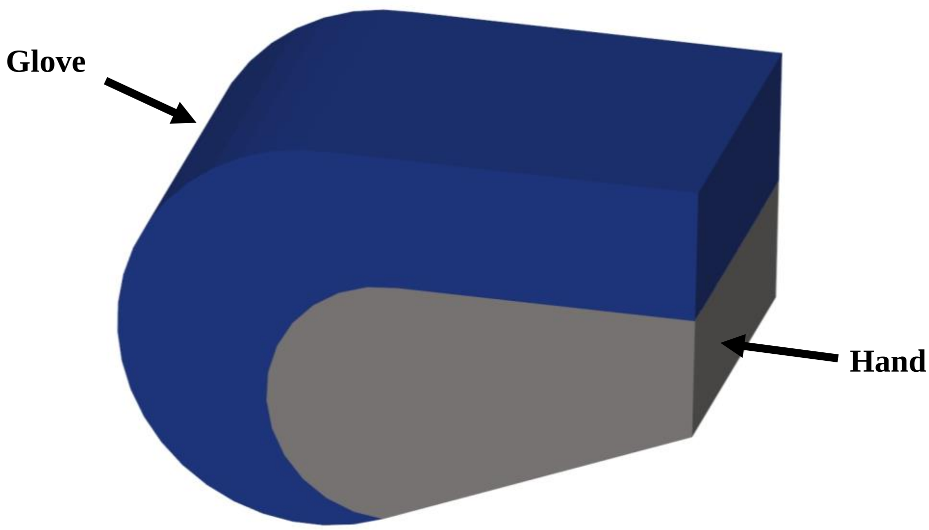

Figure 3.19. Glove and Hand Models

Table 3.11 Material Properties of the Glove and the Hand

Component	*Density* (kg/mm^3)	*Young's Modulus* (MPa)	*Poisson's Ratio*	*Mass* (kg)
Glove	3×10^{-7}	5	0.4	0.431
Hand	2×10^{-6}	8000	0.2	2.057

Table 3.12 Mesh Properties of the Glove and the Hand

Component	*Element Type*	*Element Size (mm)*	*Number of Elements*	*Component Volume* (mm^3)
Glove	Linear Tetrahedral	10	11814	1.41×10^6
Hand	Linear Tetrahedral	10	6290	1.028×10^6

3.2 Damping Defining for the Model

It was previously stated that the Rayleigh damping method was used in this study. Rayleigh damping coefficients are the multipliers of the mass and stiffness matrices of the model, and the resulting damping of the model is dependent on the frequency. In order to define a damping to model, the natural frequencies of the head need to be known.

For identification of the natural frequencies of the model, modal frequency analysis is conducted by Optistruct finite element solver (Altair Engineering Inc.).

3.2.1 Modal Frequency Analysis of Head Model for Natural Frequency Identification

The natural frequencies of the head model are obtained by normal modes analysis by Optistruct (Altair Engineering Inc.). The head model used in this model consists of the neck, skull, CSF, and brain. Headgear is not included in this study because the aim is to obtain the resonant frequencies and corresponding mode shapes of the head. The resulting mode shapes and their explanations are tabulated in Table 3.13.

Table 3.13 Mode Shapes and Corresponding Frequencies of the Head

Mode #	*Mode Description*	*Frequency (Hz)*
1	Torsional All parts move together	6.45
2	Translational All parts move together	11.10
3	Torsional All parts move together	18.36
4	Bending in Lateral Axis Brain moves with higher magnitude	297.96
5	Bending in Fore-and-Aft Axis Brain moves oppositely than other parts	349.43
6	Torsional Brain moves oppositely than other parts	448.51
7	Bending in Lateral Axis Brain moves oppositely than other parts	468.72
8	Too complex to identify	585.38
9	Too complex to identify	617.53
10	Too complex to identify	679.16
11	Too complex to identify	785.81
12	Too complex to identify	938.89
13	Too complex to identify	966.94
14	Too complex to identify	992.05

From Table 3.13, it is observed that the first natural frequency of the head model is at $6.45\ Hz$. To tune Rayleigh damping parameters for the model, the frequency response function (FRF) plot is also needed. For the FRF results, modal frequency analysis is run by Optistruct (Altair Engineering Inc.). In the modal analysis, a unit loading with a frequency changing from 0.01 Hz up to 1000 Hz with increments of 0.01 Hz is used. The input is given on the sphenoid bone location in resultant of three axes, labeled 1 in Figure 3.20. The displacement measurements are obtained in three different locations: the same point where loading is applied, above the nasal bone location, labeled 2, and on the parietal bone location, labeled 3, as shown in Figure 3.20.

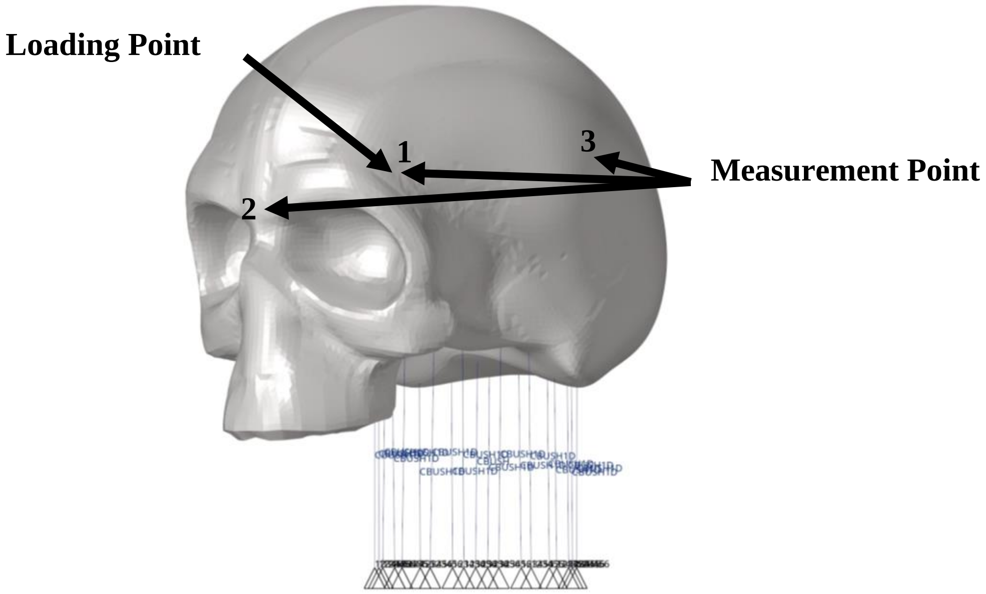

Figure 3.20. Modal Frequency Analysis Model

The response measurement points are chosen to be as far away as possible from the torsional spring axis in order to acquire higher peaks in resonant frequencies. The resulting frequency response plots are given in Figure 3.21 and Figure 3.22. Both figures display the FRF plots of three measurement points on top of each other, namely: nasal bone, parietal bone, and sphenoid bone, labeled as 2, 1, and 3, respectively, in Figure 3.20. Both figures show the response of all three locations in four directions: lateral, vertical, fore-and-aft, and total response. Lateral direction is the Y-axis, labeled A in Figure 3.21 and Figure 3.22; vertical direction is the Z-axis, labeled B in Figure 3.21 and Figure 3.22; fore-and-aft direction is the X-axis, labeled C in Figure 3.21 and Figure 3.22; directions are shown in Figure 2.2. The total response, labeled D in Figure 3.21 and Figure 3.22, is the cumulative response of a point in all three axes, with a formulation of $\sqrt{X^2+Y^2+Z^2}$.

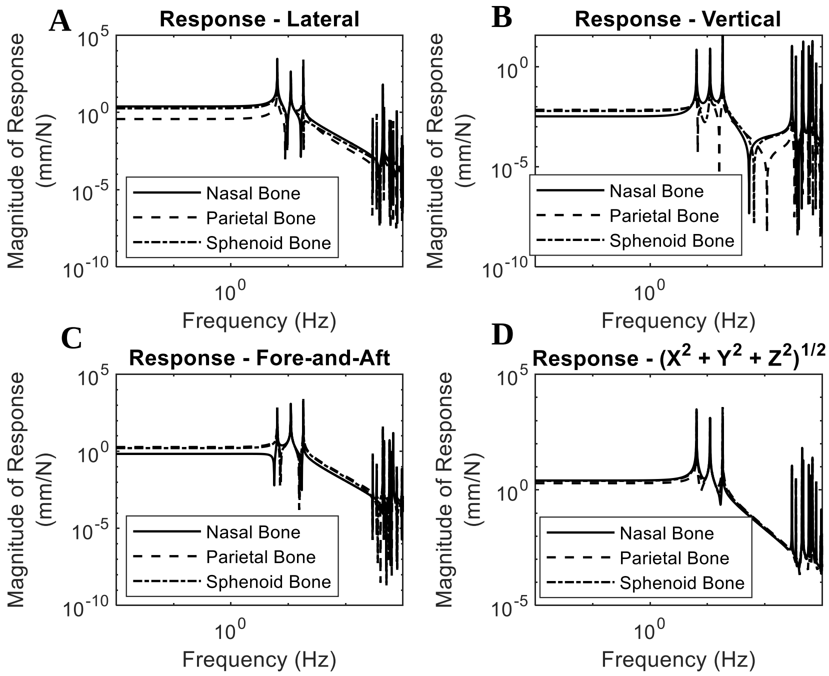

Figure 3.21. Modal Frequency Response Plots of the Head A) Lateral Direction B) Vertical Direction C) Fore-and-Aft Direction D) Total Response

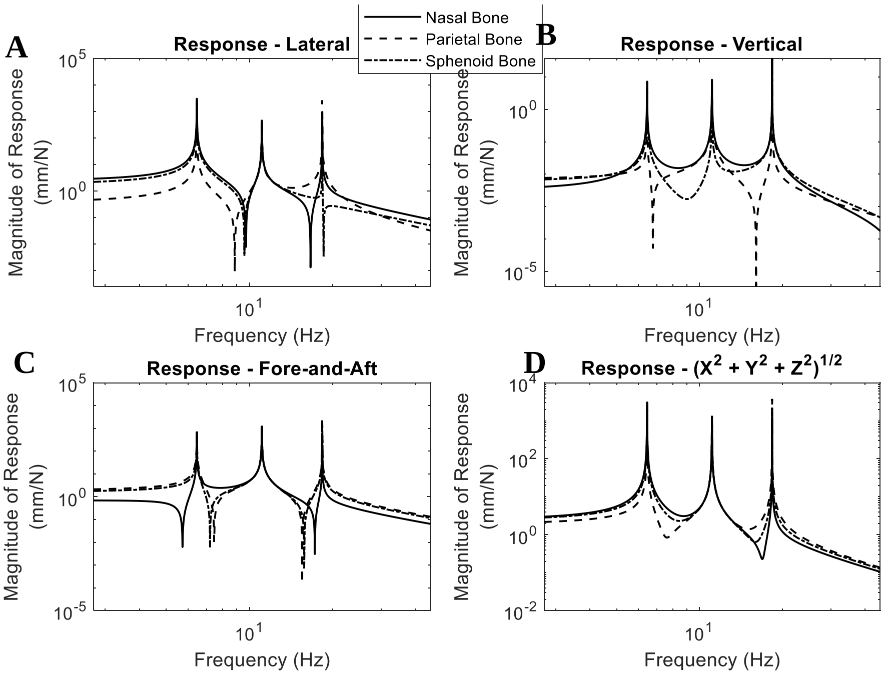

Figure 3.22. Modal Frequency Response of the Head – First 3 Modes A) Lateral Direction B) Vertical Direction C) Fore-and-Aft Direction D) Total Response

The first three natural frequencies of the head are close to each other between 6 and 20 Hz, and all the parts of the head move together. Starting in the 4th mode, the brain moves with a higher magnitude than other parts, and the mode shapes start to get hard to categorize.

The damping ratios of the human head was mentioned to be somewhere between 5% and 20%, according to studies conducted before [14], [22]. Hakansson et al. noted that the damping ratio of the head is decreasing with increasing frequency [22]; therefore, a steady-like damping ratio curve, which has approximately 5% damping ratios in the first three natural frequencies is selected.

In Eq. 2-5 the Rayleigh damping formulation was given as $\zeta = \frac{1}{2}\left(\frac{\alpha}{\omega} + \beta\omega\right)$. For the case at hand, the selected coefficients and the resultant damping plot are given in Table 3.14 and Figure 3.23 respectively.

Table 3.14 Rayleigh Damping Model Coefficients

-	Mass Matrix Coefficient (α)	Stiffness Matrix Coefficient (β)
	4	$1e-5$

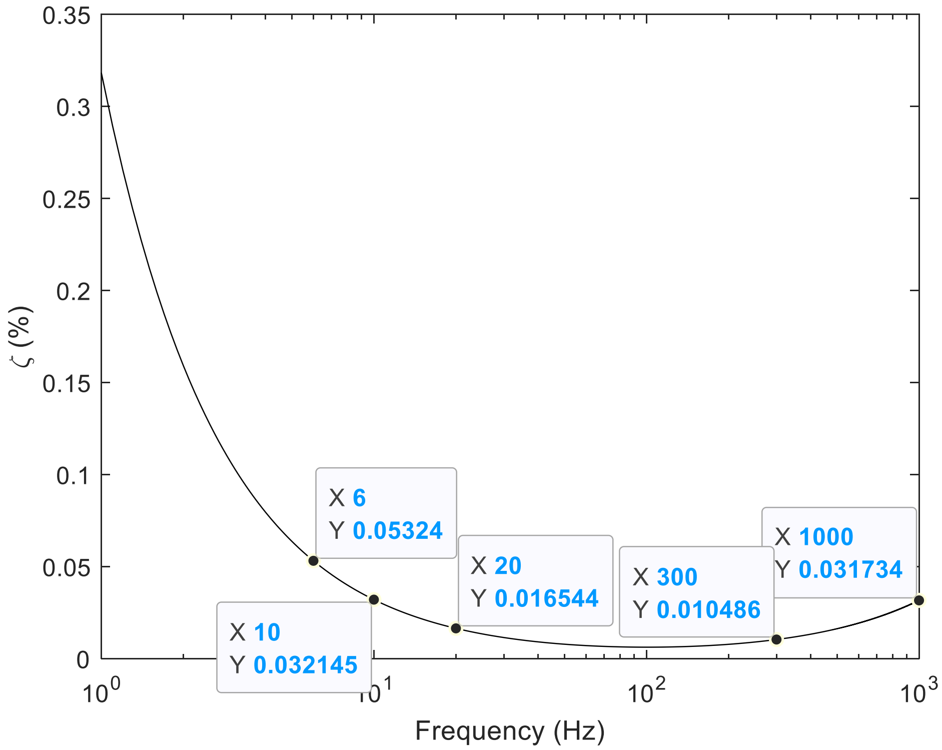

Figure 3.23. Rayleigh Damping Model Values

CHAPTER 4

SIMULATION OF HOOK PUNCH USING HEADGEAR WITH AND WITHOUT TUNED VIBRATION ABSORBER

The aim of this study is to reduce the risk of TBI for boxers. The solution generated for this problem is reducing the response level of the head at its most critical natural frequency, after the punch lands by implementing a TVA on the existing protective headgear. The most crucial motion of the head is decided to be the torsional movement around the neck, which is found to be at 6.08 Hz with headgear on, and the TVA modeling is done accordingly.

4.1 Tuned Vibration Absorber Working Principle

TVA is a single degree-of-freedom system consisting of mass and spring, with optional damper addition. TVA's working principle is to generate inertia to reduce the vibration levels of the protected structure. The protected structure in our study is the human head.

The vibration problem generally occurs at specific frequencies, at least one of the natural frequencies of the system. Modeling a TVA with a damped natural frequency to meet the main structure's high vibrational natural frequency is the first step. By matching the natural frequency of the main structure on its own, TVA absorbs the high vibrations and thus reduces the vibration levels in the main system.

The formulation of TVA adaptation on the headgear is given by the following equations:

The natural frequency for SDOF systems is formulated as follows:

$$\omega_n = \sqrt{\frac{k_{TVA}}{m_{TVA}}} \qquad \text{Eq. 4-1}$$

k_{TVA}: Stiffness of the TVA, m_{TVA}: Mass of the TVA

The damped natural frequency of the TVA is:

$$\omega_d = \omega_n\sqrt{1-\zeta^2} \qquad \text{Eq. 4-2}$$

ζ: Damping ratio of the TVA

The damping ratio of a SDOF system can be found by:

$$\zeta = \frac{c_{TVA}}{c_{crit}} \qquad \text{Eq. 4-3}$$

c_{TVA}: Damping of the TVA, c_{crit}: Critical damping of the TVA

The critical damping of a SDOF system is formulated as:

$$c_{crit} = 2\sqrt{k_{TVA}m_{TVA}} \qquad \text{Eq. 4-4}$$

By using the equations above, the formulation of TVA stiffness and damping for a given tuning frequency, TVA mass, and damping ratio is as follows:

$$k_{TVA} = \frac{\omega_d^2}{1-\zeta^2}m_{TVA} \qquad \text{Eq. 4-5}$$

$$c_{TVA} = 2\sqrt{k_{TVA}m_{TVA}}\zeta \qquad \text{Eq. 4-6}$$

A dummy SDOF system is built to better show the frequency response of a system changing with TVA implementation, as shown in Figure 4.1.

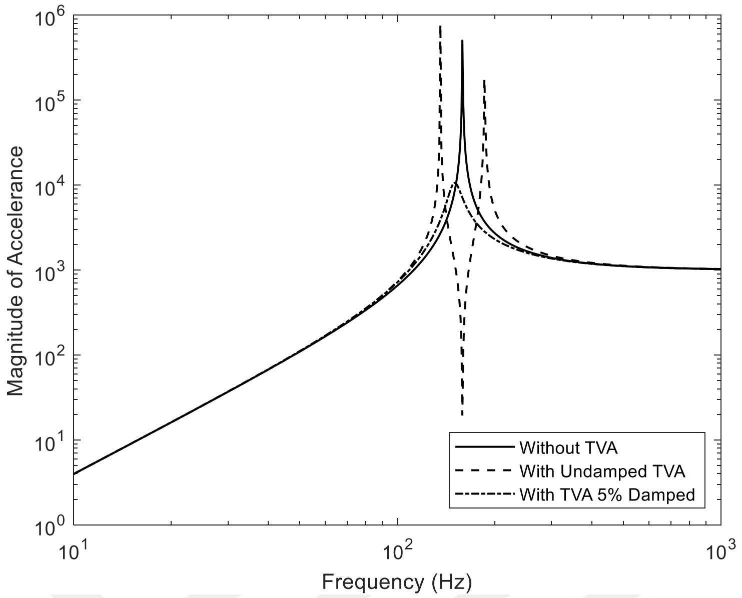

Figure 4.1. Example of TVA Effect on SDOF System

4.2 Tuned Vibration Absorber Implementation on the Headgear

TVA implementation on the existing protective headgear is a real-life challenge of this study. The idea is to install the TVA on off-the-shelf headgear without damaging it. Also, the TVA needs to be connected to the headgear as rigidly as possible to make it work as intended.

The concept of TVA in this study is a component that is fixed at both ends to the headgear with a mass in the center. The mass is connected to both ends of the TVA by means of springs and dampers. The TVA implementation on the headgear is shown in Figure 4.2 and Figure 4.3.

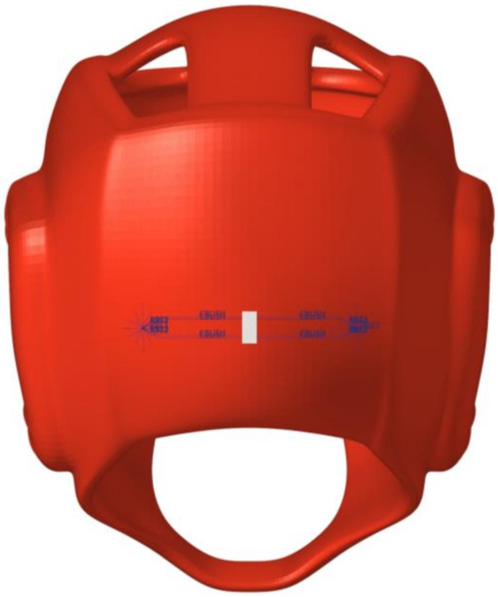

Figure 4.2. TVA Installation on the Headgear

In Figure 4.3, the real-life implementation of the TVA in finite element modeling is shown. On both sides of the headgear, an RBE3 element is created, which translates the average motion of its 25 base nodes up to a single node. From the end point of RBE3 elements, RBE2 elements are created, which translate the motion of their base nodes rigidly. Using RBE3 and RBE2 elements represents the end points of the TVA fixed on the headgear.

In the center of the TVA, a mass is created by using solid elements. The volume of the TVA mass is $790.5\,mm^3$. The material density is variable according to the required weight. The TVA mass part is connected to both ends of the TVA by using four 1-D spring elements on each side. Using four spring elements instead of one creates resistance to the rotating movements of the mass, which represents a guided mass element in real-life applications. A frictionless sliding interface condition is set between the headgear and TVA mass parts.

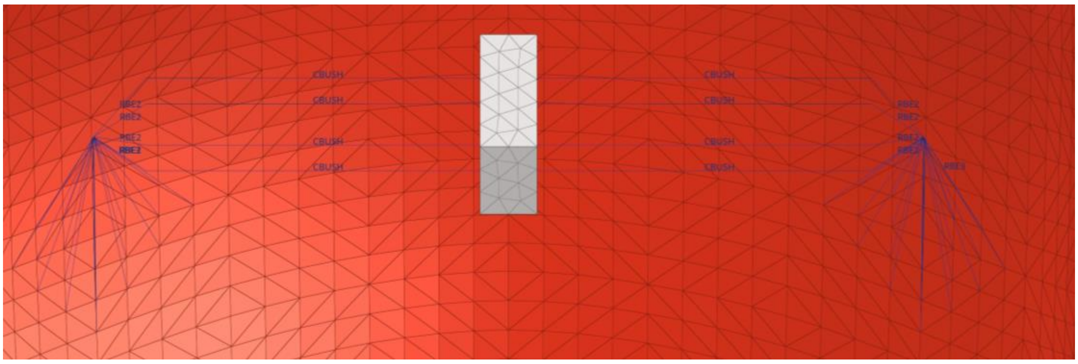

Figure 4.3. TVA Installation on the Headgear – Detailed

4.3 Modal Frequency Analysis of the Head Model for Tuning the TVA

The head model at hand is rather complicated, and TVA tuning is not possible without a trial-and-error process. TVA effectiveness is examined with two variables: the mass and damping ratio of the TVA. The modal frequency analysis method is used for this part of the study.

The damped natural frequency, ω_d from Eq. 4-2, of the TVA is set to be $6.08Hz$, which is the first natural frequency of the head model with headgear installed, and the parameter sweep review is conducted accordingly. An example response of the node on the nasal bone based on TVA implementation is given in Figure 4.4; the model used in this figure is Rayleigh-damped.

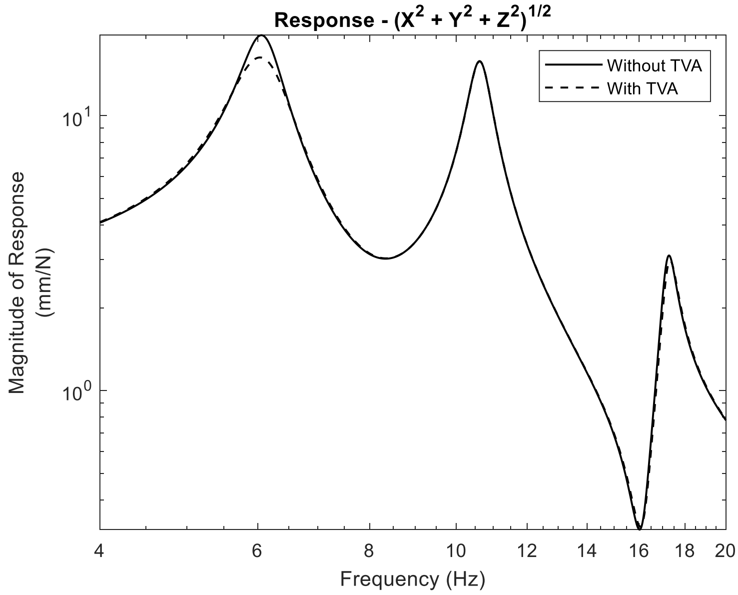

Figure 4.4. TVA Implementation Effect on Rayleigh Damped Model – Total Response

For the TVA tuning process, the first torsional mode of the head is selected in this study; therefore, selecting the foremost node from the rotation axis would give a higher response in TVA tuning. The nasal bone location, point 2 shown in Figure 3.20, is selected for the TVA tuning process. Among the four measurements, lateral, vertical, fore-and-aft, and total response, the lateral movement of the nasal bone is in accordance with the torsional movement of the head; therefore, the lateral direction is selected to be used in the TVA tuning process of this study.

Mass sweeping is conducted on the Rayleigh-damped model with a constant damping ratio of 5%. The peak values of different cases at tuning frequency are shown in Figure 4.5, in the figure the horizontal axis displays the TVA mass for different cases, and the vertical axis shows the peak lateral responses for corresponding case at tuning frequency.

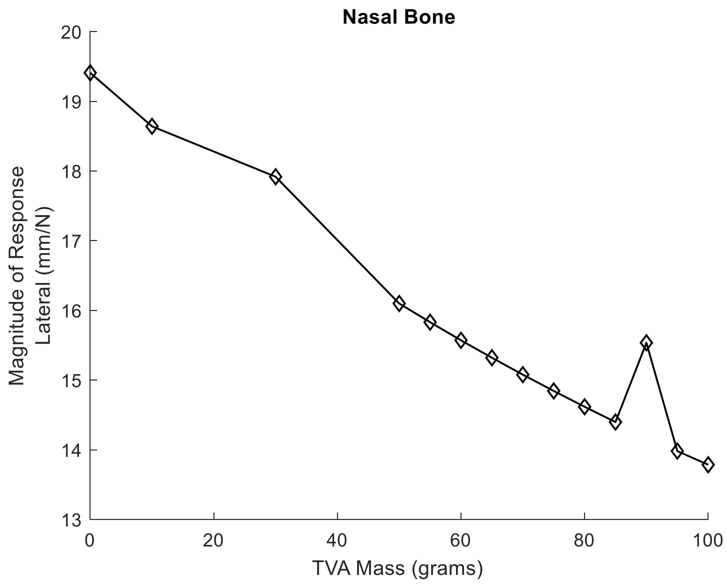

Figure 4.5. TVA Mass Sweep on Rayleigh Damped Model, TVA Damping 5%

The weight budget of TVA was set to 100 grams in 3.1.3.1, in Figure 4.5 it is observed that an increase in TVA mass decreases the response of the head except at 90 grams. For further modeling, 85 grams of TVA mass is selected.

After deciding the TVA mass of the system, the TVA damping sweep is the next step. It is observed that since the head model is already damped, high damping on TVA negatively affects the responses. Thus, a damping ratio sweep is performed between 0% and 10%, results are shown in Figure 4.6. In Figure 4.6, the horizontal axis shows the TVA damping ratio values for different cases, and the vertical axis display the lateral response of nasal bone at peak frequency. It is observed that the minimum response of the head model is acquired at 1% TVA damping in a Rayleigh-damped head model. Thus, the TVA parameters are set for the Rayleigh-damped model as 85 grams mass and 1% damping ratio.

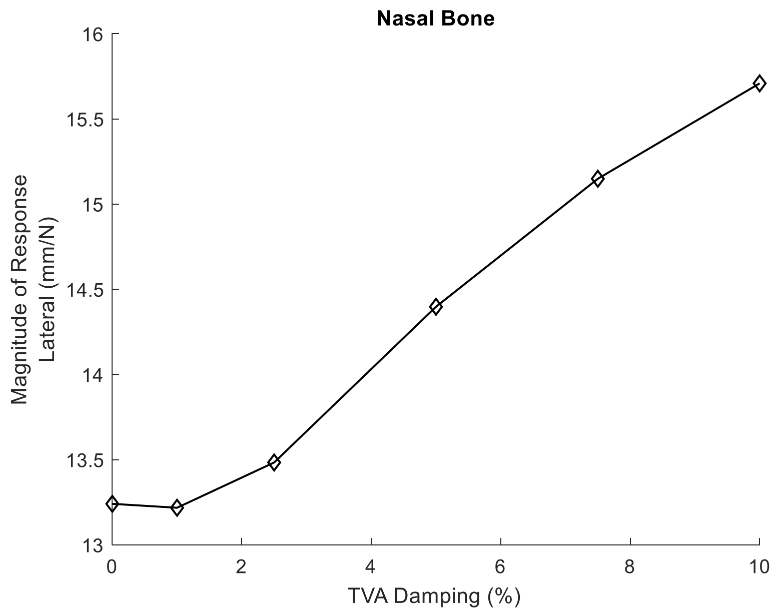

Figure 4.6. TVA Damping Sweep on Rayleigh Damped Model, TVA Mass 85 Grams

The TVA parameter sweep conducted for Rayleigh-damped model is repeated for the undamped model. It is expected to have different convergence in TVA parameters since the damping of the whole model changes considerably. The peak values of different cases at tuning frequency are shown in Figure 4.7, in the figure the horizontal axis displays the TVA mass for different cases, and the vertical axis shows the peak lateral responses for corresponding case at tuning frequency. TVA mass sweep is shown in with a constant damping ratio of 5%, it is observed that with the increase in TVA mass, the effectiveness of the TVA still rises; however, the maximum TVA mass is set to be 100 grams to prevent any unrealistic modeling. Therefore, the TVA mass for the undamped head model is selected as 100 grams.

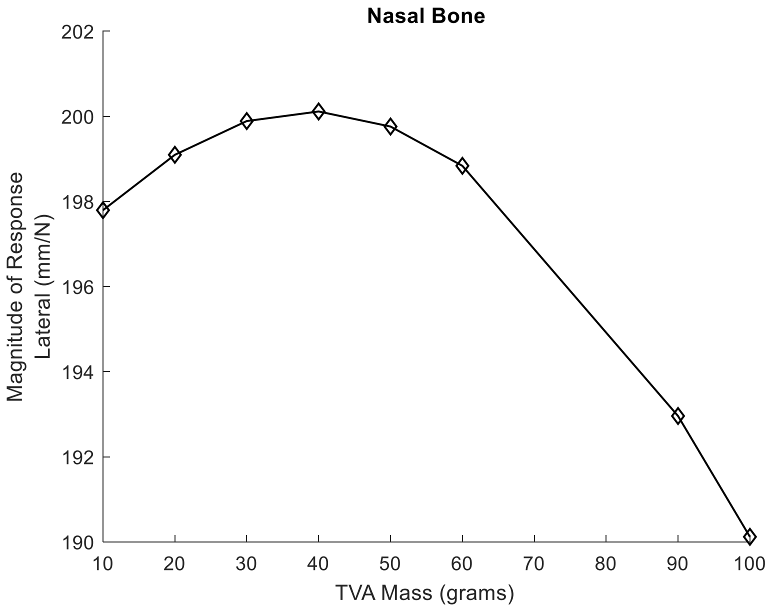

Figure 4.7. TVA Mass Sweep on Undamped Model, TVA Damping 5%

After setting the TVA mass for the undamped head model at 100 grams, the TVA damping ratio effect in response is investigated. The swept cases are shown in Figure 4.8, the horizontal axis shows the TVA damping ratio values for different cases, and the vertical axis display the lateral response of nasal bone at peak frequency. It is observed that 7.5% damping is the most effective in such a model, as shown in Figure 4.8. Thus, the TVA parameters are set for the undamped model as 100 grams mass and 7.5% damping ratio.

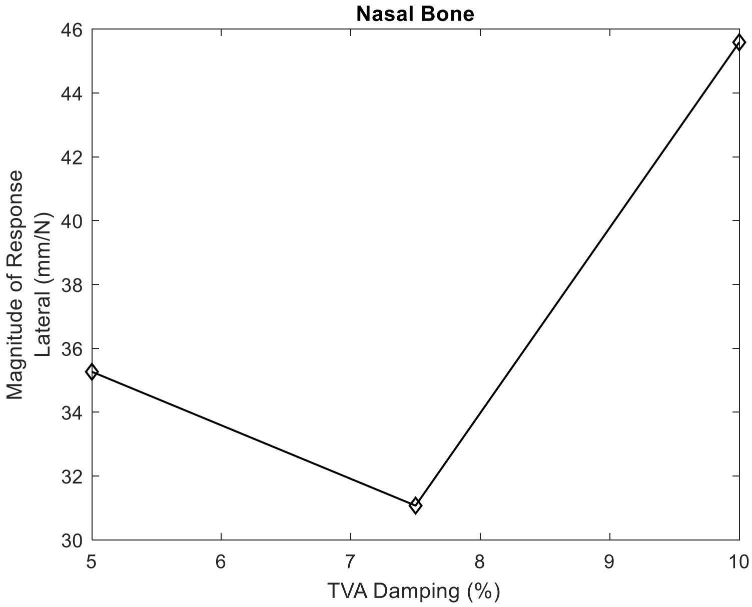

Figure 4.8. TVA Damping Sweep on Undamped Model, TVA Mass 100 Grams

The tuning process started with a selection of tuning frequency. After the tuning frequency is decided, the nasal bone location's lateral FRF peak values are selected to be the deciding factor in TVA parameter tuning. Later, a mass sweep of cases at 5% damping is performed, and the cases with the minimum peak response value are selected for both undamped and Rayleigh-damped models. After the mass of the TVA is set, the damping ratio sweeping is performed, and the minimum peak response cases are selected for damping ratios. The final TVA parameter sets for both Rayleigh-damped and undamped models are given in Table 4.1.

Table 4.1 Final TVA Parameters

Model	*Mass (grams)*	*Damping (%)*	*Tuning Frequency (Hz)*
Undamped Model	100	7.5	6.08
Rayleigh Damped Model	85	1	6.08

4.4 Simulation Details of Punch

The punch on the head is selected to be a hook punch due to its higher resultant angular motion on the head. The impact of the punch has three variables: the speed of the punch, the effective mass of the punch, and the impact location and vector of the punch. The speed and effective mass of the punch result in contact load and contact duration, which are the load inputs of the head. From the literature survey on the subject [31], [33], [34], the contact force and contact duration of the punch are selected to be around 3500 N and 10 ms respectively, which are obtained by giving the initial velocity of $6\ m/s$ to the punch. For the location and vector of the punch, the zygomatic bone and the head's lateral direction are selected, as shown in Figure 4.9, Figure 4.10, Figure 4.11, and Figure 4.12.

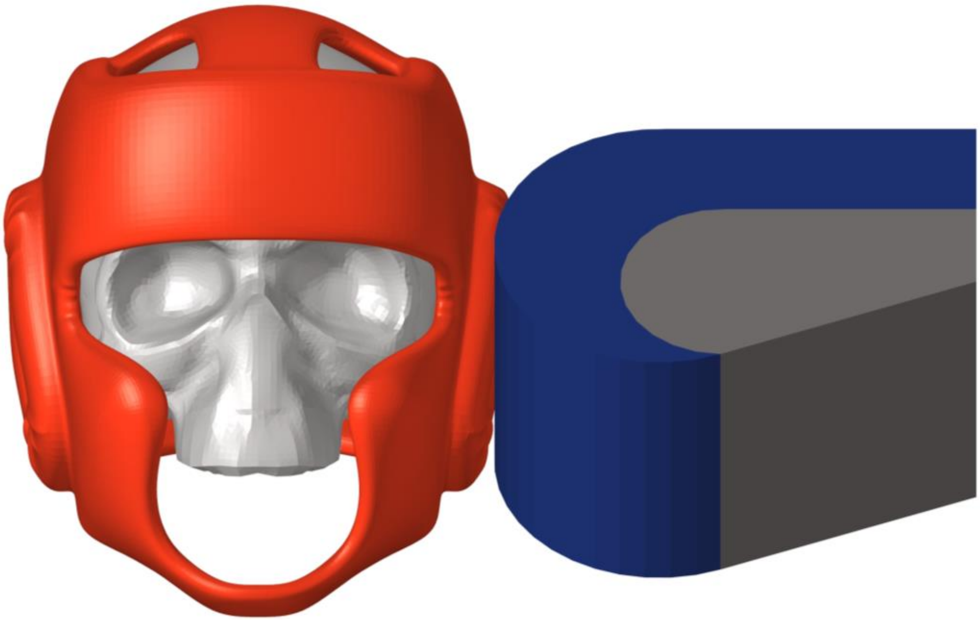

Figure 4.9. Punch Modeling – Front View

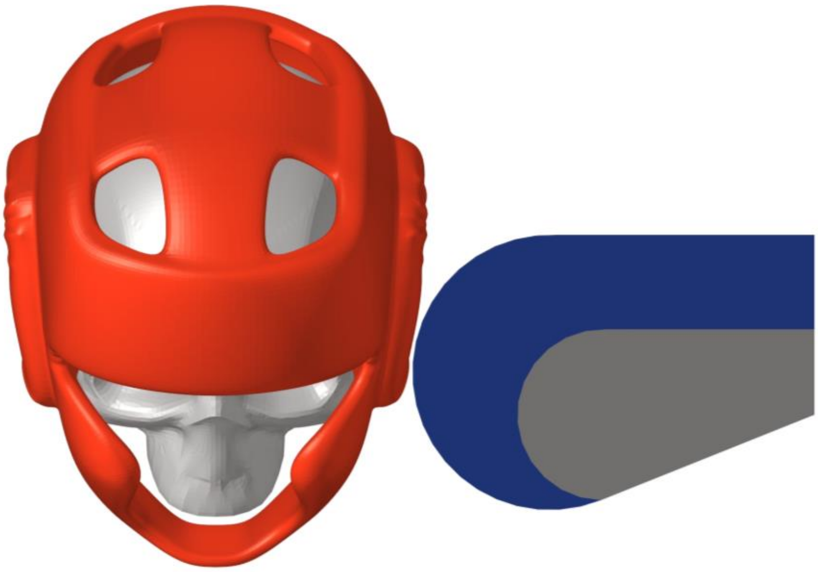

Figure 4.10. Punch Modeling – Oblique View

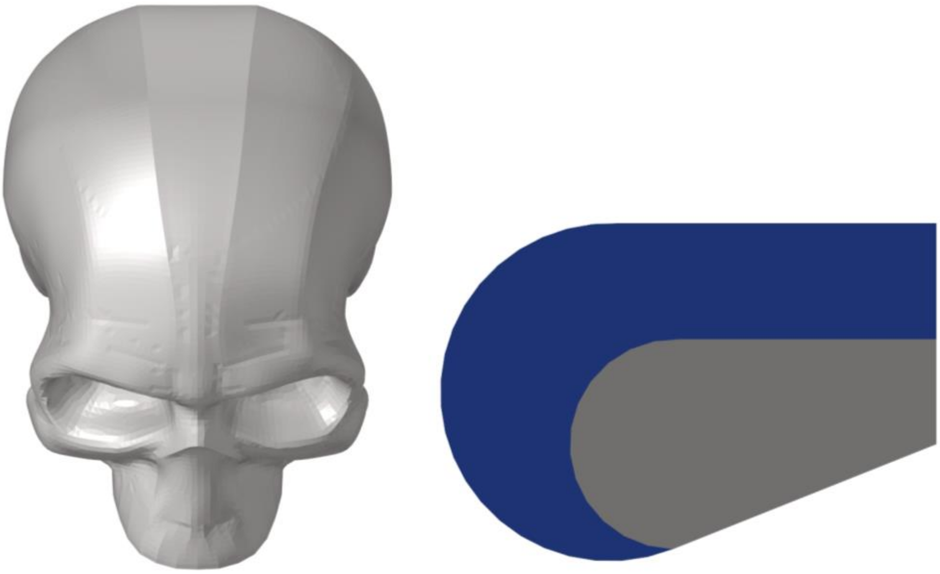

Figure 4.11. Punch Modeling – Oblique View – No Headgear

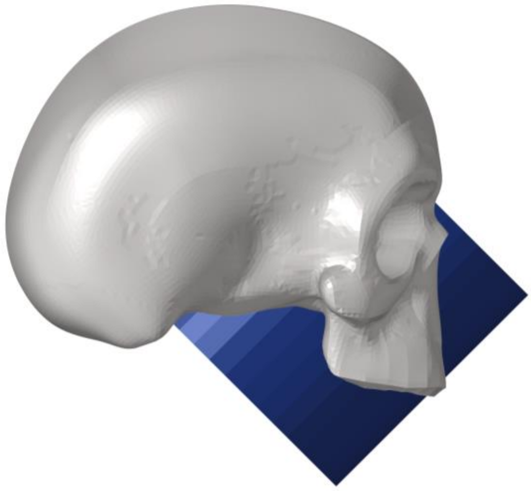

Figure 4.12. Punch Modeling – Side View – No Headgear

4.5 Simulation Settings

The simulation of the hook punch on the head is executed in three main branches: the simulation of the punch with no headgear present; with the headgear present but with no TVA installed; and finally, with the headgear present with an installed TVA. All three simulations are run for both the Rayleigh damped model and the undamped model, with their corresponding TVA designs given in Table 4.1.

Data measurements in the simulation are conducted on singular nodes, which gives an opportunity for noisy data due to numerical errors. Before the post-processing of simulation results, the data was low pass filtered at 180 Hz by SAE J211 standards to get rid of unwanted noise. Filtering out high-frequency content is also performed in similar head impact simulations [13], [20].

The severity indices to be used in this study are selected as: HIC, BrIC, and CM, formulations are given in 2.1.1. The severity indices used in the study are calculated from the peak values of linear and/or rotational velocity and acceleration values of the head. The peak velocity and acceleration values of the head are observed to occur within 10 milliseconds after the punch lands; therefore, the simulation of the punch is kept at 30 milliseconds. Simulations are run by Radioss (Altair Engineering Inc.), explicit finite element solver.

CHAPTER 5

RESULTS AND DISCUSSION

Three cases for two models are simulated: first, impact with no headgear present; second, impact on a headgear; and finally, impact on a TVA mounted headgear, for both Rayleigh damped and undamped models. For each simulation, five figures are shared: impact load, head linear acceleration, head rotational velocity, head rotational acceleration, and time history of head behavior throughout the simulation, which are the variables of HIC, BrIC, and CM. After the review of six cases separately, the results are plotted together for better comparison in time history. The severity index results are summarized in Table 5.1.

5.1 Undamped Model

In this section, the response figures of undamped model cases are displayed. Three simulations are present for the undamped model: a simulation without a headgear, a simulation with a standard headgear, and a simulation with a TVA implemented headgear. The undamped model's tuned TVA parameters are different than the Rayleigh-damped model's; therefore, with different approaches to modeling the head and different parameters on TVA, the results should vary.

5.1.1 Simulation without Headgear

In this section, five different plots are given for the undamped head FE model's hook punch simulation without headgear. The figure of punch impact force on the head, which shows the punch force, and the impact duration is given in Figure 5.1. The head resultant linear acceleration, which is the mere parameter in the calculation of HIC, is shown in Figure 5.2. Figures of head rotational velocity and movement in directions of X, Y, and Z and the resultant are given in Figure 5.3 and Figure 5.4, respectively. Head rotational velocity and acceleration peak values are used in calculations of BrIC and CM severity indices. In Figure 5.5, the motion of the head is shown at selected time steps, for better understanding the result of the impact.

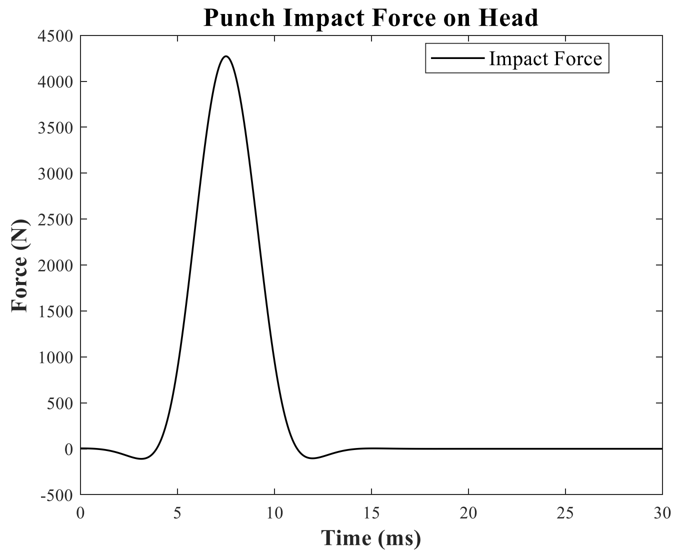

Figure 5.1. Undamped Model Simulation without Headgear – Punch Impact Force

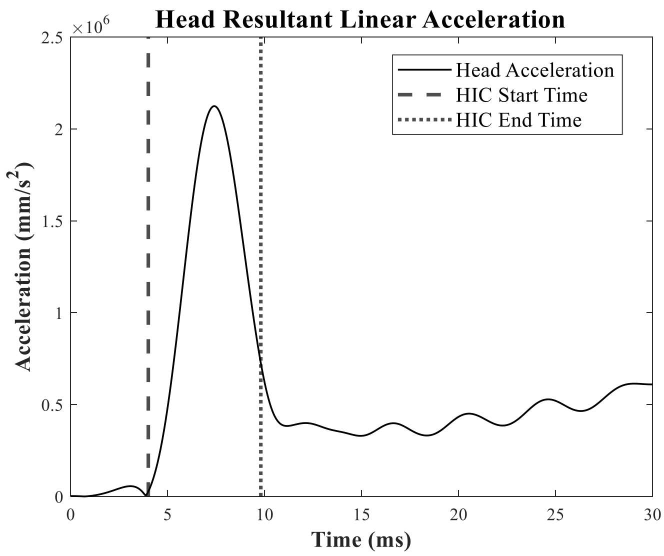

Figure 5.2. Undamped Model Simulation without Headgear – Head Resultant Linear Acceleration

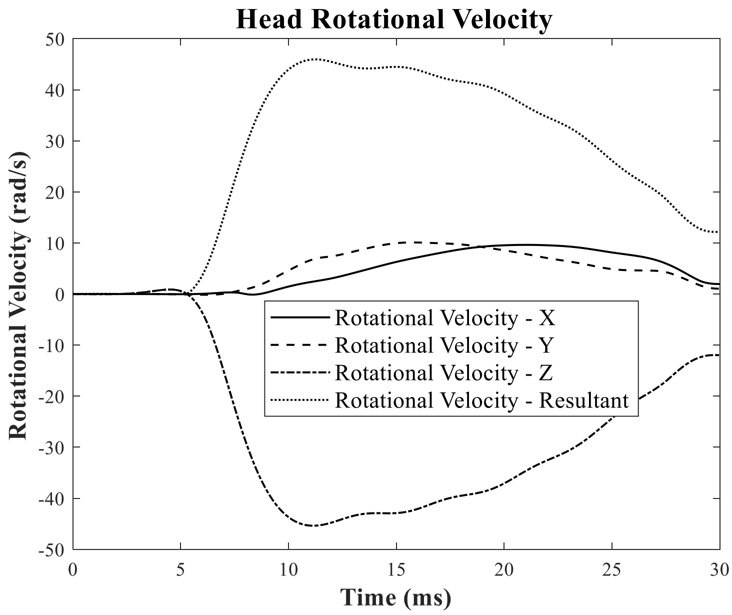

Figure 5.3. Undamped Model Simulation without Headgear – Rotational Velocity of Head

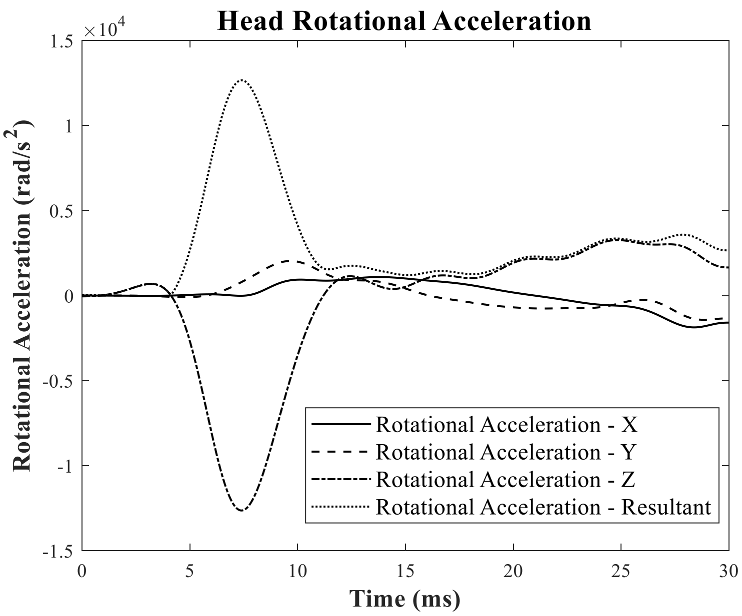

Figure 5.4. Undamped Model Simulation without Headgear – Rotational Acceleration of Head

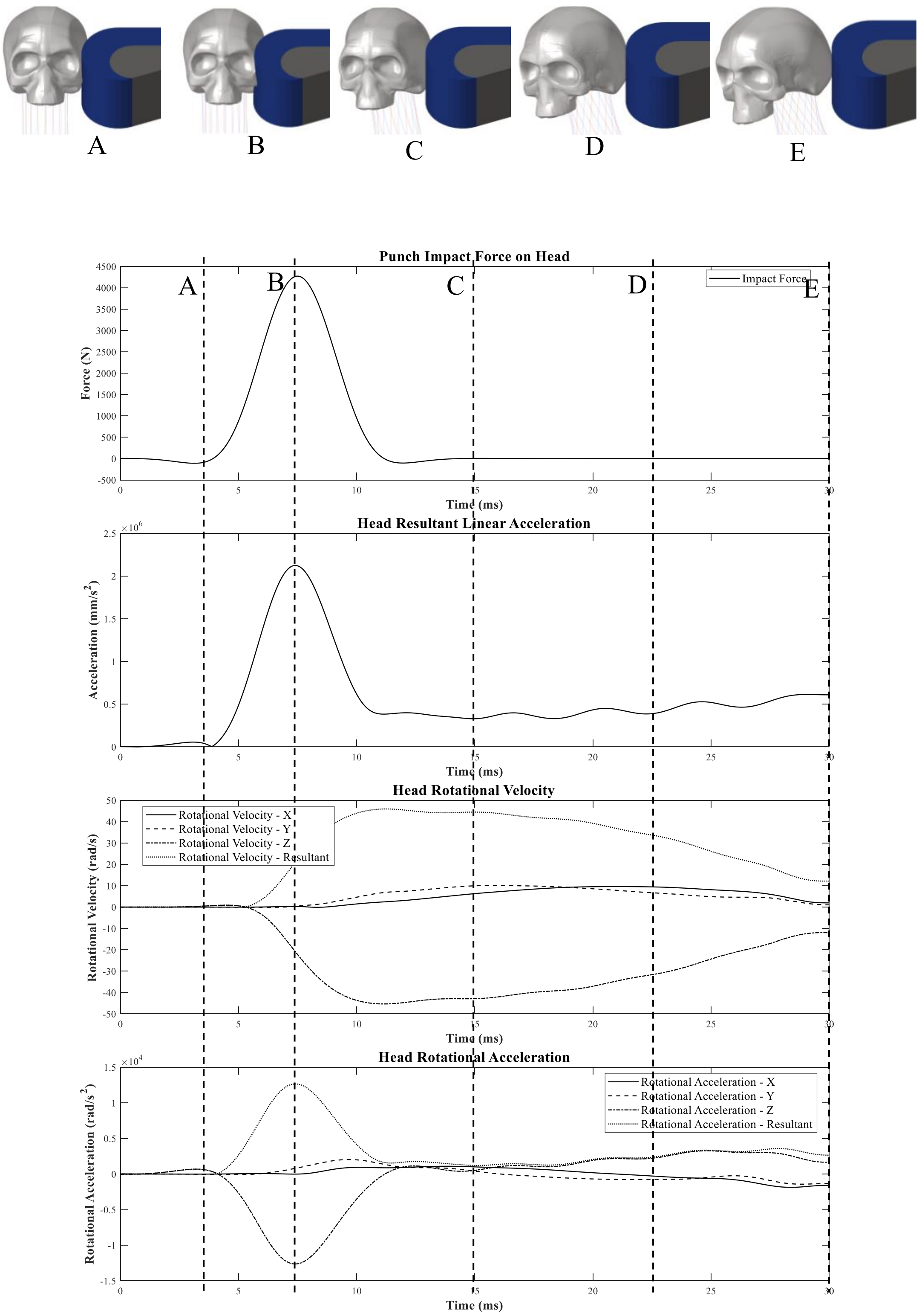

Figure 5.5. Undamped Model Simulation without Headgear – Time History of Head Dynamics

5.1.2 Simulation with Standard Headgear

In this section, five different plots are given for the undamped head FE model's hook punch simulation with standard headgear. The figure of punch impact force on the head, which shows the punch force, and the impact duration is given in Figure 5.6. The head resultant linear acceleration, which is the mere parameter in the calculation of HIC, is shown in Figure 5.7. Figures of head rotational velocity and movement in directions of X, Y, and Z and the resultant are given in Figure 5.8 and Figure 5.9, respectively. Head rotational velocity and acceleration peak values are used in calculations of BrIC and CM severity indices. In Figure 5.10, the motion of the head is shown at selected time steps, for better understanding the result of the impact.

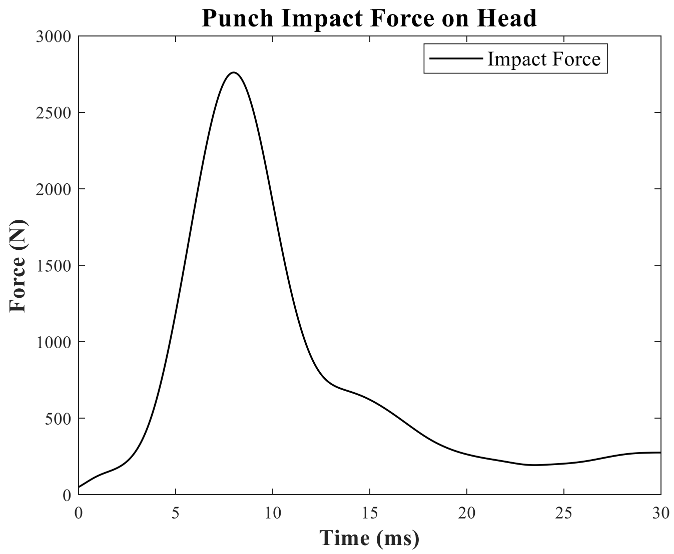

Figure 5.6. Undamped Model Simulation with Headgear – Punch Impact Force

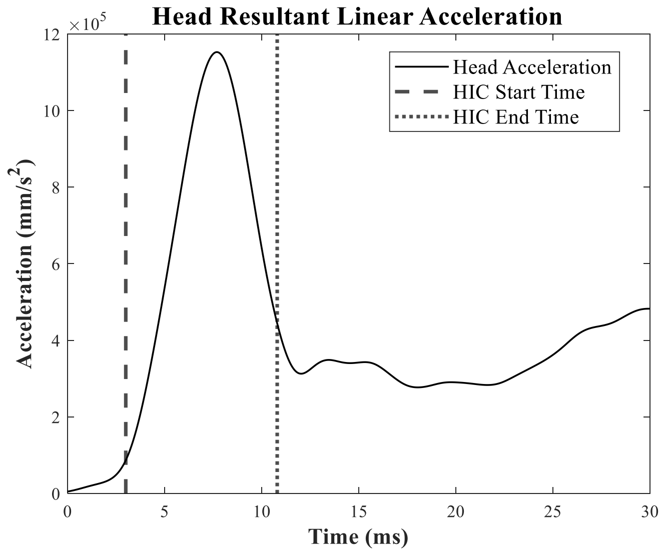

Figure 5.7. Undamped Model Simulation with Headgear – Head Resultant Linear Acceleration

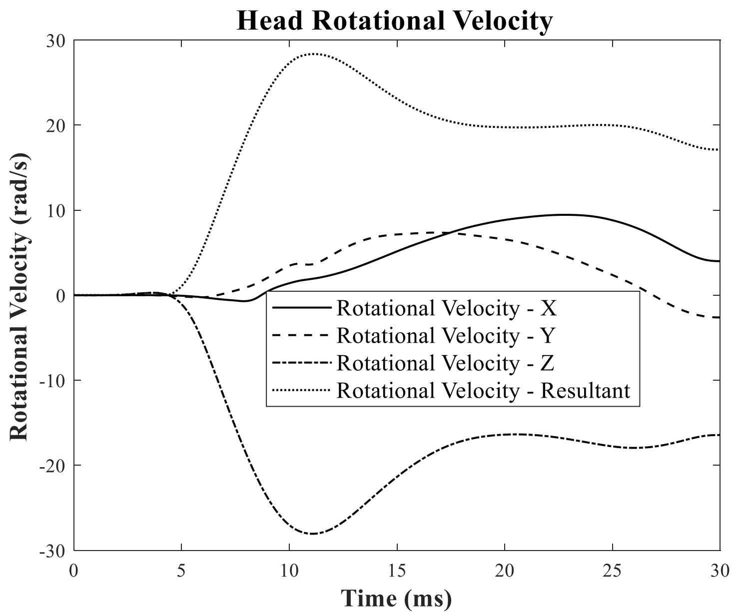

Figure 5.8. Undamped Model Simulation with Headgear – Rotational Velocity of Head

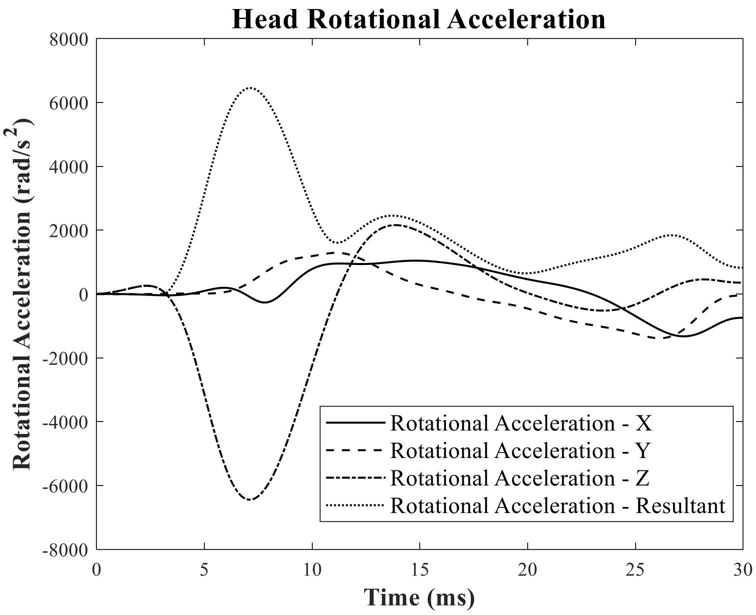

Figure 5.9. Undamped Model Simulation with Headgear – Rotational Acceleration of Head

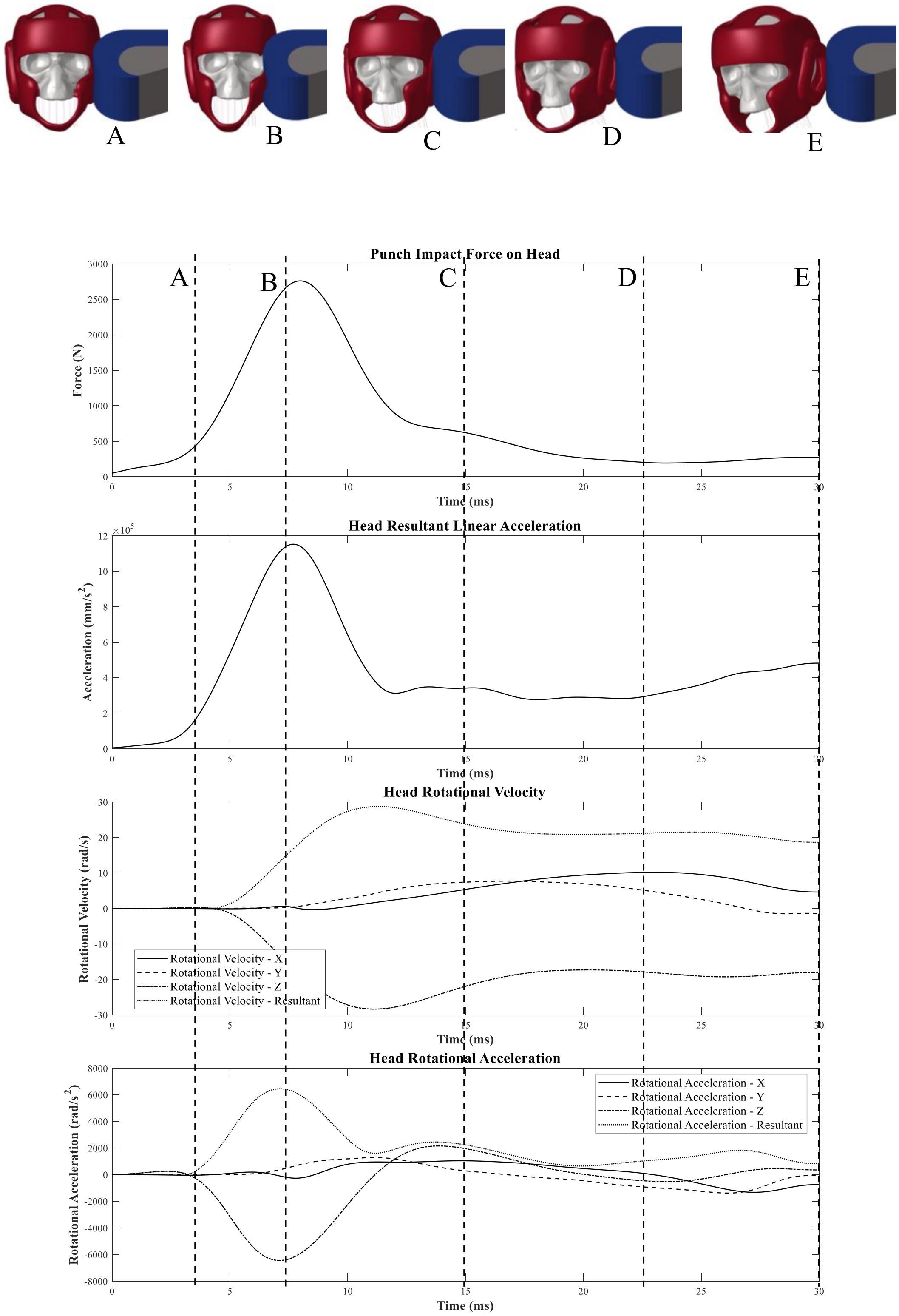

Figure 5.10. Undamped Model Simulation with Headgear – Time History of Head Dynamics

5.1.3 Simulation with TVA Implemented Headgear

In this section, five different plots are given for the undamped head FE model's hook punch simulation with TVA implemented headgear. The figure of punch impact force on the head, which shows the punch force, and the impact duration is given in Figure 5.11. The head resultant linear acceleration, which is the mere parameter in the calculation of HIC, is shown in Figure 5.12. Figures of head rotational velocity and movement in directions of X, Y, and Z and the resultant are given in Figure 5.13 and Figure 5.14, respectively. Head rotational velocity and acceleration peak values are used in calculations of BrIC and CM severity indices. In Figure 5.15, the motion of the head is shown at selected time steps, for better understanding the result of the impact.

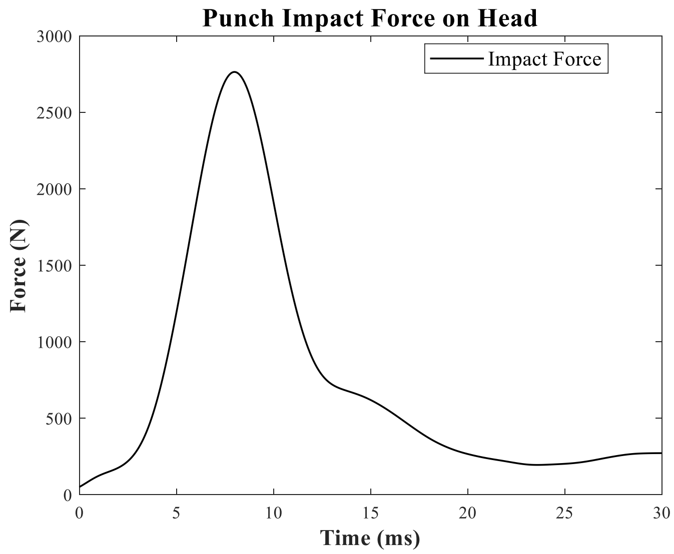

Figure 5.11. Undamped Model Simulation with Improved Headgear – Punch Impact Force

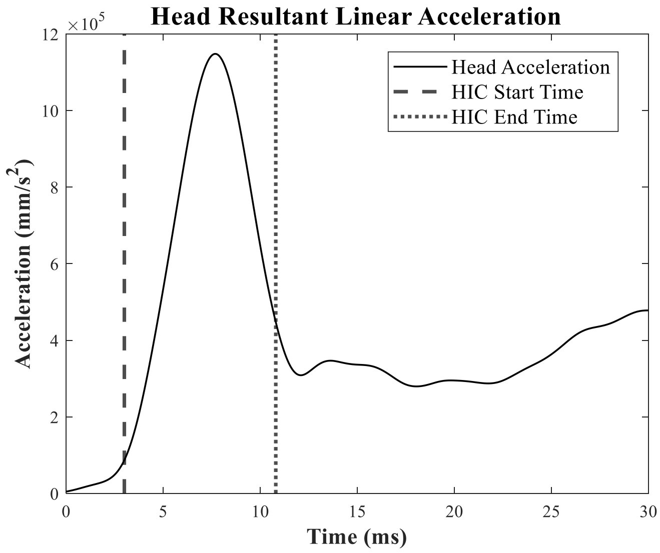

Figure 5.12. Undamped Model Simulation with Improved Headgear – Head Resultant Linear Acceleration

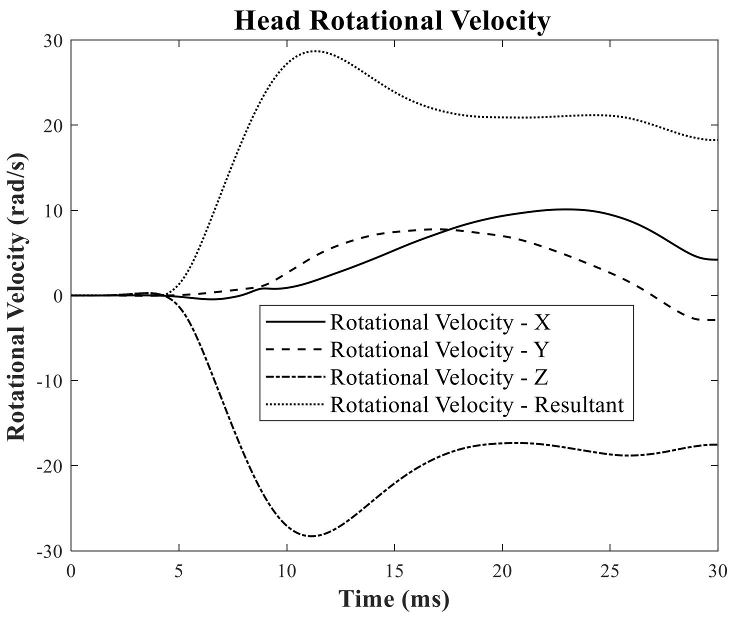

Figure 5.13. Undamped Model Simulation with Improved Headgear – Rotational Velocity of Head

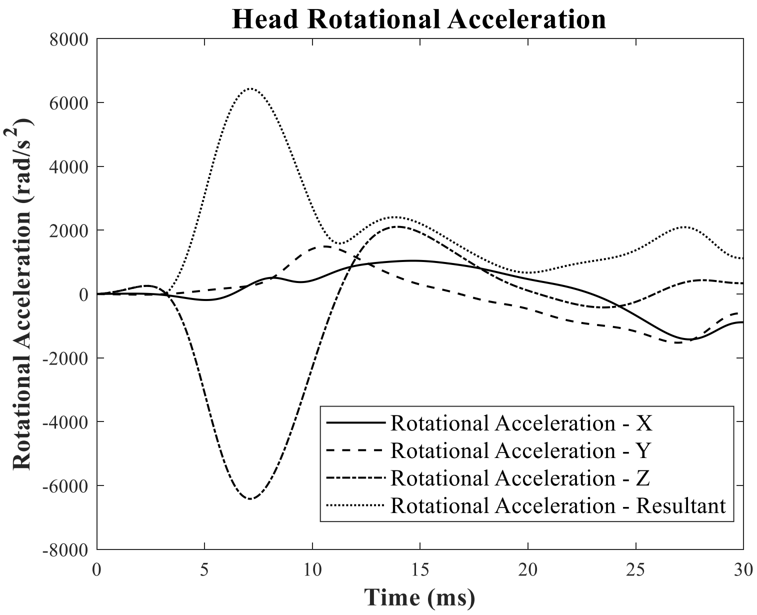

Figure 5.14. Undamped Model Simulation with Improved Headgear – Rotational Acceleration of Head

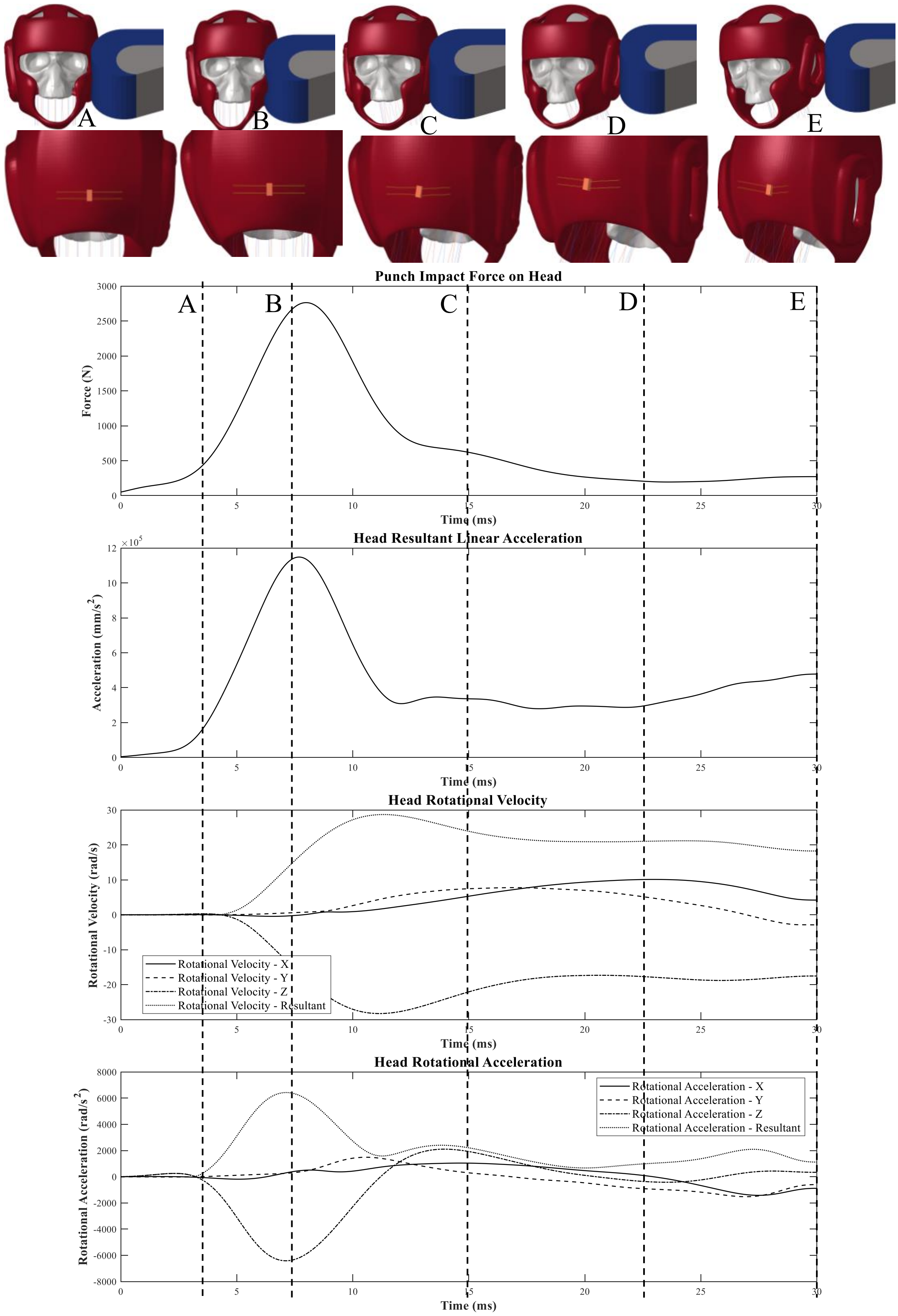

Figure 5.15. Undamped Model Simulation with Improved Headgear – Time History of Head Dynamics

5.2 Rayleigh Damped Model

In this section, the response figures of Rayleigh-damped model cases are displayed. Three simulations are present for the undamped model: a simulation without a headgear, a simulation with a standard headgear, and a simulation with a TVA implemented headgear. The Rayleigh-damped model's tuned TVA parameters are different than the undamped model's; therefore, with different approaches to modeling the head and different parameters on TVA, the results should vary.

5.2.1 Simulation without Headgear

In this section, five different plots are given for the Rayleigh-damped head FE model's hook punch simulation without headgear. The figure of punch impact force on the head, which shows the punch force, and the impact duration is given in Figure 5.16. The head resultant linear acceleration, which is the mere parameter in the calculation of HIC, is shown in Figure 5.17. Figures of head rotational velocity and movement in directions of X, Y, and Z and the resultant are given in Figure 5.18 and Figure 5.19, respectively. Head rotational velocity and acceleration peak values are used in calculations of BrIC and CM severity indices. In Figure 5.20, the motion of the head is shown at selected time steps, for better understanding the result of the impact.

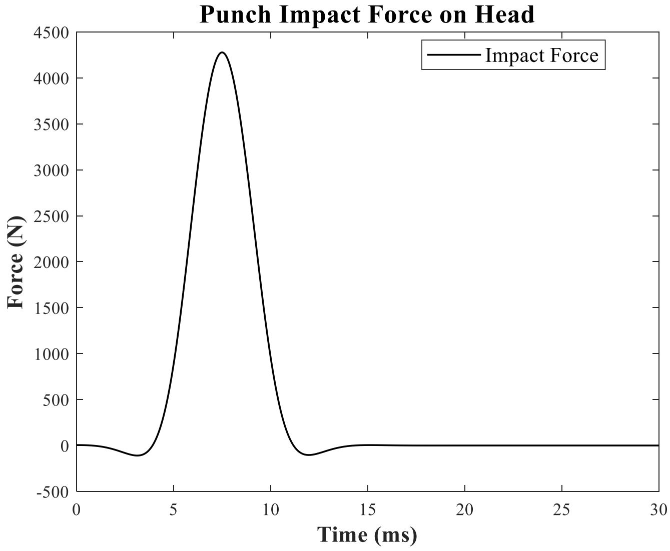

Figure 5.16. Rayleigh Damped Model Simulation without Headgear – Punch Impact Force

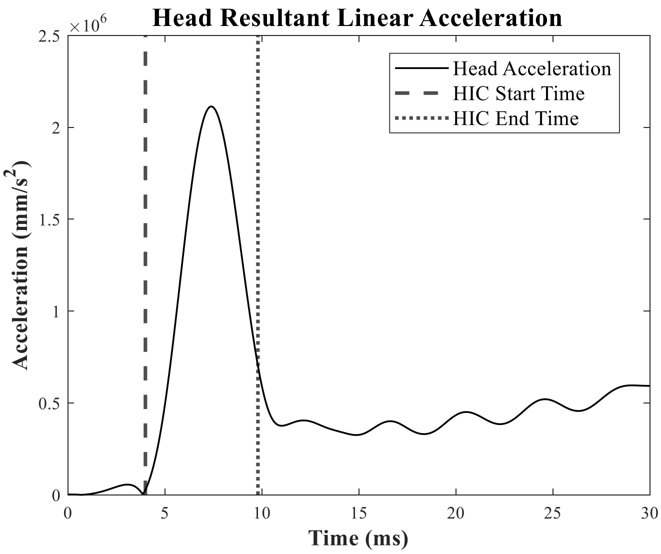

Figure 5.17. Rayleigh Damped Model Simulation without Headgear – Head Resultant Linear Acceleration

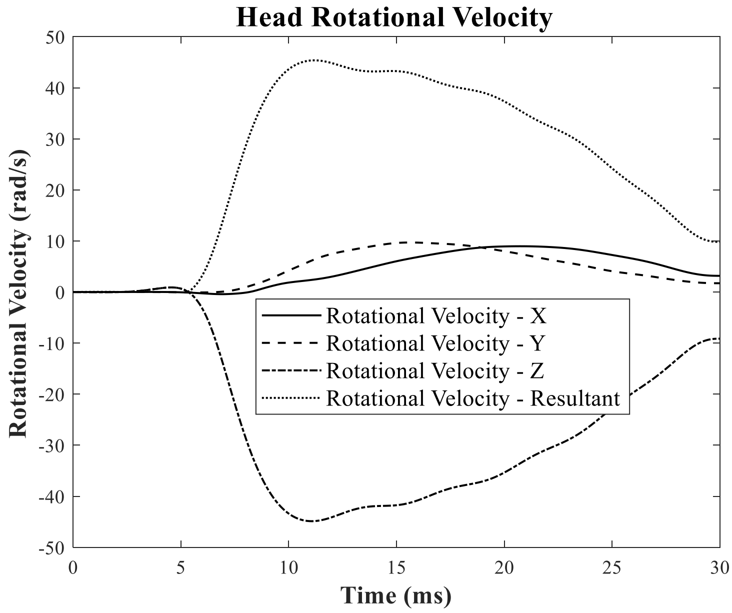

Figure 5.18. Rayleigh Damped Model Simulation without Headgear – Rotational Velocity of Head

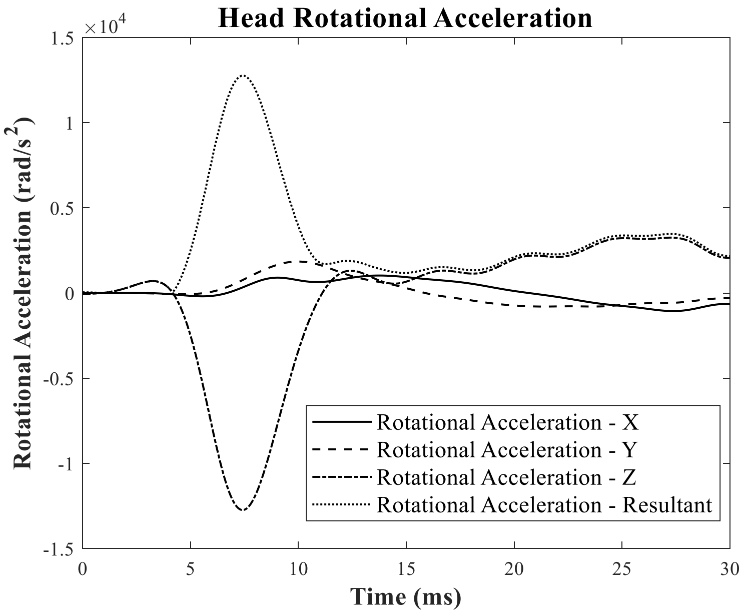

Figure 5.19. Rayleigh Damped Model Simulation without Headgear – Rotational Acceleration of Head

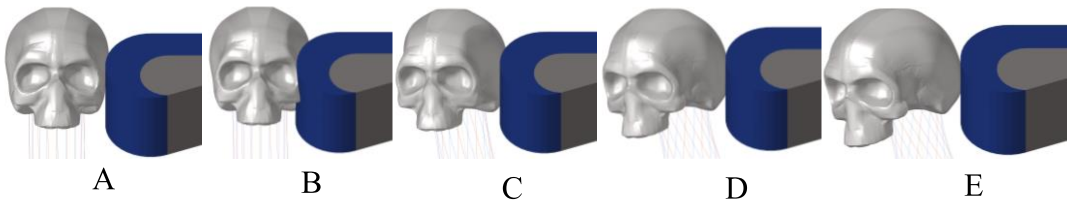

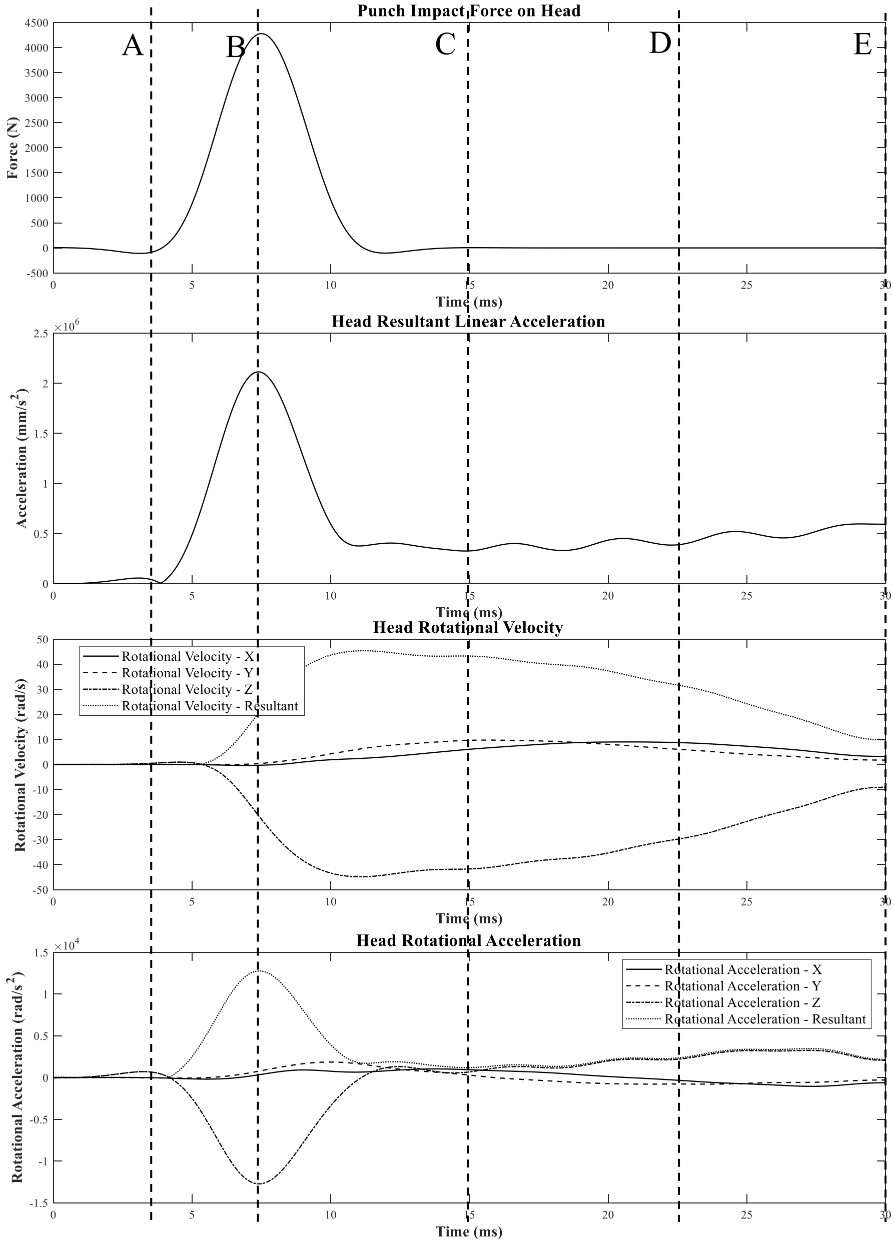

Figure 5.20. Rayleigh Damped Model Simulation without Headgear – Time History of Head Dynamics

5.2.2 Simulation with Standard Headgear

In this section, five different plots are given for the Rayleigh-damped head FE model's hook punch simulation with a standard headgear. The figure of punch impact force on the head, which shows the punch force, and the impact duration is given in Figure 5.21. The head resultant linear acceleration, which is the mere parameter in the calculation of HIC, is shown in Figure 5.22. Figures of head rotational velocity and movement in directions of X, Y, and Z and the resultant are given in Figure 5.23 and Figure 5.24, respectively. Head rotational velocity and acceleration peak values are used in calculations of BrIC and CM severity indices. In Figure 5.25, the motion of the head is shown at selected time steps, for better understanding the result of the impact.

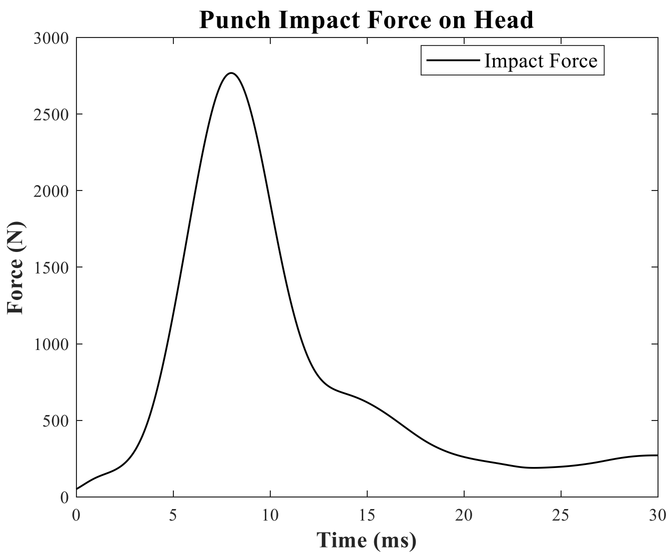

Figure 5.21. Rayleigh Damped Model Simulation with Headgear – Punch Impact Force

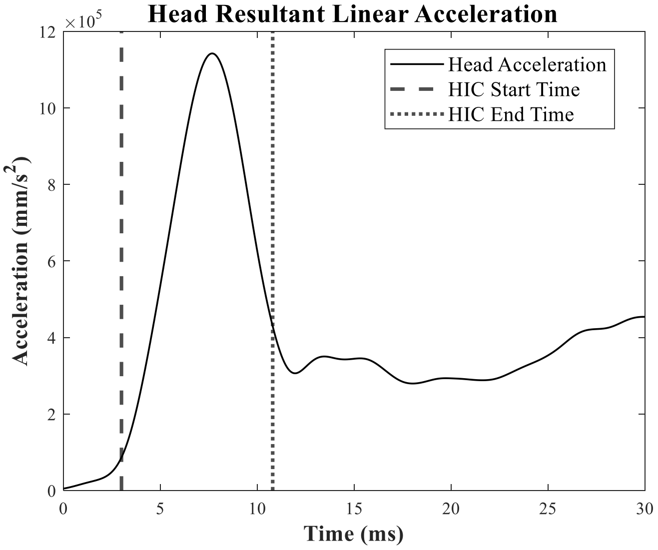

Figure 5.22. Rayleigh Damped Model Simulation with Headgear – Head Resultant Linear Acceleration

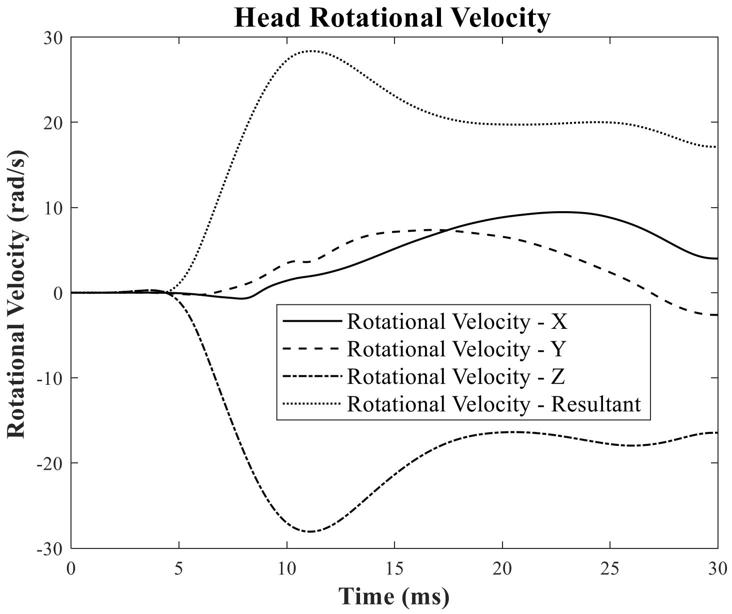

Figure 5.23. Rayleigh Damped Model Simulation with Headgear – Rotational Velocity of Head

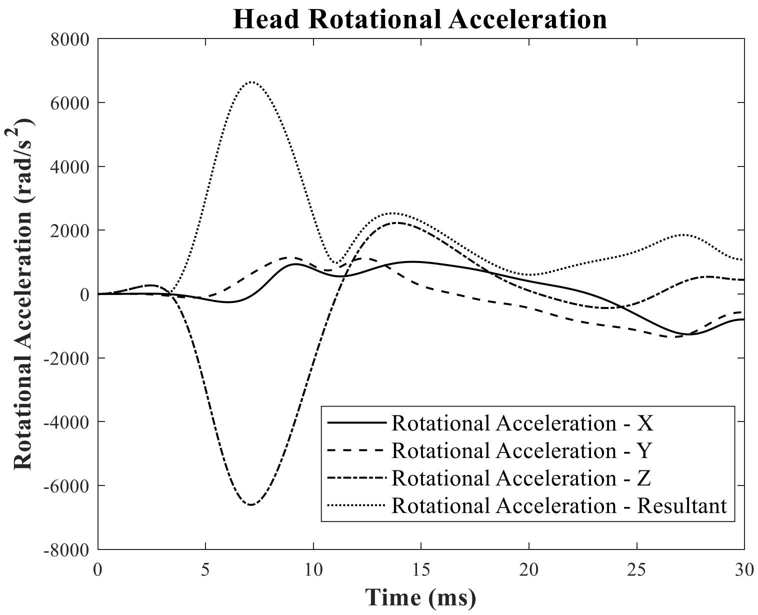

Figure 5.24. Rayleigh Damped Model Simulation with Headgear – Rotational Acceleration of Head

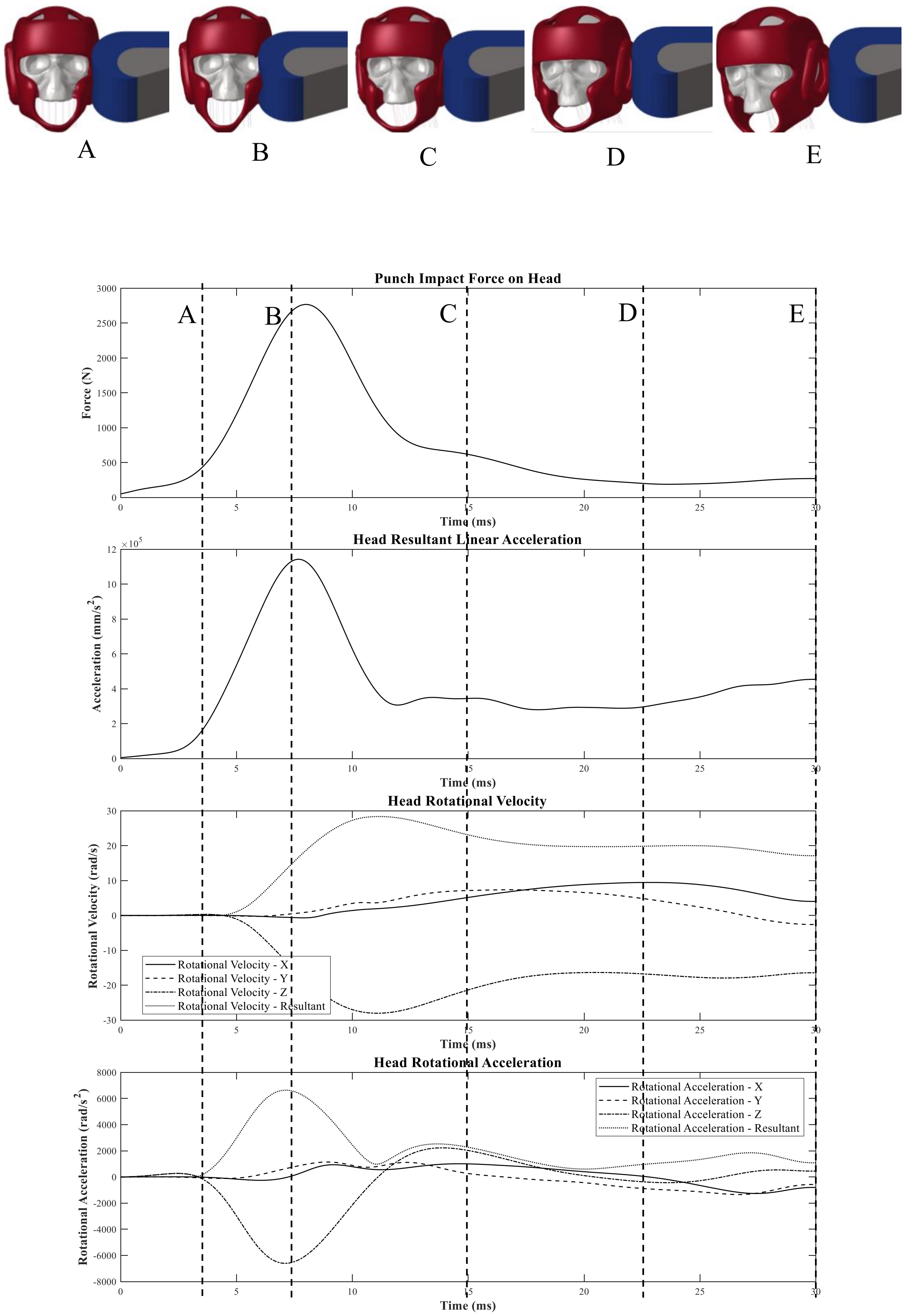

Figure 5.25. Rayleigh Damped Model Simulation with Headgear – Time History of Head Dynamics

5.2.3 Simulation with TVA Implemented Headgear

In this section, five different plots are given for the Rayleigh-damped head FE model's hook punch simulation with TVA implemented headgear. The figure of punch impact force on the head, which shows the punch force, and the impact duration is given in Figure 5.26. The head resultant linear acceleration, which is the mere parameter in the calculation of HIC, is shown in Figure 5.27. Figures of head rotational velocity and movement in directions of X, Y, and Z and the resultant are given in Figure 5.28 and Figure 5.29, respectively. Head rotational velocity and acceleration peak values are used in calculations of BrIC and CM severity indices. In Figure 5.30, the motion of the head is shown at selected time steps, for better understanding the result of the impact.

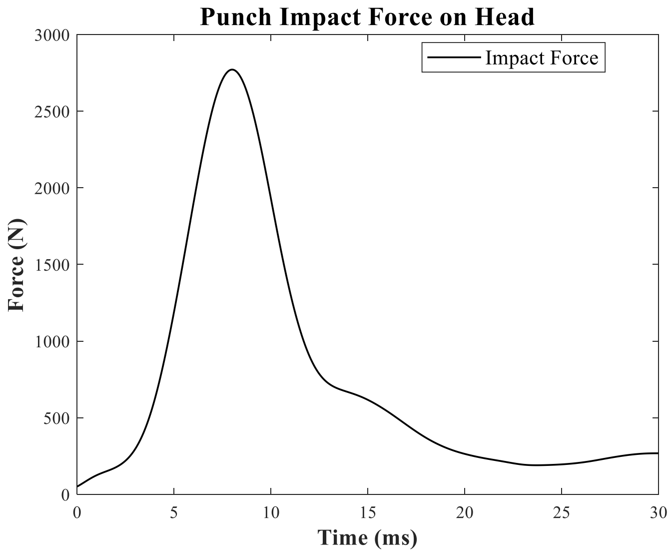

Figure 5.26. Rayleigh Damped Model Simulation with Improved Headgear – Punch Impact Force

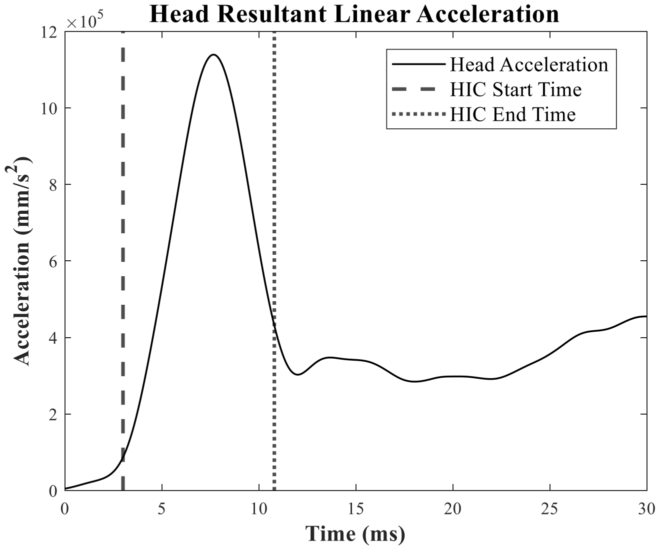

Figure 5.27. Rayleigh Damped Model Simulation with Improved Headgear – Head Resultant Linear Acceleration

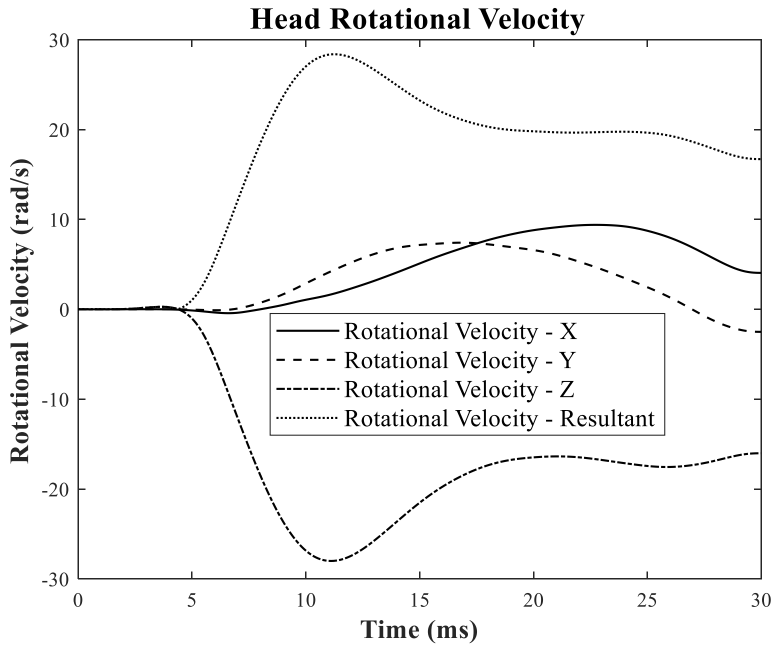

Figure 5.28. Rayleigh Damped Model Simulation with Improved Headgear – Rotational Velocity of Head

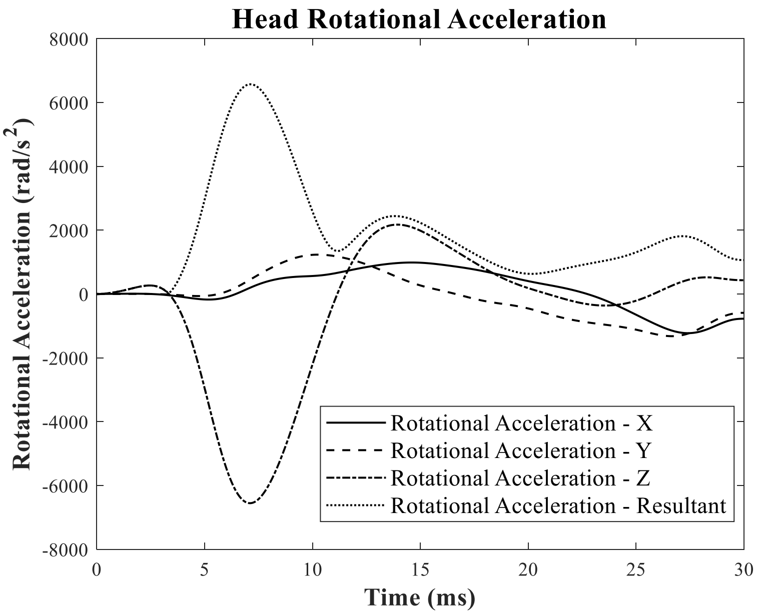

Figure 5.29. Rayleigh Damped Model Simulation with Improved Headgear – Rotational Acceleration of Head

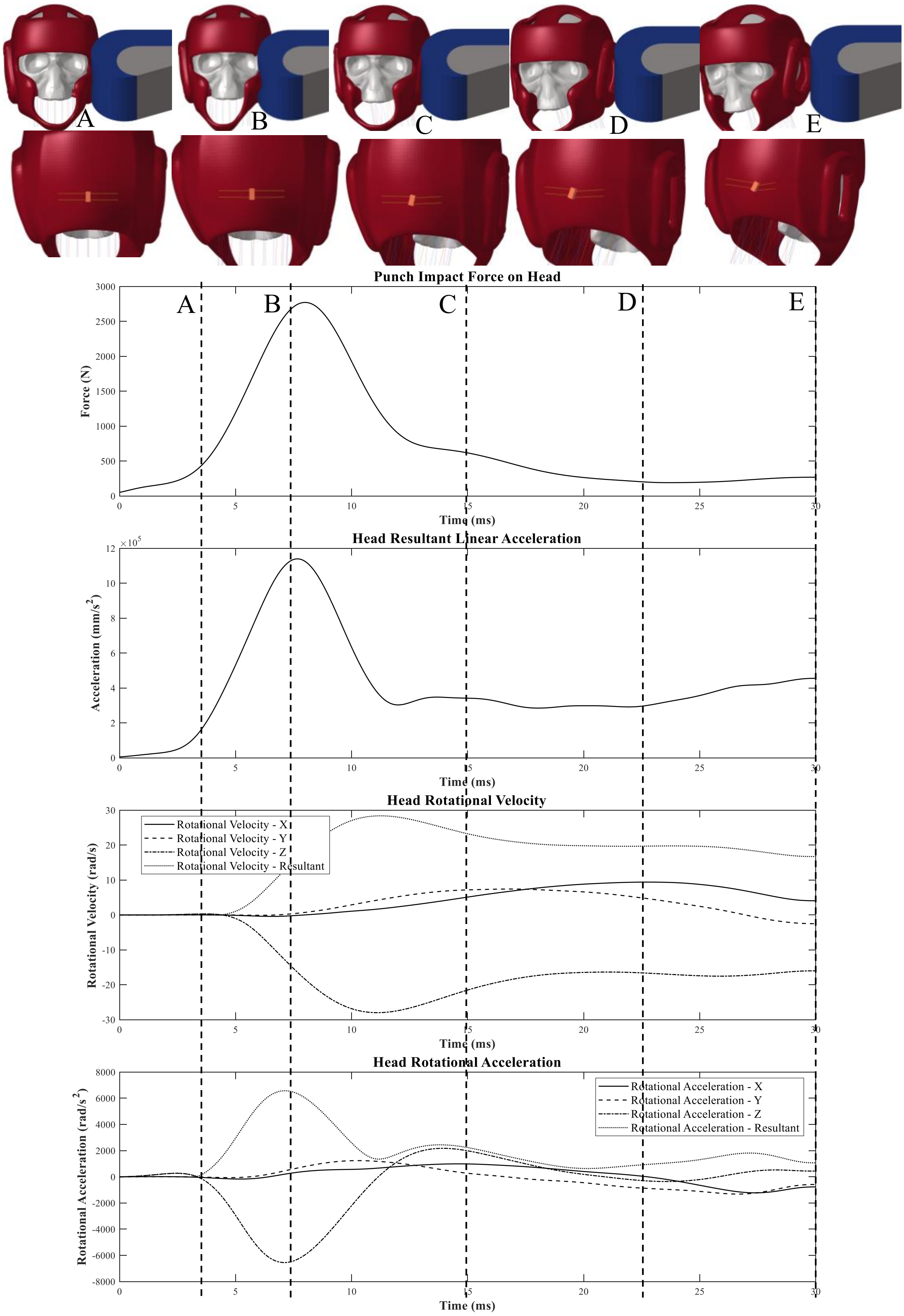

Figure 5.30. Rayleigh Damped Model Simulation with Improved Headgear – Time History of Head Dynamics

5.3 Comparison of Cases

In this section, cases where the headgear is present or not are compared with each other. The main variable for the following figures is the application of Rayleigh damping. First, a comparison of cases where no headgear is present in the model is conducted. Secondly, a comparison between cases where the headgear is present is conducted. The use of headgear is a rule by AIBA[23] in most boxing events, and the application of TVA is only possible on the headgear. The comparison of the cases without headgear is for understanding the importance of headgear usage in boxing and having a reference on the effect of Rayleigh damping in the head model.

5.3.1 Comparison of Cases without Headgear

In this section, comparisons of cases where no headgear or TVA is present are given. These results are for better understanding the application of the Rayleigh damping effect to the model.

The punch impact force on the head is compared in Figure 5.31 and Figure 5.32. It is observed that with the application of Rayleigh damping to the model, the peak impact force increased slightly.

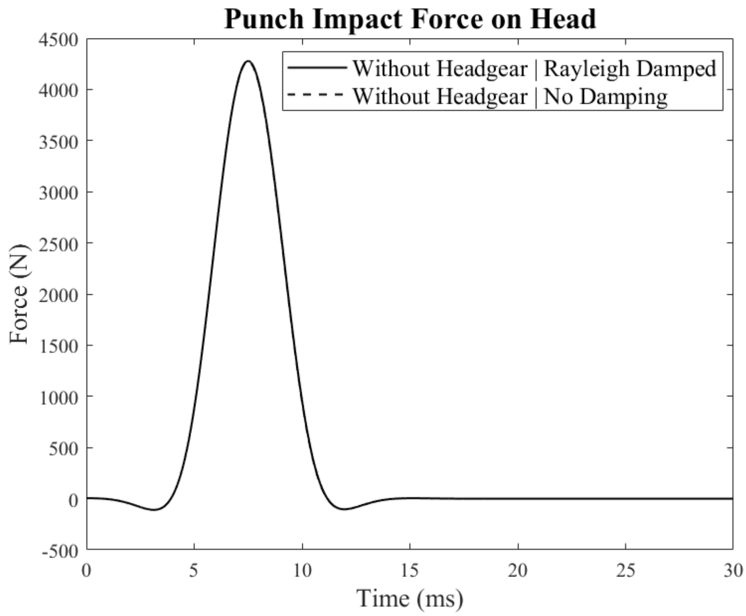

Figure 5.31. Punch Impact Force – Cases without Headgear

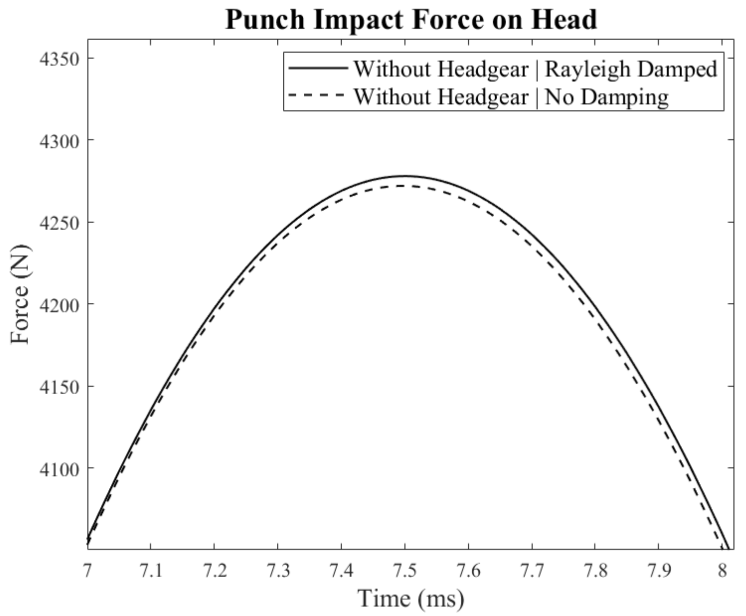

Figure 5.32. Punch Impact Force (Zoomed in) – Cases without Headgear

The head resultant linear acceleration is compared in Figure 5.33 and Figure 5.34. The effect of Rayleigh damping on head resultant linear acceleration is negligible, which would not create a significant difference in HIC criteria.

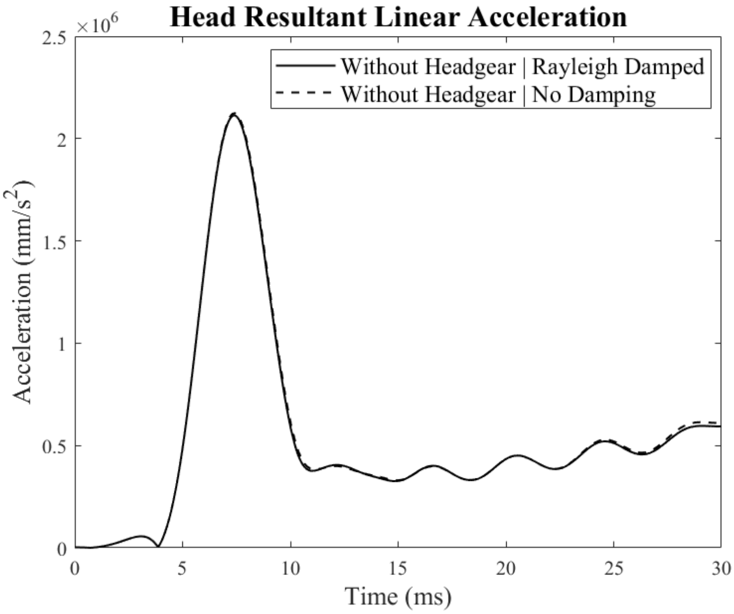

Figure 5.33. Head Resultant Linear Acceleration – Cases without Headgear

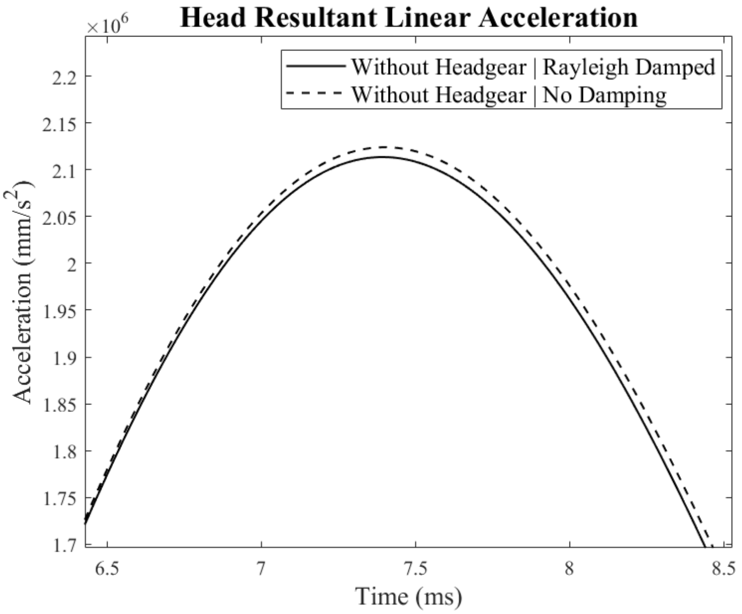

Figure 5.34. Head Resultant Linear Acceleration (Zoomed in) – Cases without Headgear

The head rotational velocities in directions of X, Y, and Z and total magnitude are displayed in Figure 5.35, Figure 5.36, Figure 5.37, and Figure 5.38, respectively. In all directions, it is observed that with the addition of Rayleigh damping to the model, the peak values decreased, and the motion of the head became smoother.

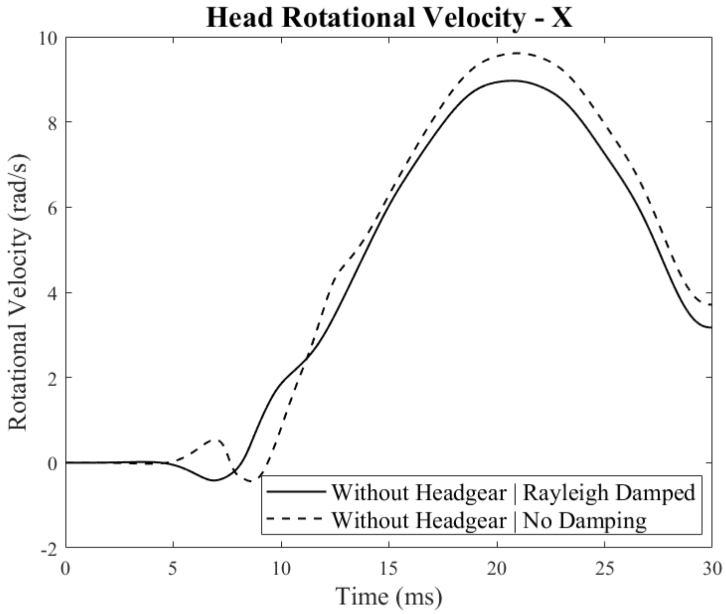

Figure 5.35. Head Rotational Velocity – X Axis – Cases without Headgear

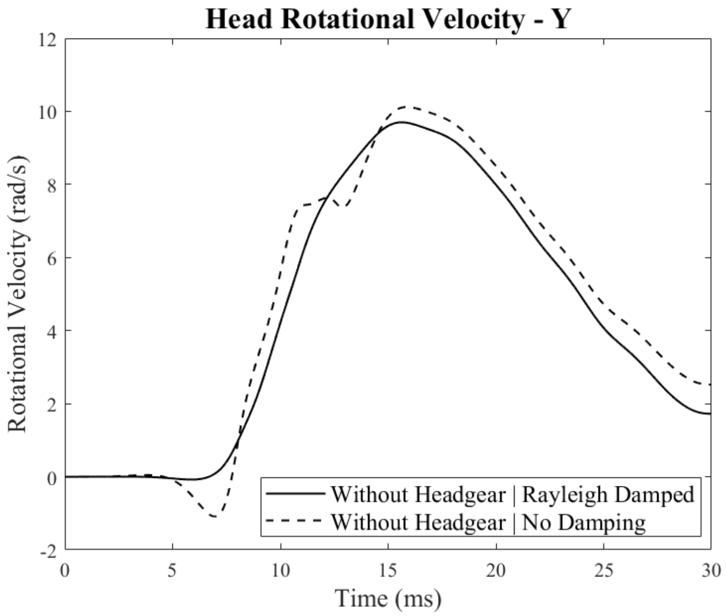

Figure 5.36. Head Rotational Velocity – Y Axis – Cases without Headgear

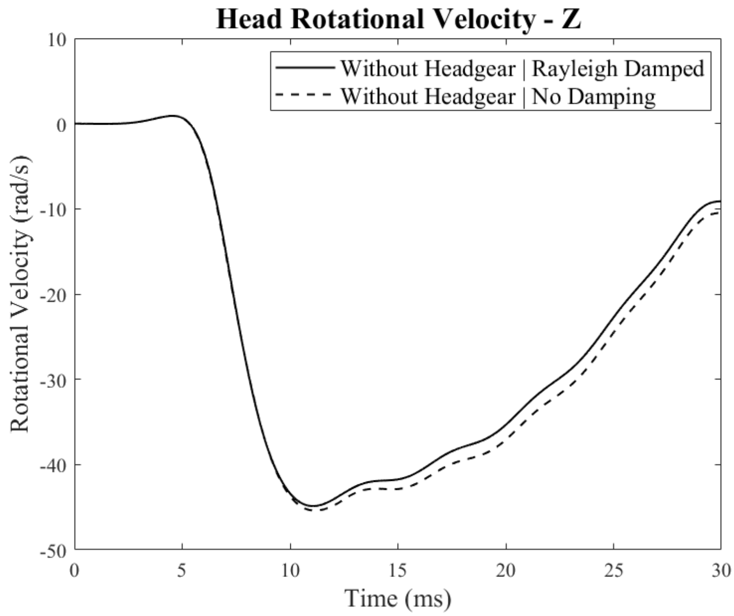

Figure 5.37. Head Rotational Velocity – Z Axis – Cases without Headgear

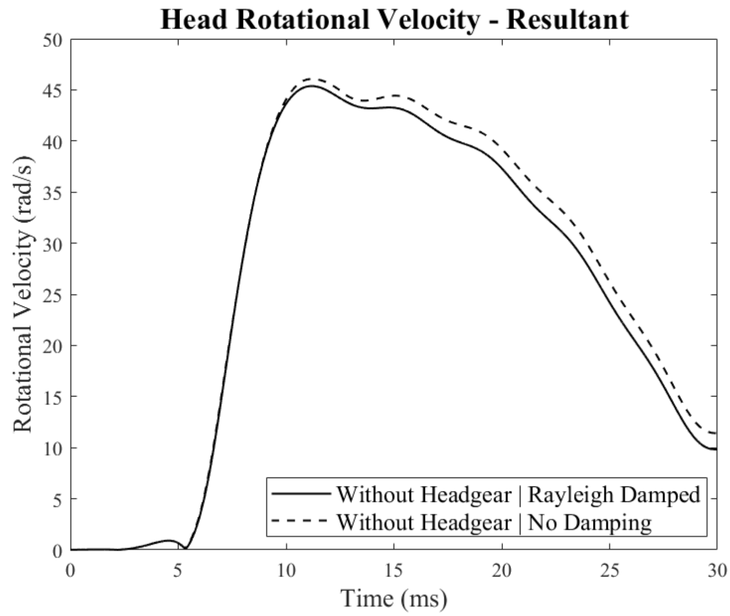

Figure 5.38. Head Rotational Velocity – Resultant – Cases without Headgear

The head rotational accelerations around directions of X, Y, and Z and their total magnitude are displayed in Figure 5.39, Figure 5.40, Figure 5.41, and Figure 5.42, respectively. Around X and Y directions, it is observed that with the addition of Rayleigh damping to the model, the peak values decreased, and the motion of the head became smoother. However, around Z direction, the application of Rayleigh damping to the model increases the peak value of the acceleration. Moreover, since the peak value of the Z direction is much higher than the X and Y directions (12 and 6 times, respectively), the resultant peak of the rotational acceleration stays increased with the application of the Rayleigh damping to the model.

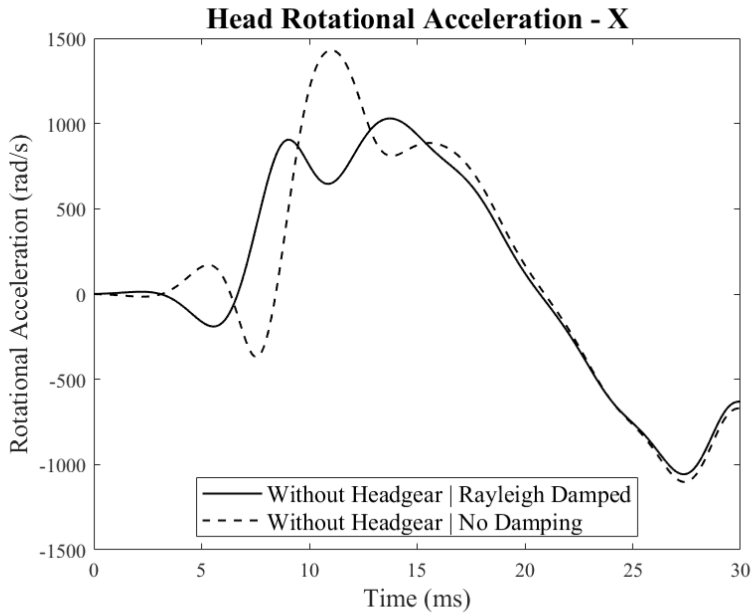

Figure 5.39. Head Rotational Acceleration – X Axis – Cases without Headgear

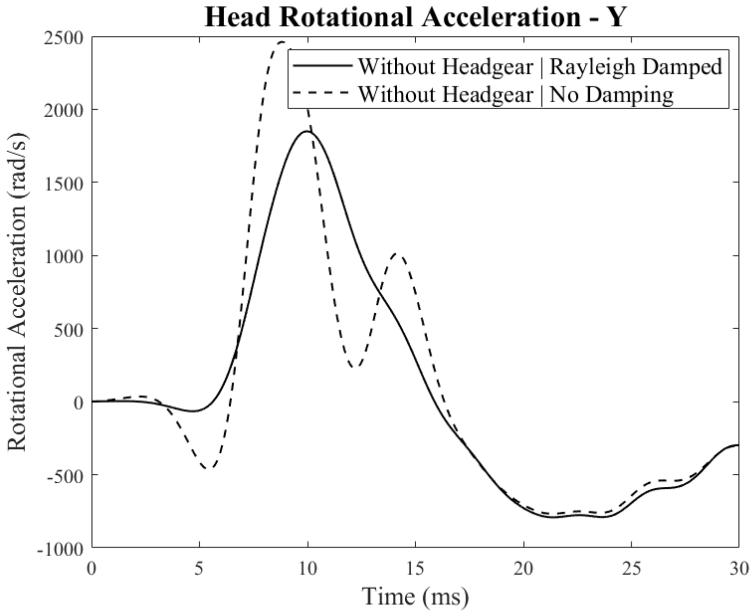

Figure 5.40. Head Rotational Acceleration – Y Axis – Cases without Headgear

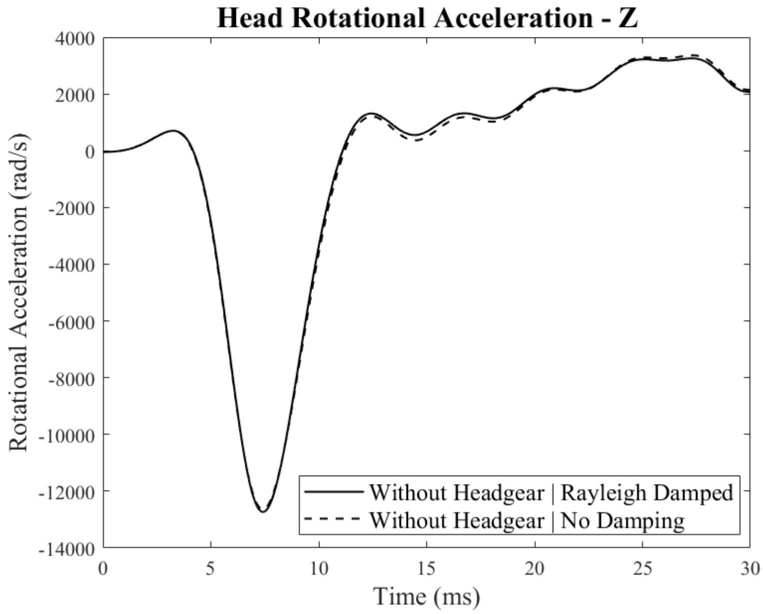

Figure 5.41. Head Rotational Acceleration – Z Axis – Cases without Headgear

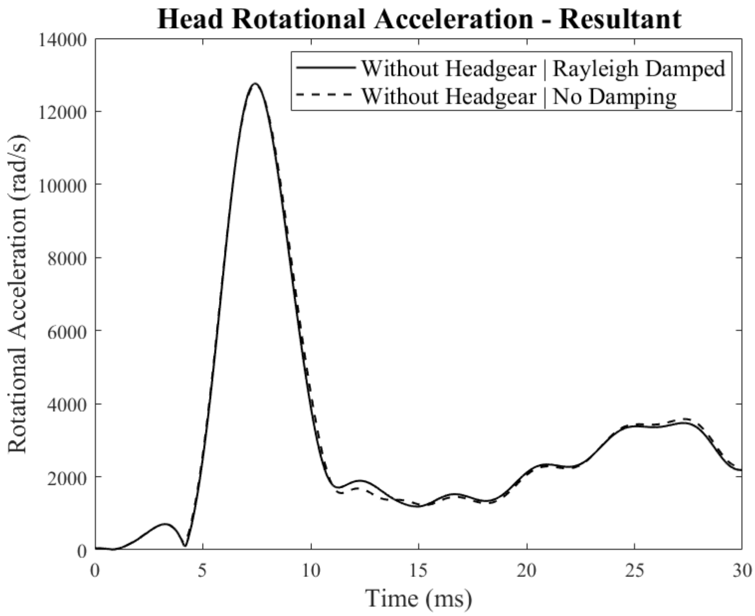

Figure 5.42. Head Rotational Acceleration – Resultant – Cases without Headgear

5.3.2 Comparison of Cases with Headgear

In this section, comparisons of cases where headgear is worn are shown. Both cases where TVA was implemented and not implemented are shown in the same figures. These results are for better understanding the effect of the TVA's application on time history.

The punch impact force on the head is compared in Figure 5.43 and Figure 5.44. It is observed that with the application of Rayleigh damping to the model, the peak impact force increased slightly, which is in accordance with the results from 5.3.1. With the implication of TVA, the peak impact force on the head for both undamped and Rayleigh-damped cases increase.

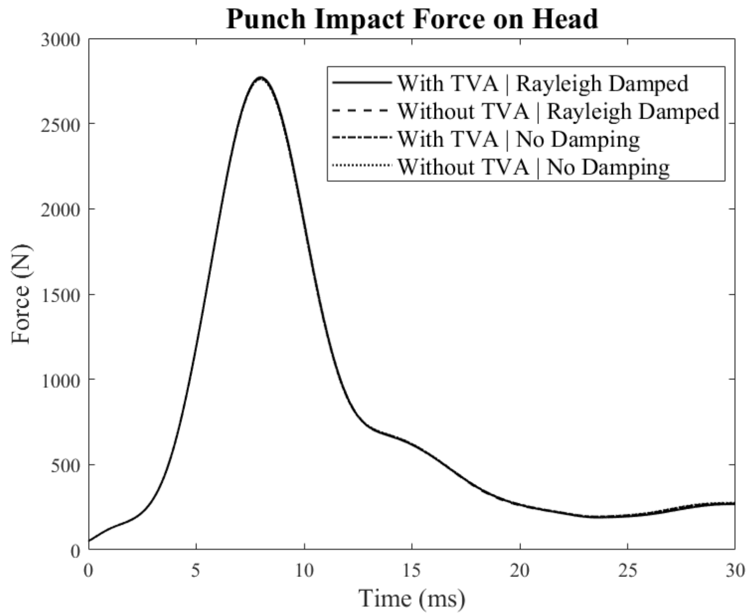

Figure 5.43. Punch Impact Force – Cases with Headgear

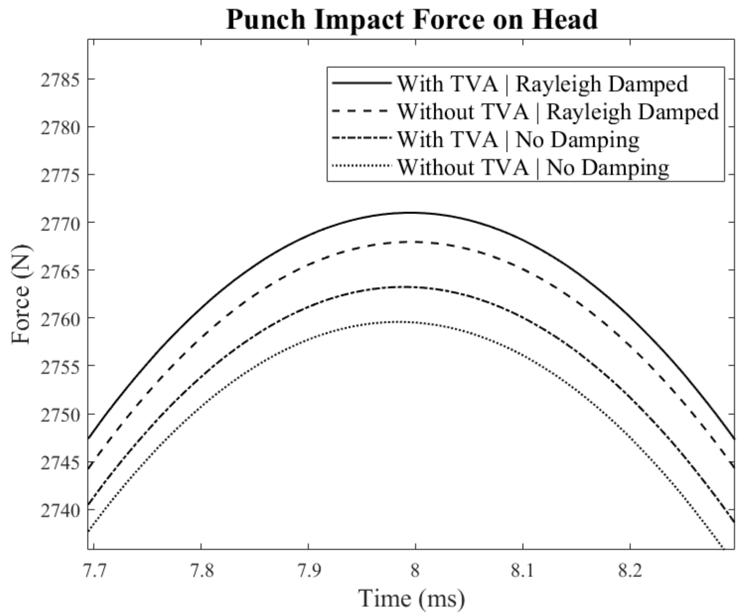

Figure 5.44. Punch Impact Force (Zoomed in) – Cases with Headgear

The head resultant linear acceleration is compared in Figure 5.45 and Figure 5.46. The effect of Rayleigh damping on head resultant linear acceleration is negligible, yet in accordance with the previous results in 5.3.1. Application of TVA has consistent effect on reducing the peak resultant linear acceleration in negligible level.

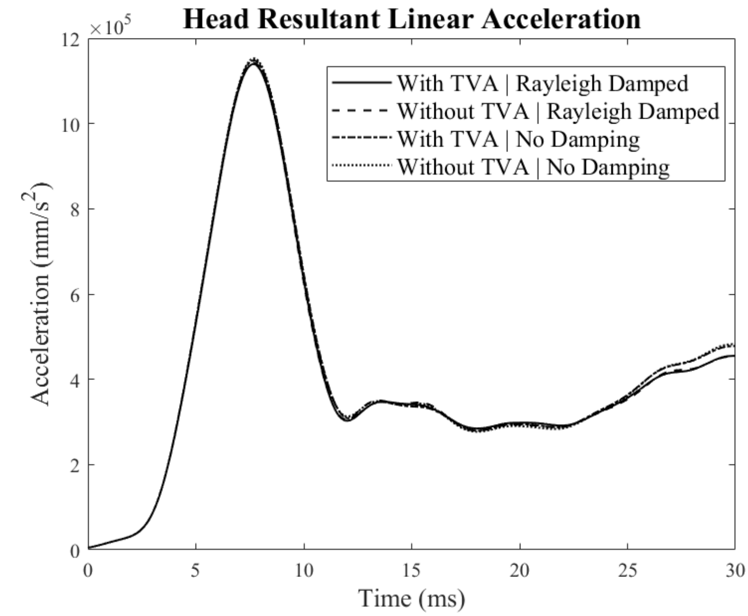

Figure 5.45. Head Resultant Linear Acceleration – Cases with Headgear

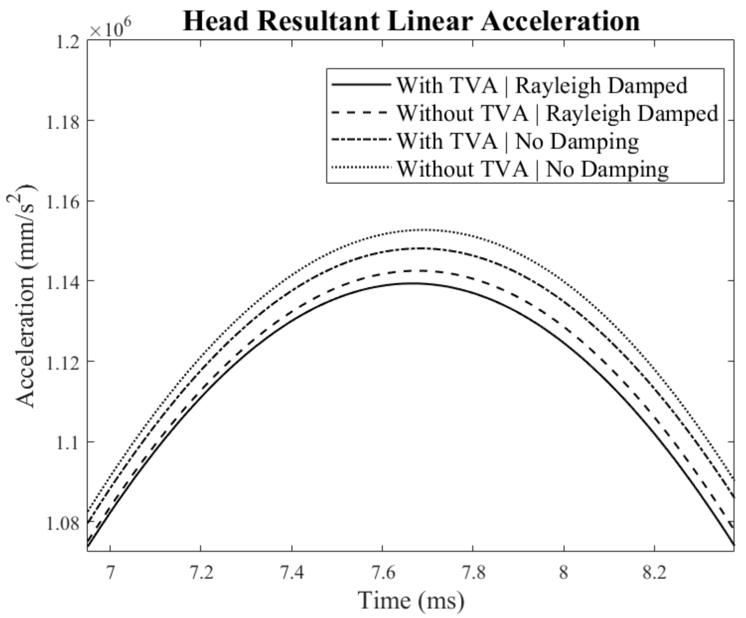

Figure 5.46. Head Resultant Linear Acceleration (Zoomed in) – Cases with Headgear

The head rotational velocities in directions of X, Y, and Z and total magnitude are displayed in Figure 5.47, Figure 5.49, Figure 5.51, and Figure 5.53, respectively, and their zoomed-on peak values in figures are presented in Figure 5.48, Figure 5.50, Figure 5.52, and Figure 5.54, respectively. In all directions, it is observed that with the addition of Rayleigh damping to the model, the peak values decreased, and the motion of the head became smoother. However, with the application of the TVA on the headgear, there is no significant or consistent change in peak rotational velocity values, which shows that the improvement on the headgear is not fruitful.

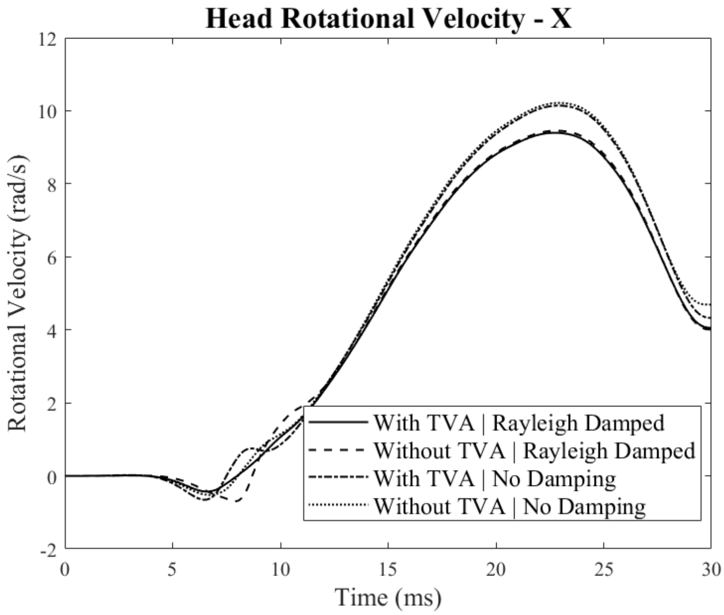

Figure 5.47. Head Rotational Velocity – X Axis – Cases with Headgear

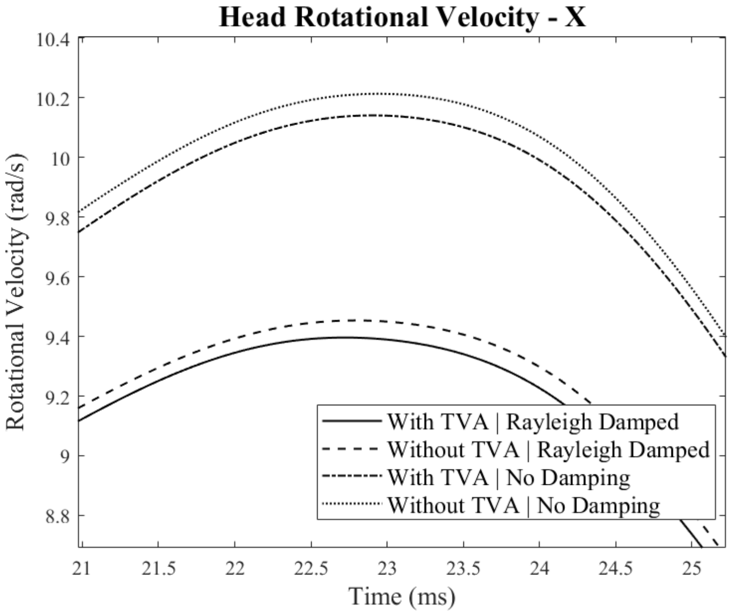

Figure 5.48. Head Rotational Velocity (Zoomed in) – X Axis – Cases with Headgear

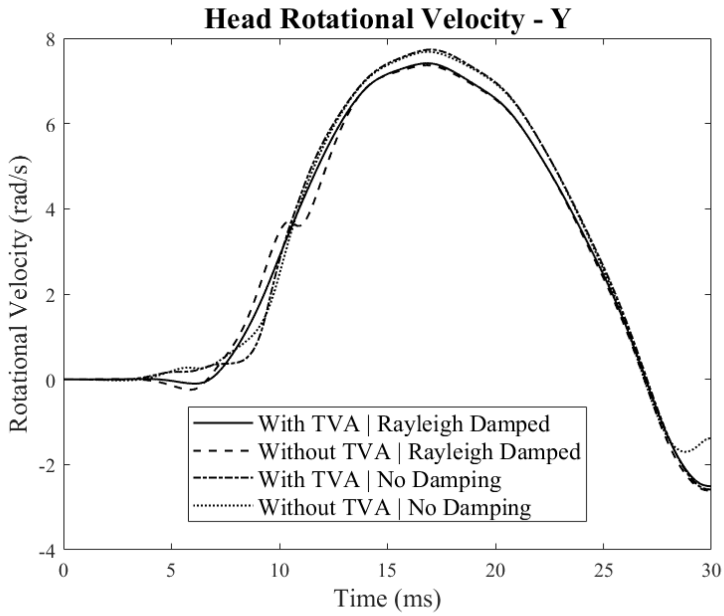

Figure 5.49. Head Rotational Velocity – Y Axis – Cases with Headgear

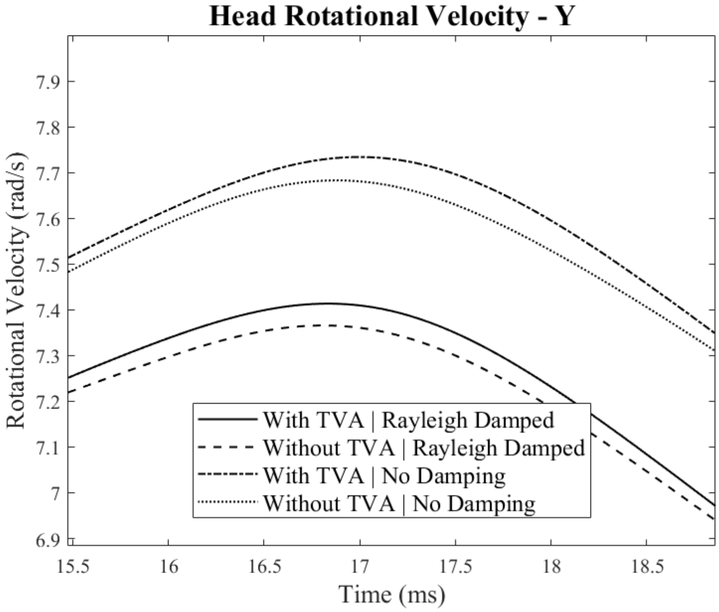

Figure 5.50. Head Rotational Velocity (Zoomed in) – Y Axis – Cases with Headgear

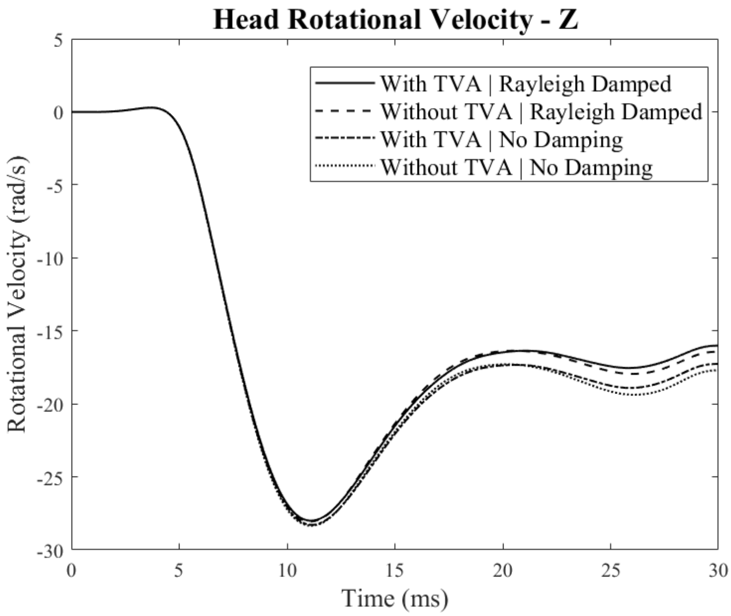

Figure 5.51. Head Rotational Velocity – Z Axis – Cases with Headgear

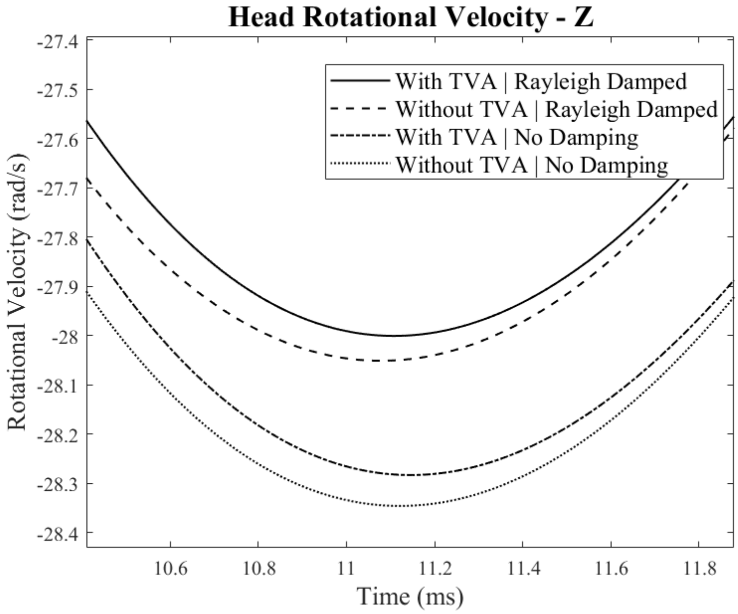

Figure 5.52. Head Rotational Velocity (Zoomed in) – Z Axis – Cases with Headgear

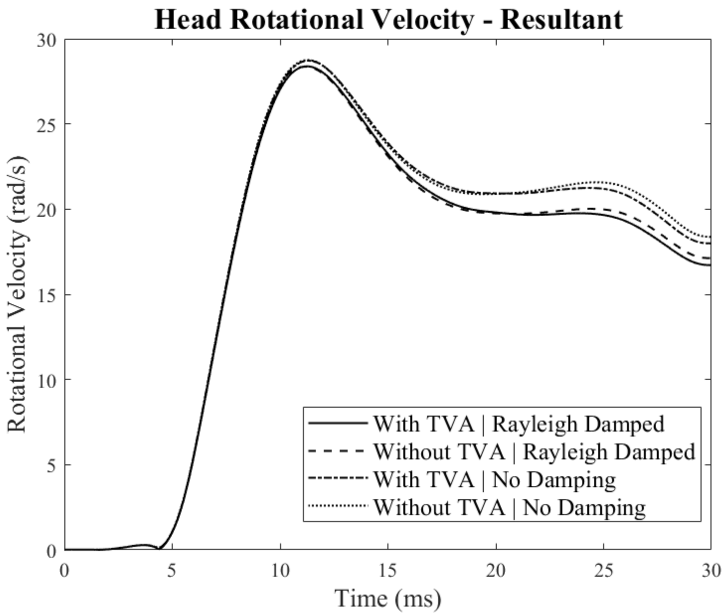

Figure 5.53. Head Rotational Velocity– Resultant – Cases with Headgear

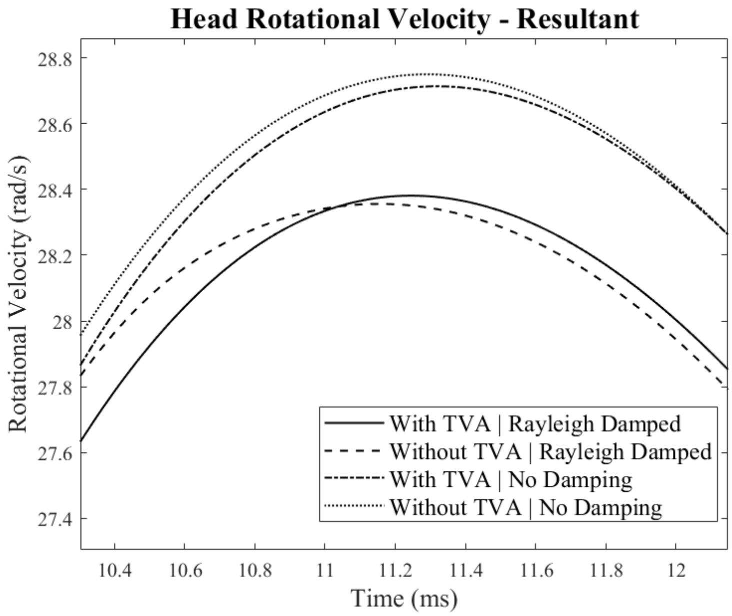

Figure 5.54. Head Rotational Velocity (Zoomed in) – Resultant – Cases with Headgear

The head rotational accelerations around directions of X, Y, and Z and total magnitude are displayed in Figure 5.55, Figure 5.57, Figure 5.59, and Figure 5.61, respectively, and their zoomed-on peak values in figures are presented in Figure 5.56, Figure 5.58, Figure 5.60, and Figure 5.62, respectively. Around all directions, it is observed that with the addition of Rayleigh damping to the model, the peak values decreased, and the motion of the head became smoother. Furthermore, with the application of the TVA on the headgear, there is no significant but consistent reduction in peak rotational acceleration values, which shows that the improvement on the headgear is changing the behavior of the head in the desired direction, but the effect is not at the desired levels.

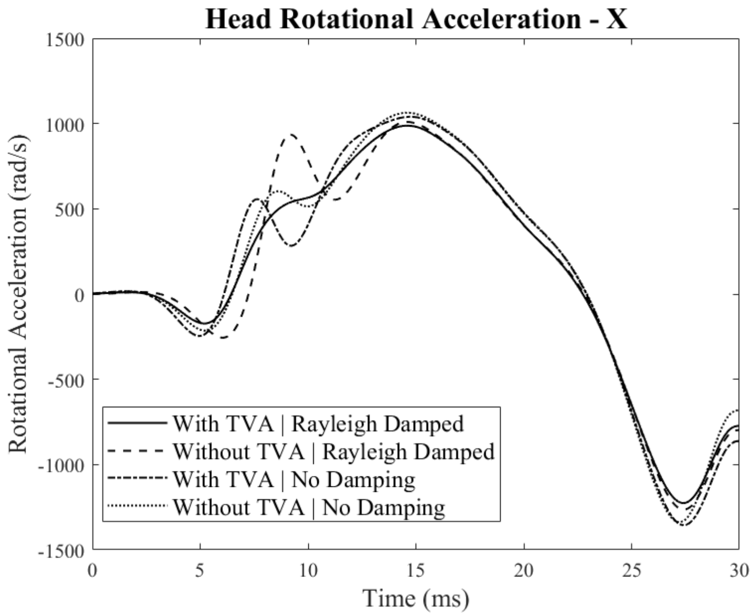

Figure 5.55. Head Rotational Acceleration – X Axis – Cases with Headgear

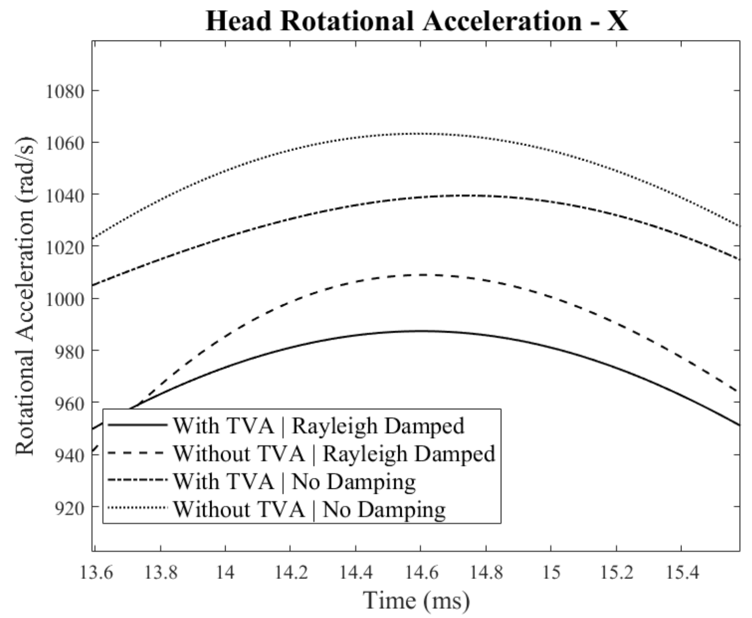

Figure 5.56. Head Rotational Acceleration (Zoomed in) – X Axis – Cases with Headgear

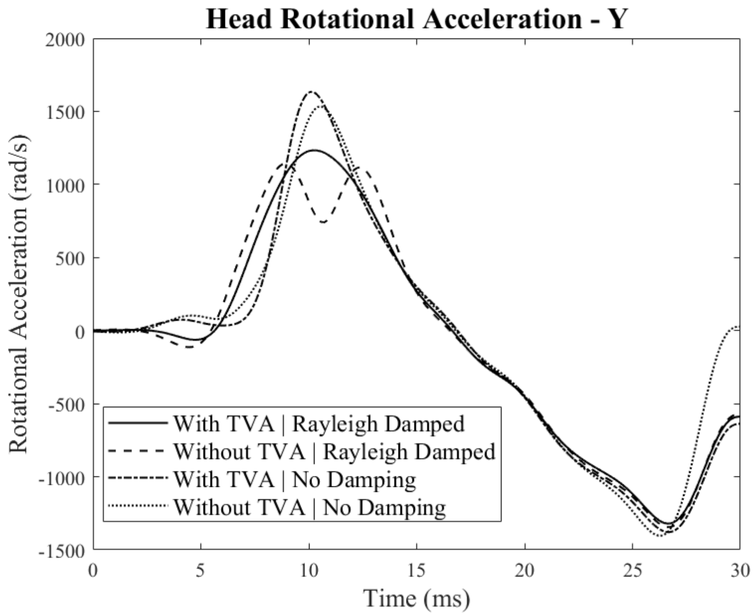

Figure 5.57. Head Rotational Acceleration – Y Axis – Cases with Headgear

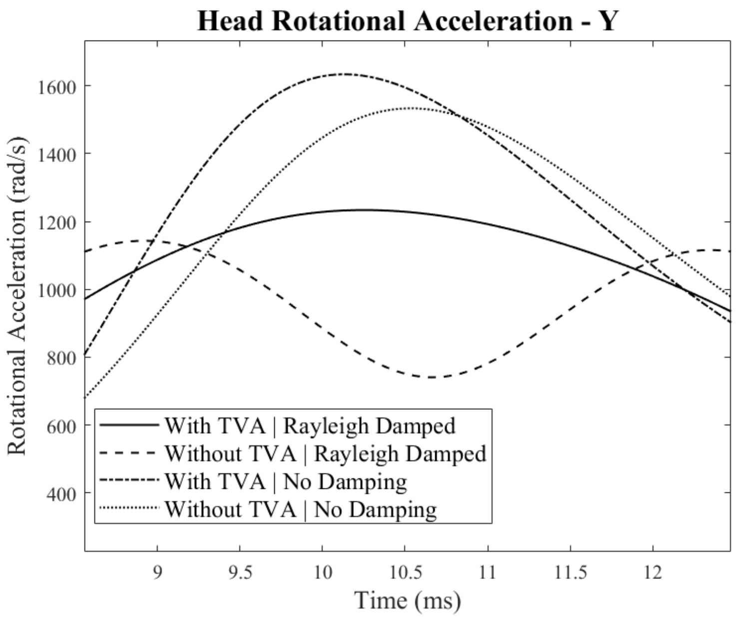

Figure 5.58. Head Rotational Acceleration (Zoomed in) – Y Axis – Cases with Headgear

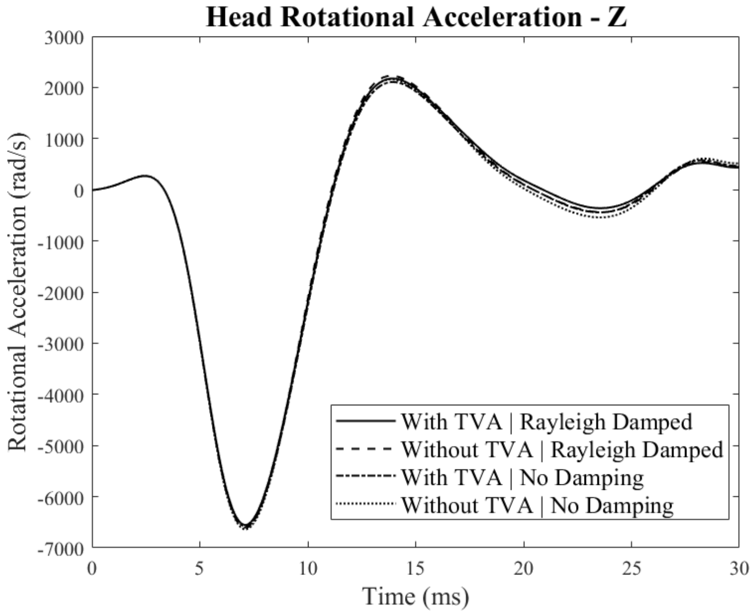

Figure 5.59. Head Rotational Acceleration – Z Axis – Cases with Headgear

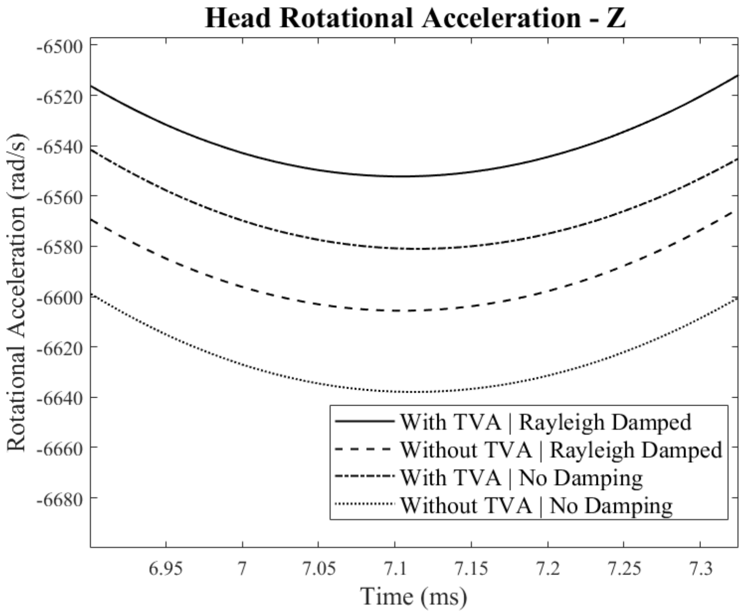

Figure 5.60. Head Rotational Acceleration (Zoomed in) – Z Axis – Cases with Headgear

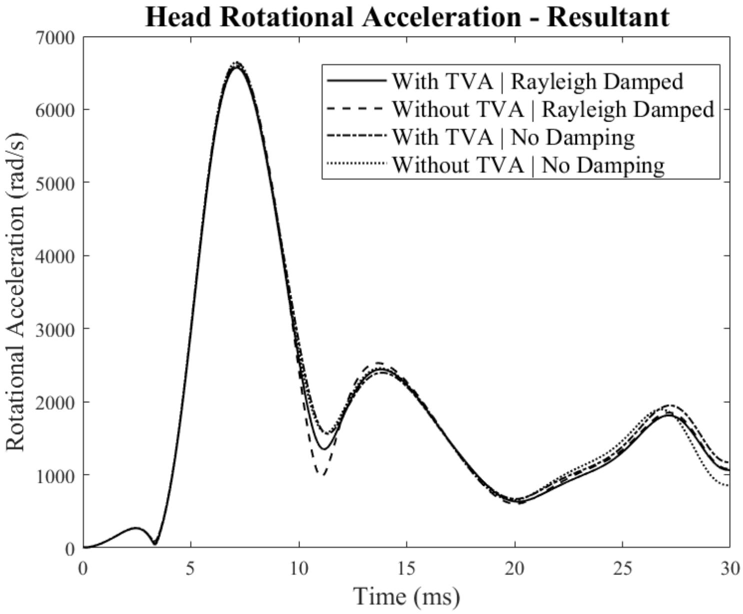

Figure 5.61. Head Rotational Acceleration – Resultant – Cases with Headgear

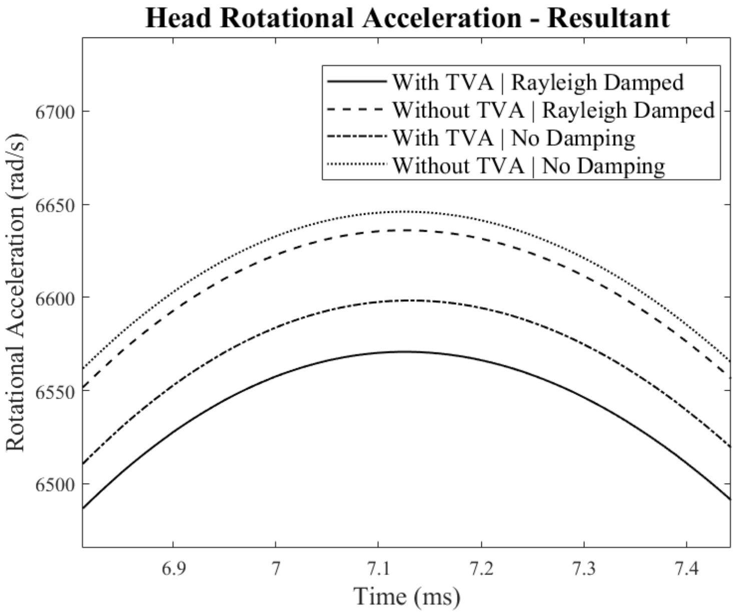

Figure 5.62. Head Rotational Acceleration (Zoomed in) – Resultant – Cases with Headgear

5.4 Discussion

The study at hand had two major goals: firstly, modeling a verified human head model to be used in dynamic analysis; and secondly, implementing a TVA on a protective headgear to reduce the risk of TBI for boxers.
The modeled human head is validated against the experimental studies and similar finite element models in the literature, which accomplished the first part of the study. To comment on the impact of the TVA implementation on the risk reduction of TBI, severity indices summarized in Table 5.1 can be used.

Table 5.1 Concussion Risk Simulation Results

	Simulation	HIC	$BrIC$	CM
Undamped Model	Without Headgear	1124.1	0.2316	0.4068
	With Headgear	363.82	0.2058	0.1725
	With TVA	362.45	0.2055	0.1717
Damped Model	Without Headgear	1103.8	0.2197	0.4023
	With Headgear	354.56	0.1935	0.1701
	With TVA	353.69	0.1934	0.1693

The study at hand was conducted in two main parts: simulation of punch impact on the undamped and damped head models. Simulations on both damped and undamped heads are conducted in order to see the overall effect of damping on the results. From the figures presented in 5.3.1, it is observed that the damping addition to the head model has a positive contribution to decreasing the linear and rotational velocity and acceleration magnitudes on the head. Apart from commenting on the authenticity of the model, this result tells us that the addition of damping to the head reduces the risk of TBI.
The effect of TVA implementation on headgear resulted in a slight decrease in severity indices. Although the decrease in TBI risk is a favorable result, the magnitude of the decrease is low.

From Figure 5.48, Figure 5.50, and Figure 5.52, it is observed that implementation of a TVA on the headgear had a positive impact on rotational velocities around the X and Z axes, yet the rotational velocity around the Y axis increased. This behavior can be seen in the following rotational acceleration figures: Figure 5.56, Figure 5.58, and Figure 5.60. Even though the resultant velocity and acceleration values of the head are decreased, the negative impact of the TVA on the Y-axis reduces the effectiveness of the TVA after all.

The design objective of the TVA-implemented headgear was to reduce the critical movement of the head, which was decided to be rotational velocity in the Z-axis. The simulations show that the aim of reducing the rapid movement in the Z-axis is achieved; however, the TVA implementation on headgear had a negative impact on rotational movements in the Y-axis. This misfortune decreases the effectiveness of TVA.

The study concluded its objective by reducing the severity indices of TBI risk; however, the effect of the TVA on the Y-axis should be discussed before carrying out the design in real life.

CHAPTER 6

CONCLUSION

The study at hand had two major goals, modeling a valid finite element human head model to carry out the required analyses and simulations, and reducing the TBI risk of a boxer who is hit by a hook punch.

The mechanism of TBI and its occurrence in boxing are investigated. After the cause-and-effect relationship between the rapid movements of the head and the risk of TBI is obtained, the solution for reducing the TBI risk is decided as the implementation of a TVA on boxing headgear.

The human head FE model is constructed and validated with experimental data available in the literature. The neck modeling is implemented on the head model by using 1-D axial and torsional springs. The boxing headgear, glove, and hand are modeled and implemented to model punch simulation. Two different cases are simulated: one with Rayleigh damping added to the whole model, the other undamped.

After completion of the modeling of the head, neck, and protective gear, the TVA tuning took place. TVA is tuned to the head's first torsional natural frequency, and the part is designed to work in the corresponding direction. There were two distinct TVA parameter tuning procedures: for the undamped model and for the Rayleigh-damped model, and their results are observed separately.

Six different cases are simulated: hook punch simulation without a headgear, with a standard headgear, and with a TVA implemented headgear, repeated for both undamped and Rayleigh-damped models. To quantify the TBI risk levels, three different severity indices are calculated: head injury criteria (HIC), brain injury criteria (BrIC), and combined metric (CM).

In the results, it is observed that the implementation of a TVA on the headgear changes the response of the head, yet the resulting behavior is not in the desired direction. The implementation of the TVA, which is tuned at the first torsional natural frequency of the head and modeled to work only around the vertical axis, did not yield the required reduction in severity indices.

The severity indices calculate the risk of TBI based on the maximum values of the linear and rotational velocity and acceleration of the head, which are dominated by both impact duration and force. The TVA tuning process, however, aims for much lower frequencies and requires a harmonic displacement in the system. Even though it is possible that the TVA may be working as designed at its tuned frequency, the TBI risk factors spike due to impact on the head, not harmonic motion. Therefore, one of the two aims of the study, TVA implementation on boxing headgear in order to reduce TBI risk, is decidedly unsuccessful. However, the modeled human head finite element model is available to be used in many more analyses or simulations. For example, car crash simulations on the human head model or analyses to improve existing boxing headgear in terms of material or design parameters can be conducted to reduce the risk of TBI occurrence.

The modeled TVA has not worked in the desired way because the tuning frequency of the TVA was too low to have a possible effect on the sharp increases in the response of the head. In the simulations it is observed that the addition of Rayleigh damping to the model decreased the TBI risk factor, which shows that the TVA implementation with higher damping ratios may yield a fruitful result. Also, it is observed that the implementation of TVA on a headgear increases movements of the head in undesired directions, which corrupts the working way of the TVA.

REFERENCES

[1] A. J. Ryan, “Intracranial injuries resulting from boxing,” *Clin Sports Med*, vol. 17, no. 1, pp. 155-168, Jan. 1998.

[2] L. C. Baird, C. B. Newman, H. Volk, J. R. Svinth, J. Conklin, and M. L. Levy, “Mortality resulting from head injury in professional boxing,” *Neurosurgery*, vol. 67, no. 5, pp. 1444–1450, Nov. 2010.

[3] M. Jayarao, L. S. Chin, and R. C. Cantu, “Boxing-related head injuries,” *Physician and Sportsmedicine*, vol. 38, no. 3. pp. 18–26, Oct. 2010.

[4] L. J. Ng *et al.*, “A mechanistic end-to-end concussion model that translates head kinematics to neurologic injury,” *Frontiers in Neurology*, vol. 8, no. 269, Jun. 2017.

[5] A. M. Nahum and R. W. Smith, “An experimental model for closed head impact injury,” *SAE Transactions*, vol. 85, pp. 2638-2651, 1976.

[6] W. N. Hardy, C. D. Foster, M. J. Mason, K. H. Yang, A. King, and S. Tashman, “Investigation of head injury mechanisms using neutral density technology and high-speed biplanar x-ray,” *Stapp Car Crash J*, vol. 45, pp. 337-368, 2001.

[7] W. N. Hardy *et al.*, “A study of the response of the human cadaver head to impact,” *Stapp Car Crash J*, vol. 51, pp. 17–80, Oct. 2007.

[8] S. Stojsih, M. Boitano, M. Wilhelm, and C. Bir, “A prospective study of punch biomechanics and cognitive function for amateur boxers,” *British Journal of Sports Medicine*, vol. 44, no. 10, pp. 725–730, Aug. 2010.

[9] D. C. Viano *et al.*, “Concussion in professional football: comparison with boxing head impacts - Part 10,” *Neurosurgery*, vol. 57, no. 6, pp. 1154–1172, Dec. 2005.

[10] J. G. Beckwith, J. J. Chu, and R. M. Greenwald, “Validation of a noninvasive system for measuring head acceleration for use during boxing competition,” *Journal of Applied Biomechanics*, vol. 23, no 3, pp. 238–244, Aug. 2007.

[11] J. Hutchinson, M. J. Kaiser, and H. M. Lankarani, “The head injury criterion (HIC) functional,” *Applied Mathematics and Computation*, vol.96, no 1, pp. 1–16, 1998.

[12] E. G. Takhounts, M. J. Craig, K. Moorhouse, J. Mcfadden, and V. Hasija, “Development of brain injury criteria (BrIC),” *Stapp Car Crash J*, vol. 57, pp. 243-266, Nov. 2013.

[13] A. Gunnarsdóttir, “Evaluation of test methods for football helmets using finite element simulations,” MSc, Medical Engineering, KTH, Sweden, 2019.

[14] A. M. Nahum, R. Smith, and C. C. Ward, “Intracranial pressure dynamics during head impact,” *SAE Transactions*, 1977.

[15] Y. Luo and Z. Liang, “Understanding how a sport-helmet protects the head from closed injury by virtual impact tests,” *Biomed Mater Eng*, vol. 28, no. 3, pp. 279–291, 2017.

[16] Z. Liang and Y. Luo, “A QCT-based nonsegmentation finite element head model for studying traumatic brain injury,” *Appl Bionics Biomech*, vol. 2015, 2015.

[17] Z. Cai, Y. Xia, Z. Bao, and H. Mao, “Creating a human head finite element model using a multi-block approach for predicting skull response and brain pressure,” *Comput Methods Biomech Biomed Engin*, vol. 22, no. 2, pp. 169–179, Feb. 2019.

[18] F. A. O. Fernandes, D. Tchepel, R. J. Alves de Sousa, and M. Ptak, “Development and validation of a new finite element human head model: Yet another head model (YEAHM),” *Engineering Computations (Swansea, Wales)*, vol. 35, no. 1, pp. 477–496, 2018.

[19] T. J. Horgan and M. D. Gilchrist, “The creation of three-dimensional finite element models for simulating head impact biomechanics,” *International Journal of Crashworthiness*, vol. 8, no. 4, pp. 353–366, Jan. 2003.

[20] E. G. Takhounts *et al.*, “Investigation of traumatic brain injuries using the next generation of simulated injury monitor (SIMon) finite element head model,” *Stapp Car Crash J*, vol. 52, pp. 1-31, Nov. 2008.

[21] K. M. Tse, L. Bin Tan, S. J. Lee, S. P. Lim, and H. P. Lee, “Development and validation of two subject-specific finite element models of human head against three cadaveric experiments,” *Int J Numer Method Biomed Eng*, vol. 30, no. 3, pp. 397–415, 2014.

[22] B. Hakansson, A. Brandt, P. Carlsson, and A. Tjellstrom, “Resonance frequencies of the human skull in vivo,” *J Acoust Soc Am.*, vol. 95, no. 3, pp. 1474–1481, Mar. 1994.

[23] *AIBA Technical and Competition Rules-1*. 2021.

[24] E. G. Takhounts, R. H. Eppinger, J. Q. Campbell, R. E. Tannous, E. D. Power, and L. S. Shook, “On the development of the SIMon finite element head model,” *Stapp Car Crash J*, vol. 47, pp. 107–133, Oct. 2003.

[25] E. Lüders, H. Steinmetz, and L. Jìncke, “Brain size and grey matter volume in the healthy human brain,” *Neuroreport*, vol. 13, no. 17, pp. 2371-2374, Dec. 2002.

[26] J. Ruan and P. Prasad, “The effects of skull thickness variations on human head dynamic impact responses,” *Stapp Car Crash J*, vol. 45, pp.395-414, Nov. 2001.

[27] V. Dirisala, G. Karami, and M. Ziejewski, “Effects of neck damping properties on brain response underimpact loading,” *Int J Numer Method Biomed Eng*, vol. 28, no. 4, pp. 472–494, Apr. 2012.

[28] J. Farmer, S. Mitchell, P. Sherratt, and Y. Miyazaki, “A human surrogate neck for traumatic brain injury research,” *Front Bioeng Biotechnol*, vol. 10, Dec. 2022.

[29] E. K. Spittle Buford W Shipley, J. Ints Kaleps, and D. Jo Miller, “Hybrid II and Hybrid III dummy neck properties for computer modeling,” systems Research Laboratories, Ohio, USA, AL-TR-1992-0049, Feb. 1992.

[30] R. Razaghi, H. Biglari, and A. Karimi, “A comparative study on the mechanical performance of the protective headgear materials to minimize the injury to the boxers’ head,” *Int J Ind Ergon*, vol. 66, pp. 169–176, Jul. 2018.

[31] X. Fan, “Kinematic analysis of traumatic brain injuries in boxing using finite element simulations,” MSc, Medical Engineering, KTH, Sweden, 2016.

[32] P. Perkins, A. Jamieson, W. Spratford, and A. Hahn, “Evaluation of ability of two different pneumatic boxing gloves to reduce delivered impact forces and improve safety,” *World Journal of Engineering and Technology*, vol. 06, no. 02, pp. 457–491, May 2018.

[33] T. J. Walilko, D. C. Viano, and C. A. Bir, “Biomechanics of the head for Olympic boxer punches to the face,” *Br J Sports Med*, vol. 39, no. 10, pp. 710–719, Oct. 2005.

[34] D. Dinu and J. Louis, “Biomechanical analysis of the cross, hook, and uppercut in junior vs. elite boxers: implications for training and talent identification,” *Front Sports Act Living*, vol. 2, Nov. 2020.